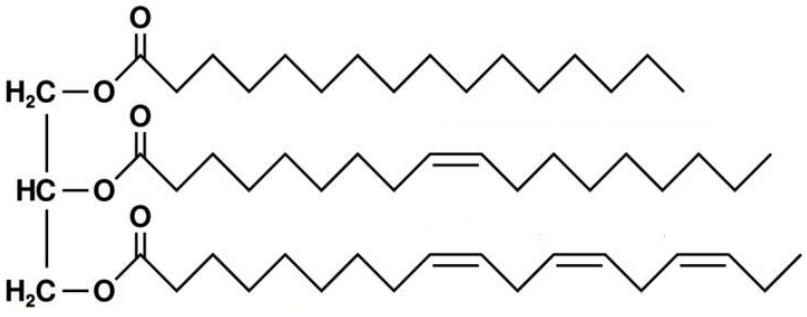

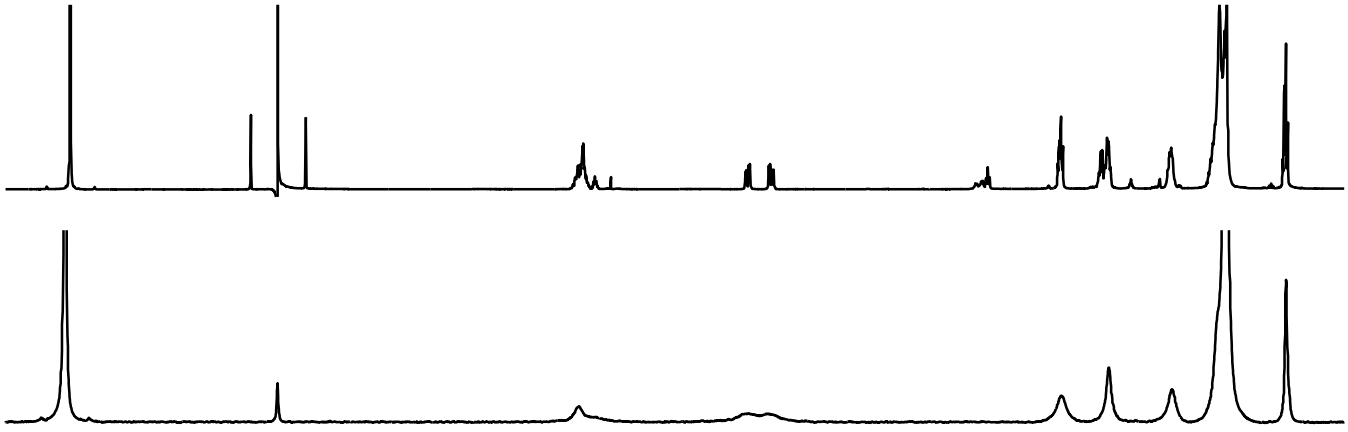

João André Gonçalves Duarte

Development, validation and biological application of a novel hybrid $^{1}H/^{2}H$ NMR method for the determination of lipid biosynthetic fluxes

Tese de doutoramento em Bioquímica, na especialidade de Bioenergética, orientada pelo Dr. John G. Jones e Dr. Shawn C. Burgess, apresentada à Faculdade de Ciências e Tecnologia da Universidade de Coimbra

2014

· U C ·

Universidade de Coimbra

João André Gonçalves Duarte

Development, validation and biological application of a novel hybrid $^{1}H/^{2}H$ NMR method for the determination of lipid biosynthetic fluxes

Tese de doutoramento em Bioquímica, especialidade em Bioenergética, orientada pelo Dr. John G. Jones e Dr. Shawn C. Burgess, apresentada à Faculdade de Ciências e Tecnologia da Universidade de Coimbra

2014

UNIVERSIDADE DE COIMBRA

Dedicado à Raquel

Prefiro escorregar nos becos lamacentos,
Redemoinhar aos ventos,
Como farrapos, arrastar os pés sangrentos,
A ir por aí...
Se vim ao mundo, foi
Só para desflorar florestas virgens,
E desenhar meus próprios pés na areia inexplorada!
O mais que faço não vale nada.

José Régio, Cântico Negro

CONTENTS

Acknowledgements

In this part of my journey through the world of since I have met multiple people to whom I owe a great deal of gratitude. It is difficult to surmise the contribution these people have given me throughout the years but I will try.

Under the supervision of Dr. Shawn Burgess I have learned a great deal about what it really means to do science. His candid mentorship is something I will forever hold dear. His door is always open and his mind is always ready for discussing science. I still do not understand why, being such an intelligent person, he still supports the Oklahoma Sooners, but to each his own I suppose.

I don't think I have ever met anyone as enthusiastic as Dr. John Jones when it comes to tackling down novel methods and ideas. He is always ready to provide his expert opinion. Without him none of this would have been possible. I am eternally grateful! Also, he is one hell of a brewmaster!

To my lab mates in the Burgess lab:

Austin Potts - who, at the very beginning of my stay in Dallas, provided me oh so important information about the American's general sense of personal space by gently pushing me away as we walked to the cafeteria – thank you for being such a good friend!

Blanka Kucejova – When Blanka tells you your presentation or data is "ok" you know you have made it big! – I hope to one day be able to reach your level of research excellence. Thank you for teaching me so much!

Justin Trombold – I find it surprising that, despite our long winded political discussions we still manage to get any work done! – Thanks for all the ideas.

Santhosh Satapati – Who tried to convince me that he had once made the best agarose gel in the world, using only water – You are an excellent researcher and I have learned a lot from you over the years. Thank you so much!

Tienteng He – You are an extremely kind and understanding person and I am constantly awed by your skill, you make the difficult seem easy. Thank you.

Xiaorong Fu – I don't think I have met anyone as efficient as you. Thank you for all the help you have given me getting my projects done!

I would also like to thank the former lab members, Nishanth Sunny and Jaimie Boney-Montoya, for always being there for me. Well, at least until you left!

To the newest member of the extended Burgess family, David Coppell, I hope you have as much fun in the lab as I did.

To my group of friend in Dallas: Albert Linden, Alexander Piala, Brody Holohan, Cindy Zoellner, Connor Gulbronson, Dan Lopes, Jared Hooks, Jessica Mayeux, Lael Ladderman, Roya Kalantari, Ryan LaRanger, Susan DeLeon. Thank you for putting up with my horrible "jokes". Keep on being awesome!

Possuo uma grande gratidão para com o Prof. Carlos Geraldes. É devido às suas aulas de espectroscopia e o seu entusiasmo que me encontro onde estou.

Ao Dr. Rui de Carvalho, que me mostrou que a máquina de RMN não é um bicho sinistro e me ensinou a domá-la, muito obrigado

André Martins, João Rodrigues, João Teixeira, Luís Nobre, Paulo Gameiro e Rui Costa. Obrigado por provarem que a amizade é intemporal e não se interessa com as distâncias físicas. Espero que consigamos manter a tradição (e o jantar do bigode obviamente!) durante muitos anos.

Aos meus pais, por todo o apoio que me deram ao longo dos anos, é difícil encontrar palavras que possam exprimir a gratidão que sinto por lá terem estado sempre para mim. Obrigado por tudo!

Finalmente, tenho de agradecer à Raquel, pela paciência, compreensão e amor que partilha comigo. És pequena e fofa e eu gosto de ti!

Abbreviations

^{1}H: Proton

^{13}C: Carbon-13

^{2}H: Deuterium

ACC: Acetyl-CoA carboxylase

BAT: Brown adipose tissue

CoA: Coenzyme A

DHA: docosahexaenoic acid

DNL: De novo lipogenesis

D_2O: Deuterated water

ELOVL: Elongation of very long chain fatty acids

FA: Fatty acid

FAD: Fatty acid desaturase

FAS: Fatty acid synthase

FAO: Fatty acid oxidation

Gly3P: Glycerol-3-phosphate

GlyNG: Glyceroneogenesis

GNG: Gluconeogenesis

HF: High fat

HFD: High fat diet

i.p.: Intraperitonial

IR: Insulin resistance

IRS: Insulin Receptor Substrate

KD: Knockdown

KO: Knockout

MIDA: Mass isotopomer distribution analysis

MS: Mass spectroscopy

mTOR: Mammalian Target of Rapamycin

MUFAS: Monounsaturated Fatty Acids

NAFLD: Non-alcoholic fatty liver disease

NAD^+: Non-protonated nicotinamide adenine dinucleotide

NADH: Protonated nicotinamide adenine dinucleotide

$NADP^+$: Non-protonated nicotinamide adenine dinucleotide phosphate

NADPH: protonated nicotinamide adenine dinucleotide phosphate

NOX: NADPH oxidase

NMR: Nuclear Magnetic Resonance

PEPCK: Phosphoenolpyruvate carboxykinase

PUFAS: Polyunsaturated fatty acids

SCD: Stearoyl-CoA desaturase

SREBP: Sterol Regulatory Element Binding Protein

STZ: Streptozotocin

T1DM: Type 1 diabetes mellitus

T2DM: Type 2 diabetes mellitus

TG-Gly: Triglyceride bound glycerol

TG-FA: Triglyceride bound fatty aids

VLDL: Very Low Density Lipoprotein

WAT: White adipose tissue

ABSTRACT

Altered lipid metabolism is a hallmark of multiple diseases such as diabetes and cancer, so there is a vast interest in the accurate determination of lipid synthesis fluxes. However, there is no gold standard for measuring these fluxes. Therefore, the initial goal of this project was to develop and validate a novel, non-invasive methodology that could be used to measure these fluxes. Here we describe a novel, hybrid $^{1}H/^{2}H$ nuclear magnetic resonance (NMR) analytical technique for the simultaneous determination of *de novo* lipogenesis, elongation, unsaturation, glycerol and cholesterol synthesis fluxes. The first chapter of this dissertation will provide the mathematical formulas necessary for the determination of these fluxes. In order to confirm that the flux readout obtained from the NMR method is actually representative of real metabolic changes, the mathematical formulas where validated by using animal models with known changes in those metabolic pathways. The NMR method was able to accurately determine the predicted changes in metabolic fluxes in all tested animal models.

One of the key aspects of diabetes is the dysregulation of lipid metabolism, as evidenced by the hypertriglyceridemia that occurs in diabetic patients. A feature of type 2 diabetes is the apparent paradox of selective insulin resistance, i.e., the glucoregulatory branch of insulin signaling becomes resistant, but the regulation of lipid metabolism remains unchanged or even elevated. However, most studies that analyze selective insulin resistance do not perform flux analysis, relying instead on mRNA or protein levels of key enzymes to determine if fluxes are changed. Chapter 2 of this dissertation will apply the NMR method described in chapter 1 to determine if lipid flux was altered in the context of diabetes and insulin resistance. Flux analysis performed in high-fat diet induced diabetic mice indicates that DNL is actually decreased in these animals, suggesting the possibility that the observed differences in mRNA and protein levels in previous studies do not necessarily translate into increased flux through the pathway.

Finally, in chapter 3 of this dissertation the NMR method will be applied to determine the effects of the cytosolic form of Phosphoenolpyruvate carboxykinase (PEPCK-C) in the regulation of lipid metabolism. PEPCK-C is considered one of the key enzymes in the regulation of gluconeogenesis, but a recent study showed that, in fact, PEPCK-C has a remarkably low impact in the regulation of hepatic gluconeogenesis.

This data raises the question: if PEPCK-C is not important for gluconeogenesis, what is its metabolic role? Previous reports have shown that PEPCK-C is associated with proper maintenance of lipid homeostasis, as animals that are whole body knockouts for this enzyme die within two days of birth, showing remarkable hypertriglyceridemia and accumulation of hepatic fat. Here it is shown that PEPCK-C has a higher control over the synthesis of fatty acids, both in the fed and fasted state, than it does for the regulation of glucose production. The potential mechanisms through which PEPCK-C regulates lipid metabolism were also investigated in mice that express varying levels of PEPCK-C, with dysregulation of shuttling of metabolites between the mitochondria and the cytosol being identified as a potential mechanism for the changes in lipid metabolism.

RESUMO

Alterações do metabolismo dos lípidos é uma das principais características de múltiplas doenças tais como cancro e diabetes, como tal, existe muito interesse em determinar de forma correta, fluxos de síntese de lípidos. Contudo, não existe nenhum "golden standard" para medir estes fluxos. Como tal, o primeiro objetivo deste trabalho foi desenvolver e validar uma nova técnica analítica híbrida de $^{1}H/^{2}H$ de ressonância magnética nuclear (RMN) para a determinação simultânea de lipogénese *de novo*, elongação, desaturação de ácidos gordos, assim como a síntese de glicerol e de colesterol. No primeiro capítulo desta dissertação serão dadas as fórmulas matemáticas necessárias para a determinação destes fluxos. Para ter a certeza absoluta que a informação de fluxos providenciada por este método são, em boa verdade, representativas de potenciais mudanças em atividade metabólica, as fórmulas matemáticas foram validadas usando modelos animais que possuem alterações previamente determinadas nessas mesmas vias metabólicas. O método de RMN foi capaz de medir com precisão as mudanças metabólicas previstas em todos os modelos animais testados.

Um dos aspetos chave da patologia da diabetes é a desregulação do metabolismo dos lípidos como evidenciado pela hipertrigliceridémia que ocorre em pacientes diabéticos. Uma particularidade da diabetes tipo 2 é o aparente paradoxo de resistência seletiva à insulina, isto é, a atividade da insulina sobre o braço glucoreglatório da sinalização torna-se resistente, mas a regulação do metabolismo dos lípidos mantem-se normal, ou mesmo elevada. Contudo, a maioria dos estudos que analisam a resistência seletiva à insulina não fazem análise aos fluxos metabólicos, recorrendo antes aos níveis de RNAm e às quantidades de proteína de algumas enzimas chave para determinar se os fluxos estão alterados. No capítulo 2 desta tese, o método de RMN descrito no capítulo 1 será aplicado para determinar se o fluxo lipogénico está verdadeiramente alterado no contexto da diabetes e resistência à insulina. Análise aos fluxos efetuada em ratinhos em que a diabetes foi induzida via alimentação de uma dieta rica em gordura indicam que a lipogénese está, de facto, diminuída nestes animais, sugerindo a possibilidade que as alterações em RNAm e níveis de proteína observadas em estudos anteriores não se traduzem necessariamente num aumento do fluxo através desta via metabólica.

Finalmente, no capítulo 3 desta dissertação, o método de RMN será aplicado para estudar os efeitos da forma citosólica da enzima fosphoenolpiruvato carboxicinase

(PEPCK-C) na regulação do metabolismo dos lípidos. PEPCK-C é considerada uma das enzimas chave na regulação da gluconeogénese, mas um estudo recente demonstrou que, de facto, a PEPCK-C tem um impacto notavelmente baixo na regulação da gluconeogénese hepática. Estes dados levantam uma questão: se a PEPCK-C não é importante na regulação da gluconeogénese, qual é o seu papel metabólico? Outros estudos indicam que a PEPCK-C é importante para a correta manutenção da homeostasia dos lípidos, visto que animais deficientes desta enzima a um nível global morrem dois dias depois de nascerem, com marcada hipertrigliceridémia e acumulação de lípidos mo fígado. Demonstramos, usando animais que expressam diferentes níveis de PEPCK-C que esta enzima tem um maior controlo sobre a síntese de ácidos gordos, quer no estado pré- ou pós prandial, do que o controlo que exerce sobre a produção de glucose. Os potenciais mecanismos através dos quais a PEPCK-C regula o metabolismo dos lípidos também foi investigado em animais que produzem diferentes níveis de PEPCK-C, sendo que alterações no transporte de metabolitos entre a mitocôndria e o citosol foram identificados como um potencial mecanismo para as mudanças no metabolismo dos lípidos.

CHAPTER 1

Development of a novel $^{1}H/^{2}H$ NMR technique to measure lipid metabolic fluxes

1 – Introduction

Obesity has reached epidemic proportions worldwide, Data from 2009 and 2010 indicates that 69.2% of United States adults where defined as overweight (BMI between 25 and 30) and 35.9% where considered obese (BMI≥30) (1). Europe follows the same trend, with a study showing that, based on BMI, 28.3% of men and 36.5 of women can be classified as obese (2). The trend is for these numbers to increase, with some studies predicting that the number of obese people in the United States might increase to almost 90% by 2030 (3). Obesity has severe consequences on individuals' health: studies show that a BMI≥30 is considered a major risk for cardiovascular diseases (4) and Type 2 diabetes mellitus (T2DM) (5). It is also an extraordinary financial burden, since studies show that about 10% of all United States medical expenses in 2008 derive from the treatment of obesity-related complications (6).

One of the consequences of obesity is increased fat mass and alterations of lipid flux and therefore there is interest in determining how these fluxes are changed in pathophysiological states.

This chapter describes the development of a NMR based technique that allows the determination of multiple lipid fluxes, namely, DNL, SCD-1 activity, elongation, NADPH synthesis, Cholesterol synthesis and triglycerie-glycerol synthesis. This method also provides lipidomic information on the analyzed sample, by determining the amount of monounsaturated fatty acids (MUFAS), polyunsaturated fatty acids (PUFAS), Saturated FA, ω-3 FA, and two individual fatty acids: linoleic acid and docosahexaenoic acid, as well as providing the average chain length of the fatty acids in the sample. Afterwards, as detailed in chapter 2 of this dissertation we will apply this method for the determination of lipid biosynthetic fluxes in High-Fat Diet (HFD)-induced type 2 diabetes.

The introduction of this chapter will briefly explain the pathways involved in lipid metabolism, followed by a review of existing methodology used to measure fatty acid metabolism. Next, in order to better understand the NMR method development, we will analyze the metabolic origin of protons and carbons of lipid moieties, cholesterol and glycerol.

2 - Lipid metabolism

2.1 – De novo lipogenesis

De novo lipogenesis (DNL) is the process through which Acetyl-CoA is converted to palmitate. The overall reaction of lipogenesis is:

$$8\ \text{Acetyl CoA} + 7\ \text{ATP} + 14\ \text{NADPH} \rightarrow \text{Palmitate} + 8\ \text{CoA} + 7\ \text{ADP} + 14\ \text{NADP}^{+} + 6\ \text{H2O}$$

There are two enzymes in DNL: Acetyl-CoA carboxylase (ACC) and Fatty acid synthase (FAS).

2.1.1 – Acetyl-CoA carboxylase (ACC)

ACC is a biotin dependent enzyme that catalyzes the conversion of acetyl-CoA into malonyl-CoA. Figure 1 shows this enzyme's mechanism of action

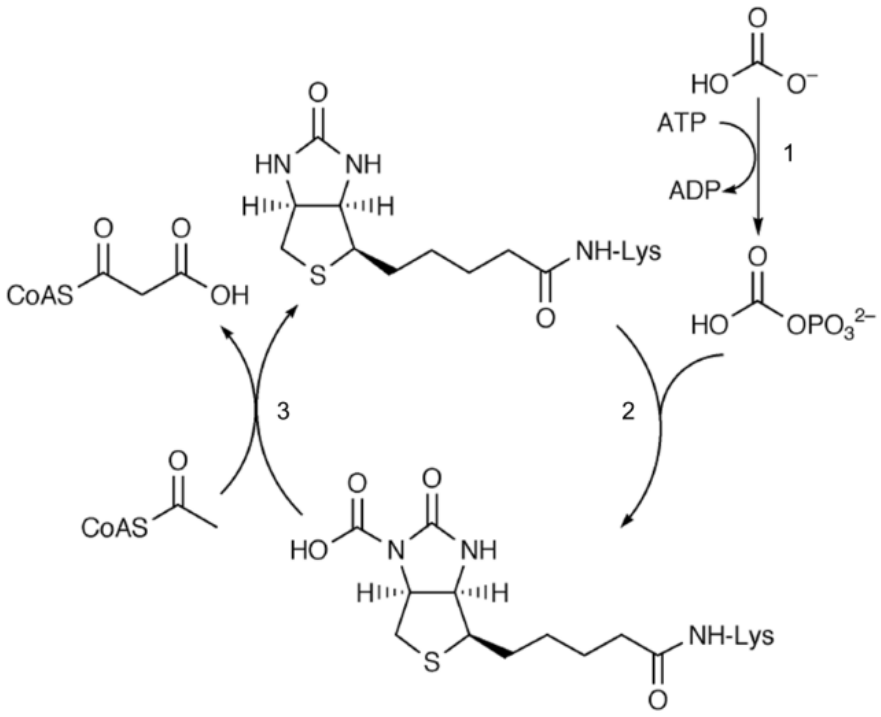

Figure 1: ACC mechanism of action: The first step in the mechanism is the phosphorylation of bicarbonate (1) followed by the transference of the carbamoyl phosphate group into the N-1 site of biotin (2) and subsequent transference to the acetyl-CoA unit, restoring the enzyme to its native conformation and creating a molecule of malonyl-CoA (3). Figure adapted from (7).

There are two isoforms of ACC, each encoded in a distinct gene (8): ACC1 and ACC2, located in the cytosol and the outer mitochondrial membrane, respectively (9). The fate of the malonyl-CoA produced by these two isoforms is distinct. ACC1-derived malonyl-CoA is used mainly as a lipogenic substrate, whereas ACC2-derived malonyl-CoA is used to regulate fatty acid oxidation by inhibiting carnitine palmitoyltransferase-I (CPT-I) (10) an enzyme essential for the entrance of fatty acids into the mitochondria, where they are oxidized. ACC1 is mainly expressed in liver, adipose tissue and mammary glands, i.e., the tissues where lipogenesis occurs to the highest extent. Conversely, ACC2 is mainly expressed in skeletal muscle, heart and liver, where β-oxidation takes place (11).

2.1.2 – Fatty acid synthase (FAS)

Fatty acid synthase (FAS) is a multimeric enzyme that catalyzes the condensation of the malonyl-CoA units produced by ACC1 to synthesize palmitate. FAS has 6 domains that catalyze the reactions necessary for the condensation of malonyl-CoA units (Figure 2). The malonyl-CoA/acetyl-CoA-ACPT-transacylase (MAT) domain catalyzes the binding of acetyl-CoA and malonyl-CoA to the acyl carrier of FAS. Then the β-ketoacyl synthase (KS) domain catalyzes the decarboxylative condensation of acetyl-CoA with malonyl-CoA, followed by a reduction catalyzed by the β-ketoacyl reductase (KR) domain, which uses NADPH as the source of proton for the reaction. The resulting β-hydroxyacyl undergoes dehydration in the dehydratase domain (DH) forming a β-enoyl product which undergoes a second reduction in the β-enoyl reductase (ER) domain. This process repeats itself for seven times, with each reaction adding two extra carbon units to the nascent fatty acid. After all of the 18 carbons of palmitate have been added, the thioesterase (TE) domain, then cleaves the newly made palmitate of the enzyme.

The mechanism of FAS will be further explored in section 3 of this chapter, in order to completely elucidate the origins of protons and carbons in the fatty acid moieties.

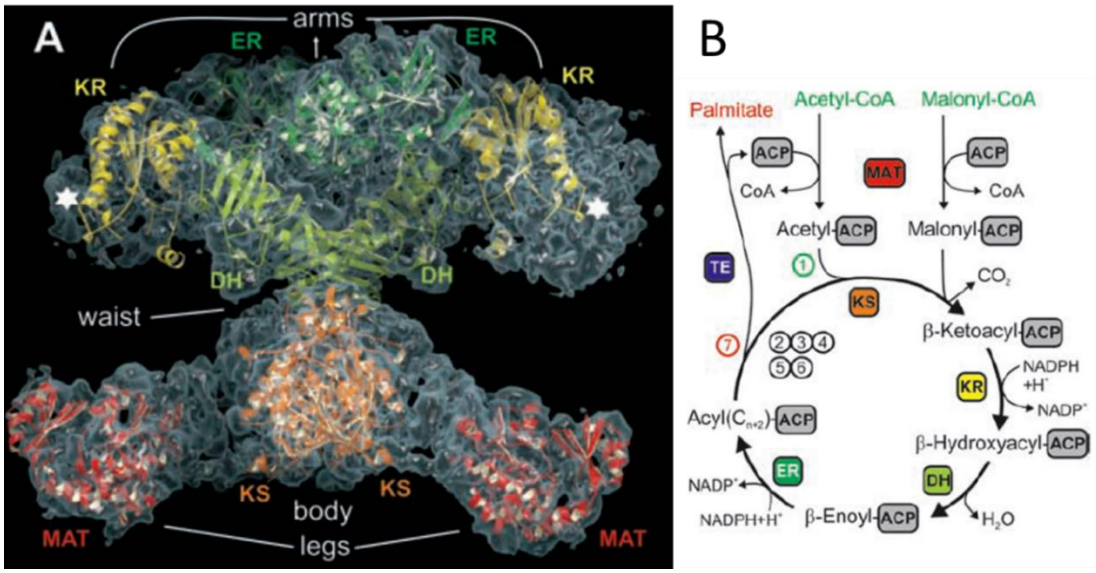

Figure 2: a) 3D structure of porcine FAS highlighting the position of some of the catalytic domains. The white stars represent the possible location of the TE domain b) Chemical reactions catalyzed by each of the domains of FAS Adapted from (12).

Each of the domains of FAS has a very precise specificity for different fatty acid carbon chains. The MAT domain has a high specificity for malonyl- and acetyl-CoA but a low specificity for higher carbon chain lengths, such as C4:0 and C6:0. The KS domain has a high specificity for C6:0 to C14:0 but not C16:0 which, coupled with the TE's domain high specificity for C16:0 (13), makes palmitate the predominant product of FAS (Figure 3).

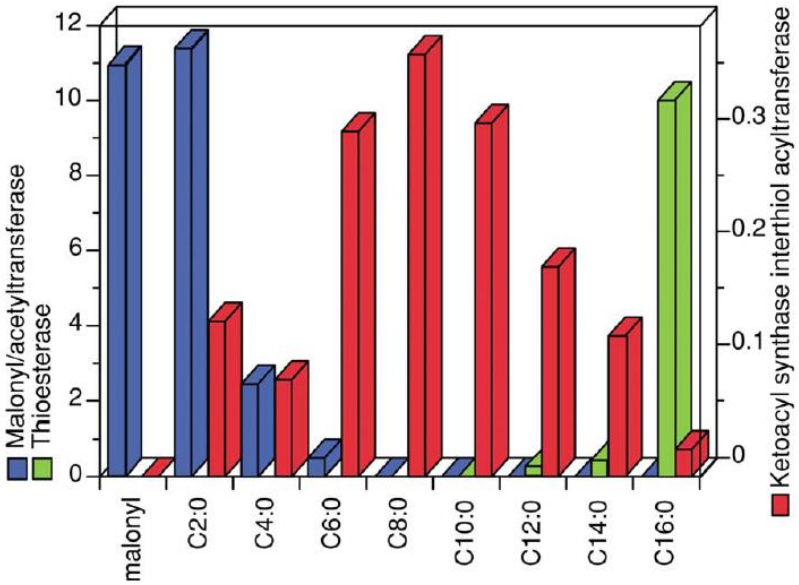

Figure 3: Chain length specific activities of malonylacyltransferase, thioesterase and ketoacyl synthase moieties of FAS. The units for the activities are µmol/min/mg. Figure adapted from (13).

2.2 – Desaturation and elongation

Fatty acids, whether they are formed by DNL or derived from the diet, can undergo further alterations, with the two most common ones being desaturation and elongation. Fatty acid's length and degree of saturation are integral in defining their physical and chemical properties. For example, the melting temperature of a fatty acid is directly proportional to its chain length and inversely proportional to its degree of saturation. The melting temperature of fatty acids is extremely important in determining membrane fluidity, and thus affecting the physic-chemical properties of cells (14). Long chain and unsaturated fatty acids also serve as precursors to other molecules, such as prostaglandins thromboxanes and leukotrienes which have important biological functions in regulation of inflammatory response (15). Finally, these fatty acids are also involved in the transcriptional regulation (16).

Since palmitate is the major product of fatty acid synthase, it is necessary to be able to generate fatty acids that have longer carbon chains and higher degree of desaturation. In order to achieve this there are two groups of enzymes – elongases and desaturases – that catalyze the fatty acid chain elongation and the introduction of double bonds in fatty acids, respectively.

There are multiple enzymes that catalyze the desaturation of fatty acids. They are classified based on the position within the fatty acid chain at which the desaturation occurs. Not every position in the fatty acid molecule is readily available to be desaturated though, since not all organisms express all the necessary desaturates. Figure 4 shows the species distribution of known desaturase enzymes, as well as the positions at which the double bond is added.

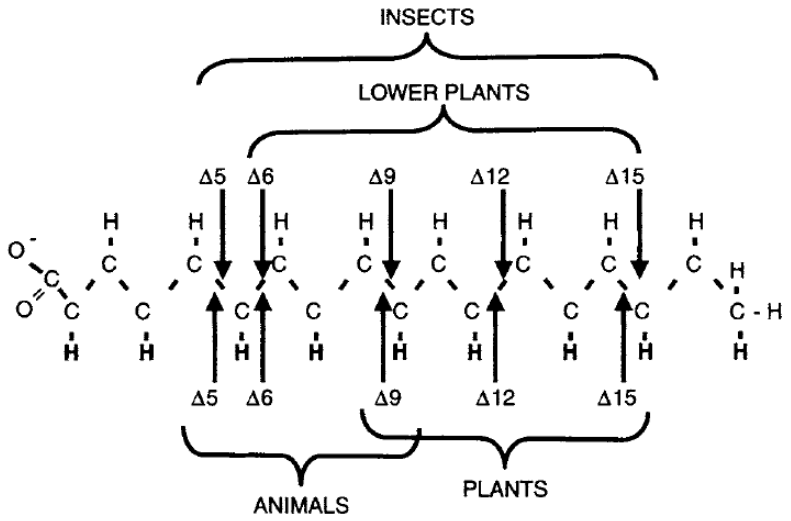

Figure 4: positions at which desaturation occurs in multiple species. Adapted from (17).

Animals possess three types of desaturases: Δ9, Δ5 and Δ6. Δ9 desaturases are referred to as SCDs (Stearoyl-CoA Desaturase) of which mice possess 4 isoforms: SCD -1,-2,-3 and -4, while Δ5 and Δ6 desaturases are designated FADS1 and FADS2, respectively (Fatty Acid Desaturases).

Since animals cannot create double bonds in position Δ12 and Δ15 they rely on plants (or insects) to provide them with linoleic and α-linolenic acid, the two major precursors of ω-6 and ω-3 fatty acids species, respectively. Hence, these fatty acids are essential, since they can only be derived from the diet.

SCD's mechanism is the best understood. In animal tissues, SCD desaturates fatty acids by a three-component enzyme system involving flavoprotein-NADH-dependent cytochrome *b*5 reductase, cytochrome *b*5, and the SCD protein itself, in the presence of molecular oxygen (Figure 5).

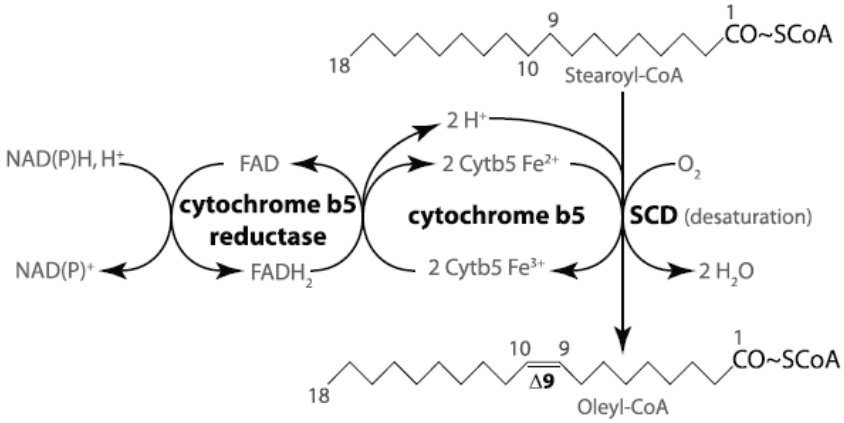

Figure 5: The mechanism of SCD action. Adapted from (18).

The distinct isoforms of SCD are differently expressed in rodent tissues. SCD-1 is mainly expressed in adipose tissue and liver (19), SCD-2 is abundant in the brain (20), SCD-3 is only present in sebaceous glands (21) and SCD-4 is found exclusively in the heart (22). SCD-1, -2 and -4 preferentially catalyze the conversion of stearoyl-CoA (18:0) to oleyl-CoA (18:1), while SCD-3 preferentially catalyzes the conversion of palmitoyl-CoA (16:0) to palmitoleyl-CoA (16:1) (23).

FADS are involved in the metabolic processing of essential fatty acids linoleic (18:2 n-6) and α-linolenic (18:3 n-3) acid, in order to generate PUFAS (Figure 7). (24)

In order to synthesize fatty acid chains longer than 16 carbons, palmitate can undergo chain elongation. This is achieved by a series of enzymes that catalyze the addition of carbon units in a molecular mechanism that is similar to that of FAS to

previously existing fatty acids (whether derived from *de novo* lipogenesis or from diet). There are 4 enzymes associated with elongation of fatty acids (Figure 6). The first step is a condensation catalyzed by ELVOL (Elongation of very long chain fatty acids), followed a reductase catalyzed by KAR (α-ketoacid reductase), a dehydratase catalyzed by HADC (3-hydroxyacyl-CoA dehydratase) and another reductase catalyzed by TER (trans-2,3,-enoyl-CoA reductase).

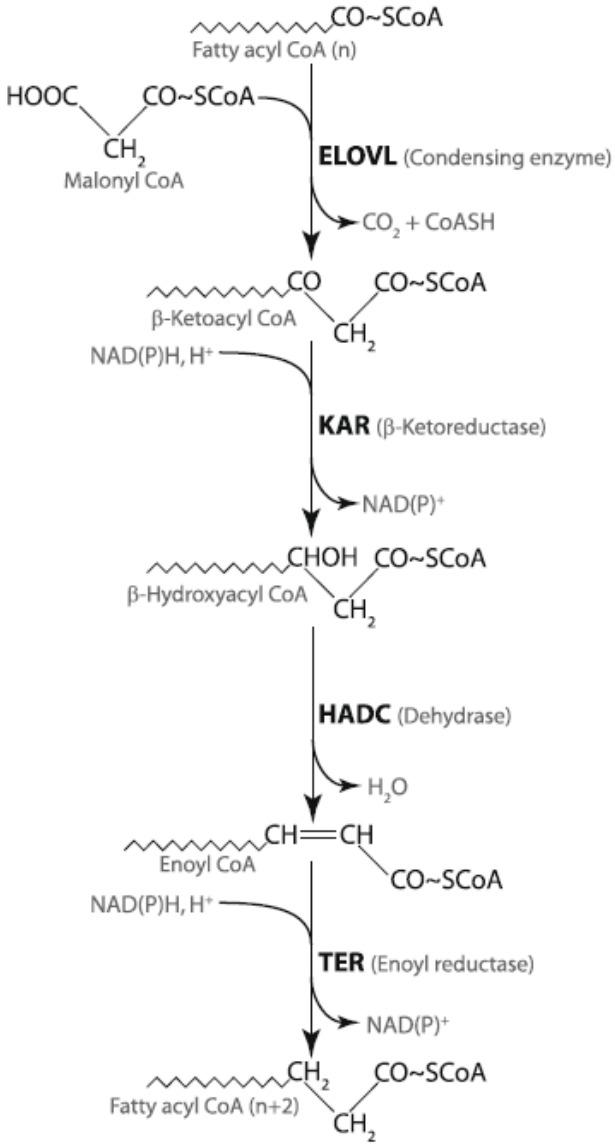

Figure 6: Mechanism of fatty acid elongation. Adapted from (18).

There are 7 isoforms of Elovl (1-7), each with distinct substrate preferences and tissue distribution (18). There are also 4 isoforms of HADC (HADC 1-4) (25) with are expressed in different tissues.

Elovl, Scd and Fads enzymes act in tandem to synthesize a plethora of fatty acid species. Figure 7 shows the reactions catalyzed by these enzymes in the production of long chain polyunsaturated fatty acids from a palmitate precursor (derived from FAS and, to a lesser extent, diet) or from essential fatty acids linoleic acid (18:2 n-6) or α-linolenic acid (18:3 n-3) (Figure 7).

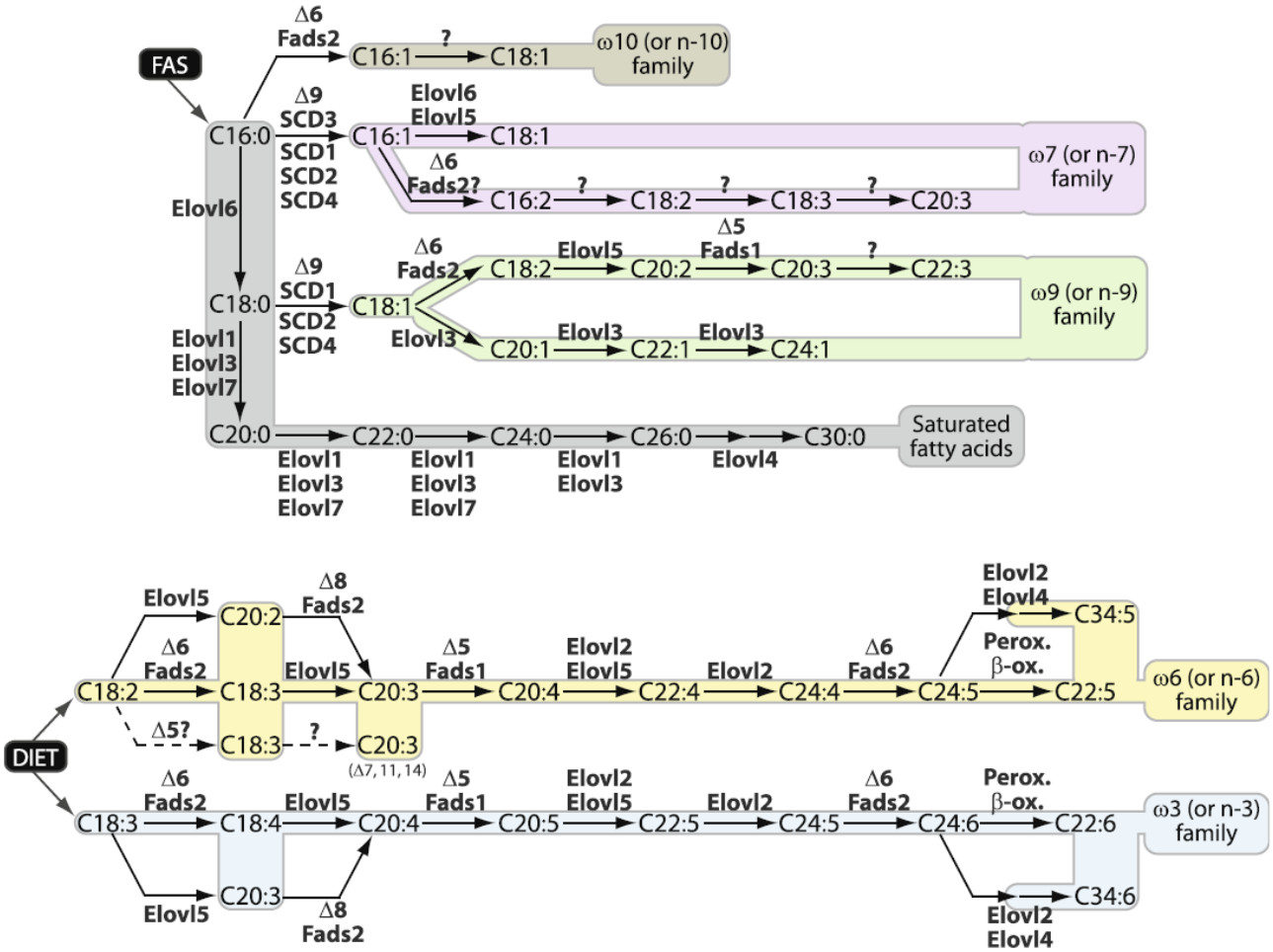

Figure 7: Metabolism of fatty acids, highlighting the desaturation and elongation reactions catalyzed by Elovl and Fads. Figure adapted from (18).

2.3 – Triglyceride-Glycerol synthesis

Free fatty acids might have deleterious effects in the development of insulin resistance and/or diabetes (26). Therefore it is necessary to store fatty acids in a less reactive but still accessible form. Normally this is achieved by esterifying fatty acids. One of the possible metabolites used for esterification is glycerol-3-phophate (Gly3P), forming glycerolipids. Therefore, an accurate determination of the synthesis rate of Gly3P is also important.

There are three pathways through which Gly3P is synthesized: glycolysis, glyceroneogenesis or through the action of glycerol kinase (Figure 8).

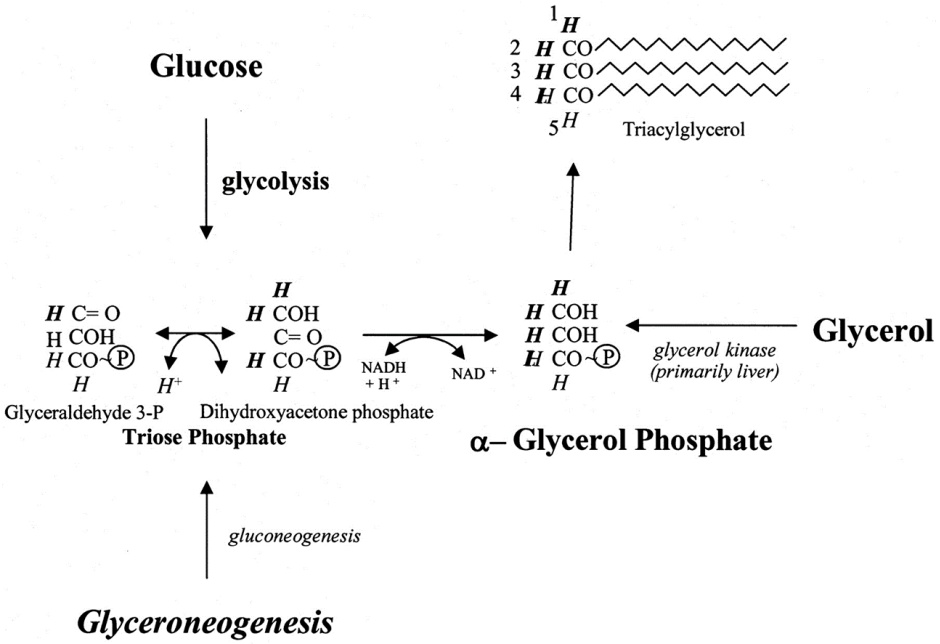

Figure 8: Differential contributions of pathways of glycerol synthesis towards labeling of the glycerol moiety of fatty acids. Italized protons are derived from glyceroneogenesis and bold protons are derived from glycolysis Adapted from (27).

Glycolysis produces triose phosphates - glyceraldehyde-3-phosphate and dihydroxyacetone phosphate – and the latter can be converted to Gly3P via glycerol-3-phosphate dehydrogenase (G3PDH).

Glyceroneogenesis is essentially a truncated from of gluconeogenesis, in which the triose-phosphates made in this process do not continue reacting further up the gluconeogenic pathway, but are converted to Gly3P via G3PDH.

Lastly, free glycerol can be directly phosphorylated by glycerol kinase to Gly3P but the expression of this enzyme is limited to some tissues – mainly the liver – and is absent from the WAT, where Gly3P production plays an important role in lipid homeostasis.

All of these pathways are simultaneously active to different extents and their relative contributions to the pool of Gly3P are dependent on numerous factors, such as pathophysiology.

2.4 – Cholesterol Synthesis

Cholesterol is another important lipid species that plays an important role in whole body homeostasis, serving as a precursor to bile acids and steroid hormones, as well as an integral part of the plasma membrane.

The cholesterol biosynthetic pathway starts with condensation of acetyl-CoA and acetoacetyl-CoA to form 3-hydroxy-3-methyl-glutaryl-CoA (HMG-CoA), followed by its reduction to mevalonate by HMG-CoA reductase, which is the committed step of cholesterol synthesis. The pathway involves numerous other steps, catalyzed by multiple enzymes, which include several phosphorylation, condensation, reduction and dehydration reactions, to ultimately form cholesterol (Figure 9).

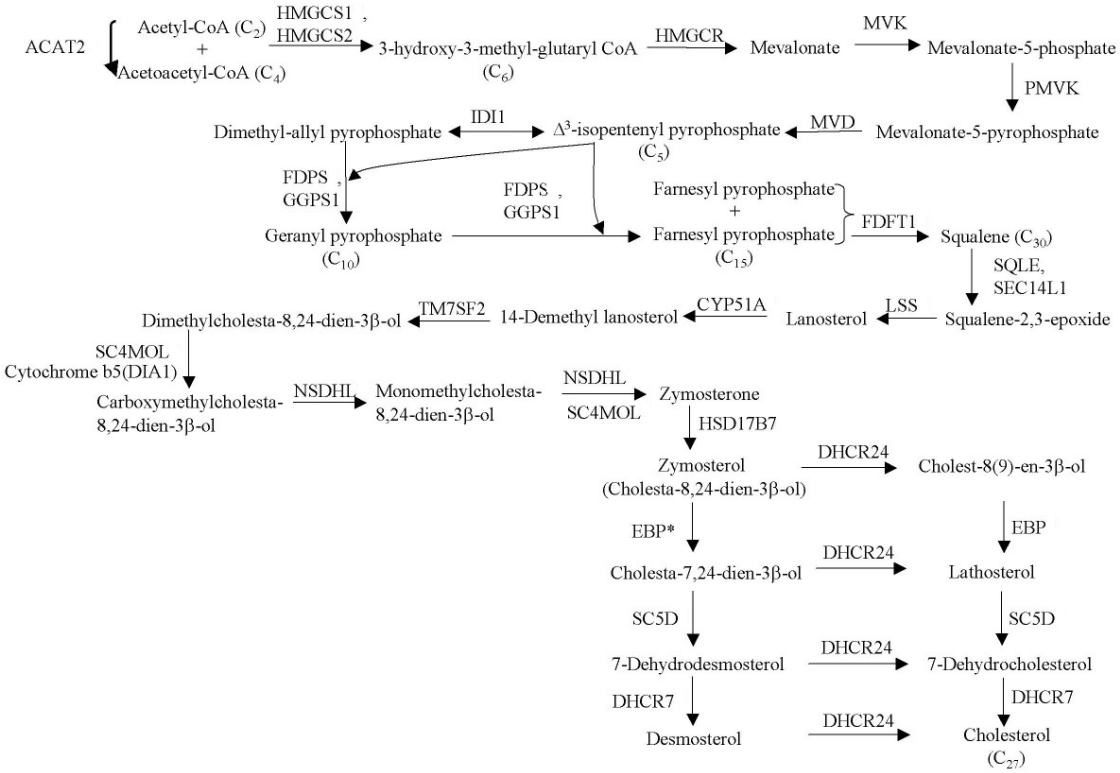

Figure 9: Pathway of Cholesterol biosynthesis, figure adapted from (28).

3 - Review of isotope-based techniques for measuring lipid flux

Due to importance of lipid biosynthetic fluxes to whole body homeostasis, it is import to be able to accurately measure them directly. And, for that purpose, multiple methodologies using isotopes (stable or otherwise) were developed to track lipid synthesis.

Historically, tracer experiments to measure lipid synthesis were first developed using of radioactive tracers, such as ^{14}C labelled acetate, ^{3}H labelled water and ^{14}C and ^{3}H labeled fatty acids. However, due to the negative effects of radioactivity (even though both ^{14}C and ^{3}H undergo β-decay – the least dangerous type of radioactive decay) they are not safe for in vivo studies, and require specific facilities and methodologies, which significantly raise the cost of studies. Nevertheless, the mathematical models and insights created by radioactive tracer research laid the groundwork for stable isotope tracer research.

With stable isotopes, it became possible to perform in vivo experiments while using higher amounts of substrate without any of the negative toxicity effects associated with radioactivity.

There are multiple choices for stable isotope tracers capable of measuring lipid biosynthetic fluxes, these include:

3.1 – Labeled fatty acids:

Some studies use either ^{13}C or ^{2}H labeled fatty acids to measure fatty acid uptake, esterification and/or SCD1 activity. Using fatty acids as a precursor usually limits the number of molecules that will have label incorporated into them as, barring extensive recycling of the fatty acid precursor used, it will only be possible to examine the enrichment of the same fatty acid used (tracer dilution analysis) or fatty acids directly derived from the precursor (for example, fatty acids derived from elongation or desaturation of the precursor).

Tracer dilution analysis of labeled fatty acids is a common methodology to measure the incorporation of exogenous fatty acids into the pools of interest, allowing, for example, the determination of the contribution of dietary fatty acids, adipose tissue derived fatty acids and hepatic lipogenesis to hepatic triglyceride pools in human subjects with NAFLD (29). Another study used a similar technique to determine the uptake of FA into muscle and WAT in human subjects (30).

Similarly, multiple studies have used labeled fatty acids to probe specific pathways, such as the oxidation and desaturation of stearate using either D_5-18:0 or D_7-18:0 in rats (31). Another study analyzed the activity of SCD1 over palmitate in human macrophages

and dendritic cells using D_3-16:0 (32). These techniques can be applied to multiple systems, as exemplified by Mosley *et al.* who used ^{13}C-18:1n-7 (vaccenic acid) to measure the synthesis of conjugated linoleic acid in lactating cows (33).

However, these precursors do not directly provide information about *de novo* lipogenesis and, even though it is possible to determine fluxes through specific pathways (such as desaturation) these are normally constrained to analyzing fatty acids that are direct products of the labelled fatty acid chosen as tracer, therefore narrowing the amount of obtainable data.

Another important fact to consider is that specifically labeled fatty acids are expensive, significantly increasing the costs of studies, especially in when studying large biosystems, such as humans or large animals.

3.2 – Labeled fatty acid precursors

Another possible class of stable isotope tracers used to measure lipid biosynthetic fluxes are fatty acid precursors. Essentially, since the most basic building block for fatty acid synthesis is acetyl-CoA it is possible to use any metabolite that gives rise to labeled acetyl-CoA as tracers, such as, acetate, glucose, glutamine and pyruvate, among others.

Using this type of tracers it is possible to measure the incorporation of label into a plethora of fatty acids, significantly increasing the possible analyzable pathways. An additional layer of information can be added as the simultaneous use of different tracers with distinct labeling patterns can be used to determine the specific contribution of specific pathways to lipid biosynthetic fluxes.

As an example, Collin *et al.* (34) determined the contributions of acetate, glucose, pyruvate and glutamine to lipogenesis in human differentiated adipocytes using 1-^{13}C acetate, U-^{13}C glucose, U-^{13}C pyruvate and U-^{13}C glutamine and found the percent contributions were 16.6, 42.4, 12.3 and 10.4, respectively.

There are some issues with using labeled acetate as a tracer. Namely, in some tissues, like the liver, zonation across can cause a gradient in precursor enrichment, potentially leading to an underestimation of trace/tracer ratios (35). Another factor to bear in mind, is selective uptake of acetate by specific tissues. When given orally, acetate is readily taken up by the liver, and thus, the enrichment of acetate in the peripheral blood is much smaller than that of the portal blood, which become an issue where the goal of the experiment is to study extra-hepatic lipid metabolism (35).

Other tracers that originate acetate or acetyl-CoA, such as glucose or glutamine also have some issues, in the sense that they undergo extensive metabolic cycling, causing an effective dilution of label and the appearance of distinct acetate isotopomers, which must be accounted for in the calculations. Therefore, additional experiments need

to be made in order to determine how much of the label from the tracer actually gets to acetate and how it is distributed. Since these parameters are affected by numerous metabolic pathways it is difficult to rely on tabled values and/or previously published data, as a simple change in one pathway might cause a completely distinct acetate isotopomer pattern.

Finally, as with labeled fatty acids, an experiment using labeled acetate or glucose in large amounts can become prohibitively expensive, especially if there is a need for a long exposure to the tracer (for example, to measure DNL in human adipose tissue).

3.3 – Labeled water

Water is a ubiquitous presence in many metabolic reactions and, therefore, has the potential to trace several metabolic fluxes simultaneously. Deuterium labeled water (D_2O) can easily be administered either in an oral bolus or via i.p. injection, where it rapidly equilibrates with the organism's body water, achieving complete equilibration in about 10 min (36). With an estimate of the body water percentage of the organism it is easy to calculate the necessary amount of D_2O that needs to be administered in order to achieve a certain enrichment. For example, the body water pool has been estimated between 60 and 70% in rodents (27, 36-38). Once the D_2O bolus is administered, it is possible to supplement drinking water so that it is enriched to the bolus' goal. Using this protocol, it is possible to maintain the deuterium enrichment of body water as long as necessary, with the caveat that, presumably due to the production of metabolic unlabeled water by the organisms, there will be a slight dilution of the final body water enrichment (39).

D_2O freely and uniformly distributes itself across any tissue and, therefore, there are no issues with enrichment zonation or selective uptake which, couple to its low cost and ease of continued administration, make it an excellent tracer to determine whole body lipogenesis.

Labelled D_2O will be incorporated into both acetyl-CoA and NADPH but the extent to which this exchange occurs depends on several factors. NADPH can be derived from two sources in mammals: the malic enzyme pathway or the pentose phosphate pathway, the former being in equilibrium with body water, but the latter not (40). It has been estimated that the maximal contribution of pentose phosphate pathway to NADPH synthesis in the mouse adipose tissue is about 60% (41). Acetyl-CoA enrichment also depends on its source (40), but under the assumption that pyruvate is the main source of acetyl-CoA, and that the exchange of the methyl protons of pyruvate with body water is 80-95% complete (42, 43) it's enrichment will approach that of body water.

The major caveat of using D_2O comes from the fact that the majority of stable isotope methods commonly used employ gas- or liquid- chromatography mass spectroscopy (MS) to analyze the incorporation of label. Since MS techniques are unable to determine the positional enrichment within the fatty acid moieties, there are several assumptions that need to be made when analyzing labeling patterns. Since the enrichment ratio of tracer/trace is one of the most important parameters that needs to be to measure metabolic flux, the fact that, for all intents and purposes, when using D_2O to trace lipogenesis, there are multiple sources of label incorporation (Acetyl-CoA, Body water and NADPH), severely impairs the MS-based techniques' ability to determine the "true" precursor enrichment.

In order to circumvent issues that arise from incorrect determination of the true precursor enrichment, a statistical analysis method entitled Mass Isotopomer Distribution Analysis (MIDA) was developed by Hellerstein *et al.* in 1992 (44). Essentially, MIDA considers that, in the synthesis of polymers (fatty acids can be considered a polymer of acetyl-CoA) the enrichment of the final polymer follows a binomial distribution which is a function of the enrichment of the monomers (the *p* value) and the number of monomers that constitute the polymer (the *n* value). Therefore, if both the *p* and the *n* value are known, the synthesis rate of the polymer can be determined based on the polymer's enrichment ratio.

Lee et al. applied MIDA to determine the synthesis rate of palmitate in isolated Hep G2 cells (45) and *in vivo* in several rat tissues (37) and determined the *n* value to be 17 and 20 respectively. Another study by Diraison (46) found this value to be 22 for rat plasma palmitate. Showing that the true precursor enrichment is prone to variability and should be calculated for every new experiment.

Correct determination of the *n* value becomes more complicated for fatty acids that have undergone chain elongation as those fatty acids can be generated from palmitate that was previously labeled or unlabeled palmitate. Each of these two pools will have a distinct *n* value associated with them and, furthermore, the presence of two distinct precursor pools makes it so that the incorporation of deuterium label into long-chain fatty acids can no longer be approximated as a binomial distribution. In order to circumvent this issue, Ajie *et al.* (47) essentially assume that the *n* value for palmitate is 21 and that each subsequent two-carbon unit added to palmitate has an *n* value of 3. This approximation is predicated on both the complete equilibration of body water enrichment with NAPDH and no significant acetyl-CoA enrichment. If these assumptions are made, it is possible to plot the theoretical mass isotopomer distributions that would be obtained in the most extreme cases, i.e. all long chain fatty acids being synthesized *de novo* or all fatty acids being synthesized by chain elongation and then perform linear regression

analysis to fit the isotopomer distributions to the biologically calculated values, therefore determining the percentage contribution of both DNL or elongation. Additionally, fatty acid elongation also occurs, to a lesser extent, in mitochondria (48) and the carbon source for this pathway is acetyl-CoA as opposed to the more prevalent elongation that occurs in the endoplasmic reticulum and uses malonyl-CoA as a source of carbons.

Another important component of lipid metabolism, as highlighted above, is the synthesis of Gly3P. MIDA has also been applied to probe not only the changes in total Gly3P production but also the relative contributions of glyceroneogenesis and glycolysis to its synthesis. Essentially, the math associated with the calculation of total Gly3P synthesis is the same as for the calculation of the synthesis of fatty acids: the *n* value is calculated from the mass isotopomer ratios and is then compared with the number of deuteriums in the Gly3P molecule (36).

Once the *n* value of Gly3P is known it is possible to determine the contribution of glyceroneogenesis and glycolysis to its synthesis. This is only possible in tissues where the contribution of glycerol kinase to the synthesis of Gly3P is negligible, such as the adipose tissue. In order to perform this calculation it is first assumed that the number of incorporated deuteriums in the Gly3P molecule is 3.5 or 5, if the source is glycolysis or glyceroneogenesis, respectively (27, 49). Therefore, the contribution of each of these pathways to the *n* number is given by:

$$n = 5x + 3.5(1 - x) \quad Eq\ (1)$$

Where x is the fraction of Gly3P derived from glyceroneogenesis. Solving Eq. 1 for x we have:

$$x = \frac{n - 3.5}{1.5} \quad Eq(2)$$

Finally, MIDA can also be applied to determine the synthesis of cholesterol, in a fashion similar to that of palmitate, as described in (37, 45-47, 50).

In order to perform MIDA analysis it is necessary to make multiple assumptions about *n* values and, since previous papers show the great variability of the *n* value, assuming any integer value for this variable is somewhat misleading and might lead to an incorrect determination of lipid flux.

In this chapter we will describe and validate a novel methodology for measuring lipid biosynthetic fluxes that overcomes these issues by the use of NMR-based isotopomer detection, since NMR is able to provide some information about not only the deuterium enrichment value, but also the deuterium enrichment position. Namely, since both the terminal methyl group and the α2 protons of fatty acids appear as a discrete peaks in the NMR spectra it is possible, by comparing the deuterium enrichment at both

ends of the molecule, to determine not only de novo lipogenesis but also elongation with less need for assumptions about the number of exchanging protons. This method also allows the determination of glycerol and cholesterol synthesis, as will be described later in this chapter.

Since the positional information at which deuterium incorporation occurs is of extraordinary importance to the analysis of the data, the following section discusses the pathways through which each of the protons in fatty acids, cholesterol and glycerol-3-phosphate might become labeled.

4 - Analysis of the chemical origin of protons and carbons within the fatty acid moieties

In order to develop a novel stable isotope technique to determine fatty acid flux it is imperative to understand the origin of protons and carbons in the moieties to be analyzed. Figure 10 shows the mechanism of FAS. During DNL malonyl-CoA and acetyl-CoA bind to FAS and a condensation reaction occurs. This condensation happens in such a way that the terminal methyl group of fatty acids is derived from acetyl-CoA, with all the other carbons being derived from malonyl-CoA. All the protons in the terminal methyl group are derived from acetyl-CoA, the even numbered carbons have one proton derived from water and one proton derived from malonyl-CoA and the odd numbered carbons have both of their protons derived from NADPH (41, 51).

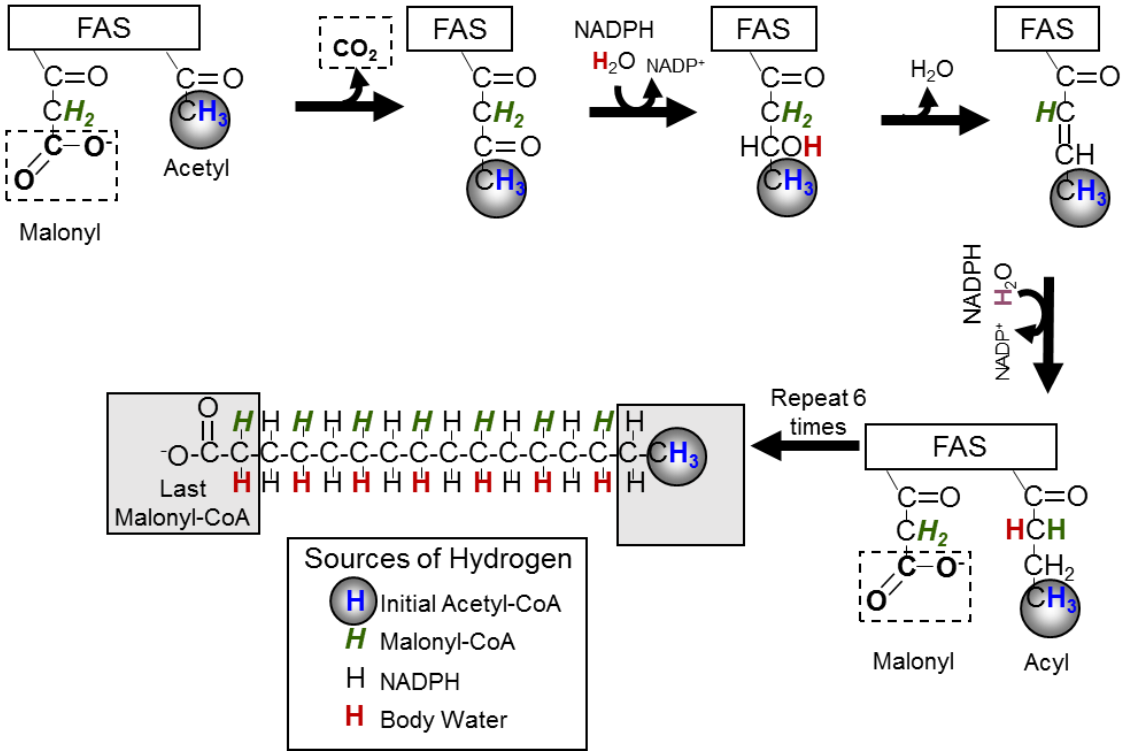

Figure 10: Mechanism of action of fatty acid synthase, highlighting the origin of each proton and carbon in the nascent fatty acid moiety.

During fatty acid desaturation there are no new protons incorporated into fatty acids either as part of the reaction or via any enzymatic intermediate and, therefore, there is no incorporation of label during this reaction.

Fatty acid elongation can occur in either the endoplasmic reticulum or the mitochondria. The former is the most active prevalent and uses malonyl-CoA as a

substrate, while the latter uses acetyl-CoA as a precursor (48). As previously mentioned the mechanism for elongation is exactly the same as that of de novo fatty acid synthesis, with the substrate being added to the carboxyl terminal of the preexisting fatty acid chain. Therefore protons attached to carbons closer to the carboxyl terminal of fatty acids are labeled through both DNL and elongation, while the terminal methyl group of fatty acids can only be labeled via DNL.

It is also important to understand the origin of the protons in the glycerol moiety of fatty acids. Figure 11 indicates the protons that are derived from the three possible pathways of glycerol synthesis, i.e., glyceroneogenesis, which labels all protons, glycolysis, which labels protons 1, 2, 3 and either 4 or 5. If glycerol kinase is the source of Gly3P, there is a rapid equilibrium of this newly formed glycerol with the triose phosphate pool, leading to the appearance of label in protons 1, 2 and 3.

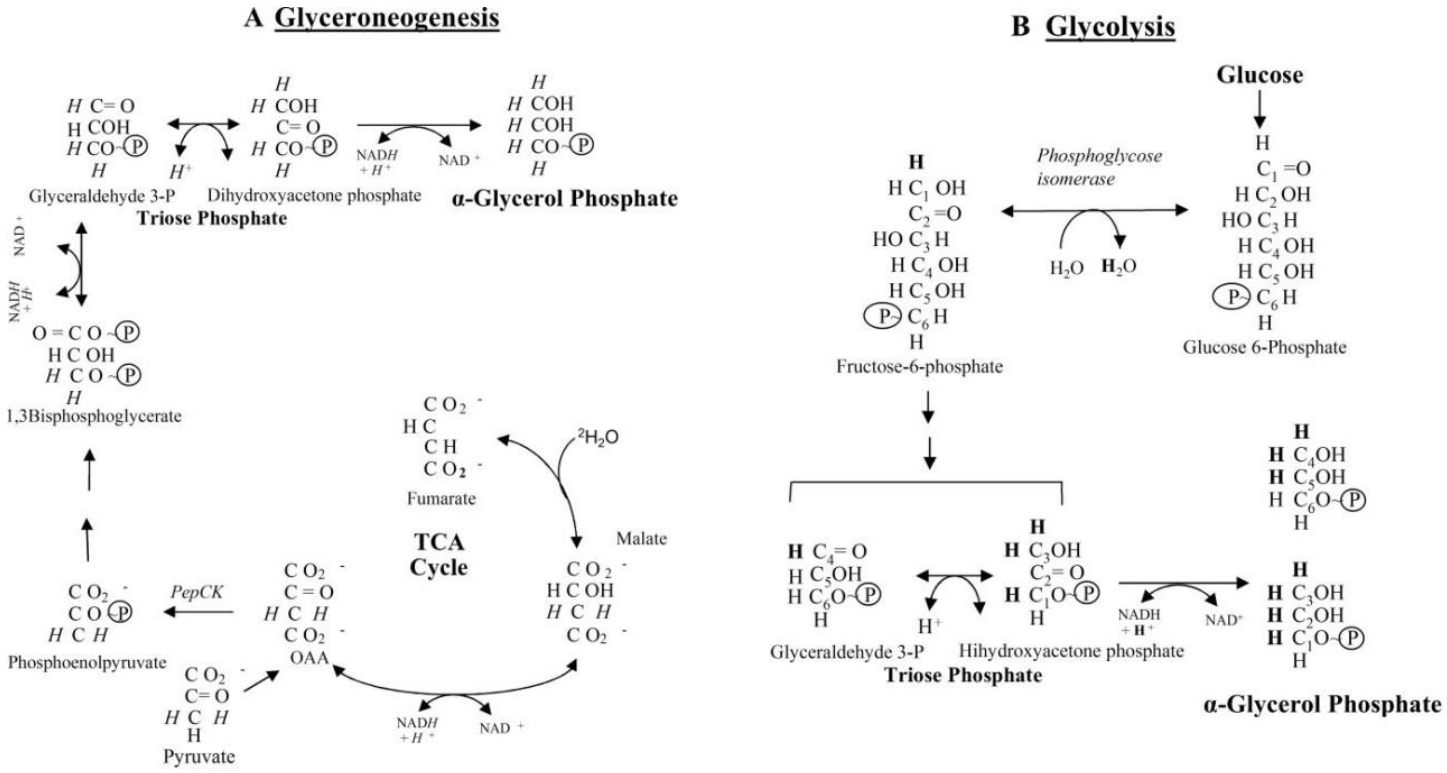

Figure 11: Contributions of glyceroneogenesis and glycolysis to the incorporation of deuterium in the glycerol-3-phosphate molecule. Adapted from (27).

It is also possible to track the incorporation of deuterium into cholesterol during its synthesis. As for fatty acids, there are three possible sources for each proton in the cholesterol molecule: acetyl-CoA, NADPH and water (52). Figure 12 shows the origin of each proton in the cholesterol molecule.

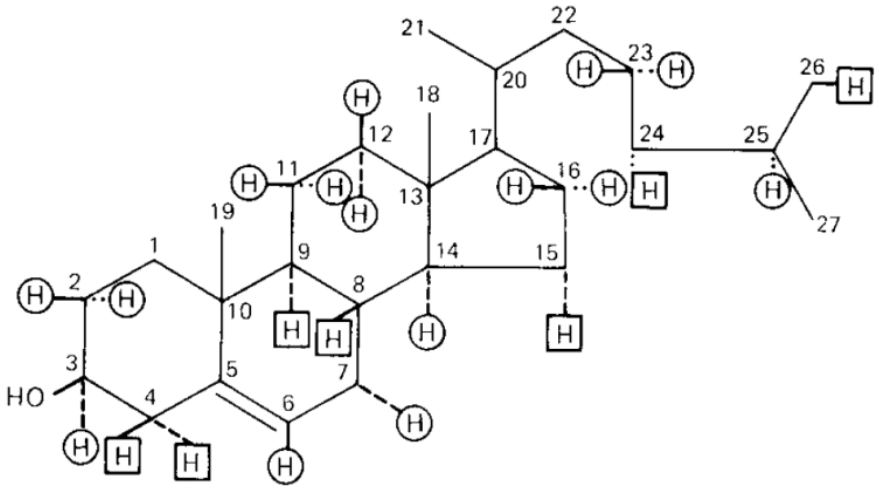

Figure 12: Origin of each individual proton in the cholesterol molecule. Circled protons are derived from NADPH, squared protons are derived from water and the remaining are derived from acetyl-CoA. Adapted from (52).

As previously stated, one of the biggest advantages of NMR techniques is its ability to provide positional enrichment information. For some molecules, different protons/deuteriums are observable in NMR spectra as distinct resonances based on their chemical environment and therefore it is possible to determine the deuterium enrichment in specific position of the molecule. As we detailed in this section there are multiple pathways through which specific protons are incorporated and multiple origins for those particular protons. This information will be used in the next section to develop a NMR method for measuring synthesis fluxes in all the lipid moieties referred to in this section.

5 - Development of a novel nuclear magnetic resonance technique for measurement of lipid flux

Delgado *et al.* published (53) a method that uses deuterated water and NMR spectroscopy in order to determine the percentage of hepatic lipids that were *de novo* synthesized during the labeling period. Here we expand and validate that method, using it to calculate not only *de novo* lipogenic flux but also elongation flux, SCD-1 activity, triglyceride-bound glycerol (TG-gly) synthesis and. This method can also be used to perform a limited lipidomic analysis, allowing the calculation of ω-3 FA, saturated FA, MUFAS and PUFAS well as two specific fatty acids: linoleic acid and docosahexaenoic acid. Finally the expanded method allows the determination of average fatty acid chain length and molecular weight.

The basic premise of this method is the analysis of the deuterium labeling patterns that are generated after mice are injected with D_2O. Post-injection, these mice are returned to their cages and given *ad libitum* access to water which has been enriched with D_2O, in order to maintain the body water enrichment achieved by the injection. Figure 13 shows a typical ^1H and ^2H NMR spectra of a mouse's hepatic purified triglyceride fraction according to the method of Hamilton and Comai (54).

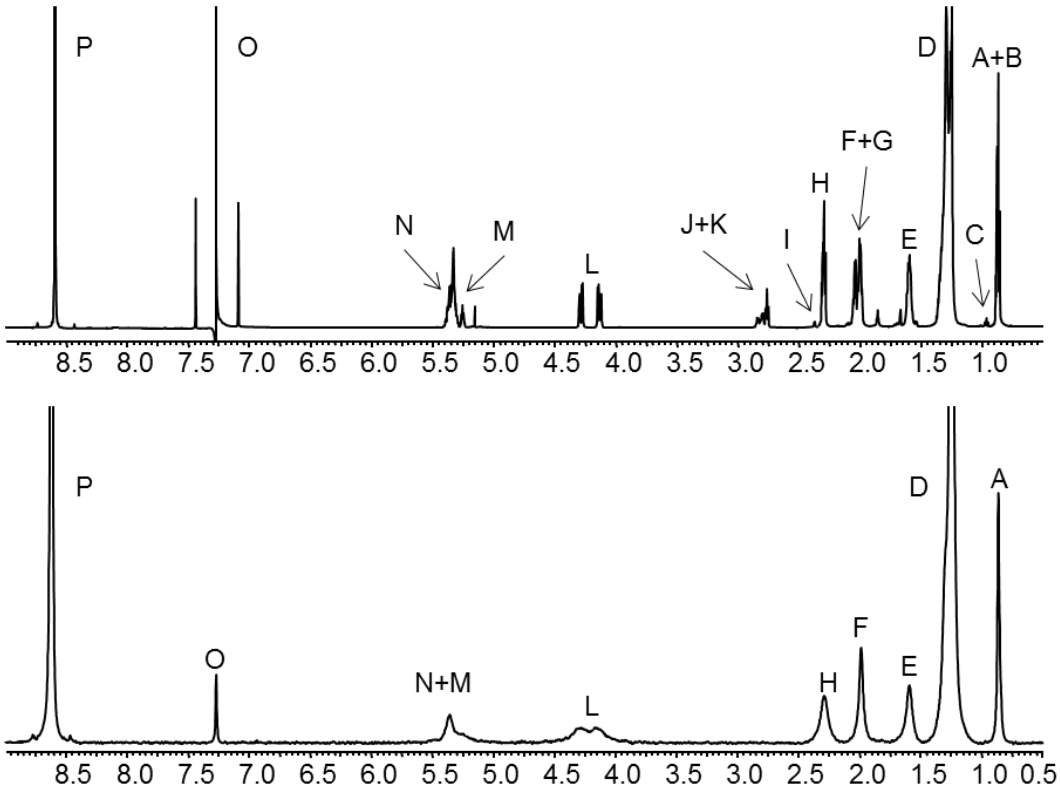

Figure 13: 1H (upper) and 2H (lower) NMR spectra of a purified triglyceride fraction. A: Non ω-3 methyl; B: Partial ω-6 methyl; C: ω-3 methyl; D: Aliphatic chain; E: α3 aliphatic; F: Protons

adjacent to monounsaturated olefinic; G: protons adjacent to polyunsaturated olefinic; H: α2 aliphatic; DHA α2 and α3 ally; J: Linoleic acid bisallylic; K: Other bisallylic; L: sn1,sn3 of esterified glycerol; M: sn2 of esterified glycerol; N: Olefinic; O: Chloroform; P:Pyrazine standard.

As mentioned in the previous section, the incorporation of deuterium into each specific position of the fatty acid moieties is dependent on the activity of lipid synthesis pathways. Therefore is possible to determine, based on deuterium enrichment, the lipid synthesis fluxes.

As mentioned in section 4 of this chapter, acetyl-CoA is the precursor for the synthesis of both fatty acids and cholesterol. Providing the carbon backbone and most of the protons for these molecules and, therefore, knowing its enrichment is extremely important. However, there are some issues with sampling acetyl-CoA, namely its low tissue concentration and its instability. Under the assumption that pyruvate is the main source of acetyl-CoA, and that the exchange of the methyl protons of pyruvate with body water is 80-95% complete (42, 43) the enrichment of body water – which is easier to measure (55) – can be used as a proxy for acetyl-CoA enrichment. Bearing that in mind, the paper by Delgado *et al.* (53) defined the % of newly synthesized fatty acids as:

$$\%\, DNL = 100 \times \frac{\%\ enrichment\ terminal\ methyl}{\%\ body\ water\ enrichment}\ Eq.3$$

Even though the assumptions are sound, the measurement of this flux wasn't, however, validated using a model known to have high lipogenic activity. Furthermore, the incorporation of deuterium label into other positions of the fatty acid moieties can be explored to extract further flux information from the ^{2}H NMR spectra. The following sections of this chapter will expand this method to determine additional lipid biosynthetic fluxes as well as perform a partial lipidomic analysis of the fatty acid moieties. All of these flux measurements will be validated using different animal models.

5.1 – Validation of body water enrichment as surrogate precursor enrichment

As previously mentioned, in order to be able to extract flux information from a tracer experiment it is imperative to be able to determine the tracer to tracee ratio, i.e. the enrichment in the administered substance and the enrichment in the native substance. Since acetyl-CoA – i.e. the direct precursor to fatty acid synthesis – is hard to sample, the use assumption that body water enrichment can be used as a surrogate to the true precursor enrichment needs to be validated.

In order to confirm that acetyl-CoA enrichment is equivalent to body water a chemical biopsy method was used. In this method a xenobiotic that forms an adduct with the metabolite of interest is administered. The adduct is then usually excreted (for example in urine) making subsequent analysis easier. In the particular case of acetyl-CoA we used para-aminobenzoic acid, which is acetylated to N-acetyl-para-aminobenzoic acid (Figure 14C) and excreted in urine.

Six male C57/Bl6 mice were individually housed and received para-amino benzoic acid (PABA) to sample hepatic acetyl-CoA and determine its enrichment. D_2O was administered as described above. Drinking water was enriched to 3% and supplemented with 2.5mg/L of PABA for 3 days to allow the animals to adapt to the compound. One day prior to urine collection the drinking water was replaced with 3% D_2O and 2.5mg/L PABA (2% PABA-d_4). Overnight urine was collected and stored at 4º until further processing. N-Acetyl-PABA was purified and processed and analyzed via ^1H and ^2H NMR as previously described (56). The total ^2H-enrichment of carbon 2 from the acetyl moiety of *N*-acetyl PABA were calculated by comparing the area of N-Ac-PABA CH_3 (2.1 ppm) signal with the mean areas of the pair of aromatic PABA-d_4 (2.0% ^2H) signals at 7-8 ppm, which serve as internal standard. Body water enrichment was calculated using ^2H NMR as previously reported (55). Briefly, 10 µl of plasma was added to 190 µl of acetone and a ^2H NMR spectrum was acquired. Enrichments were calculated by comparing the ratio of the deuterium signal of acetone and water in biological samples with those of of standards with a known enrichment.

Analysis of N-Acetyl-PABA purified from mouse urine was used to determine the acetyl-CoA moiety's enrichment. Typical ^1H and ^2H NMR spectra of the purified N-Acetyl-PABA are shown in figure 15A and Figure 14B, respectively. There was no significant difference in the enrichment of the acetyl moiety of N-Acetyl-PABA when compared to that of body water (Figure 14D).

These results indicate that, under these conditions, the deuteriums in water and acetyl-CoA are completely interchangeable, and, therefore, it is possible to directly use body water enrichment as a surrogate for acetyl-CoA, which greatly facilitates flux calculations.

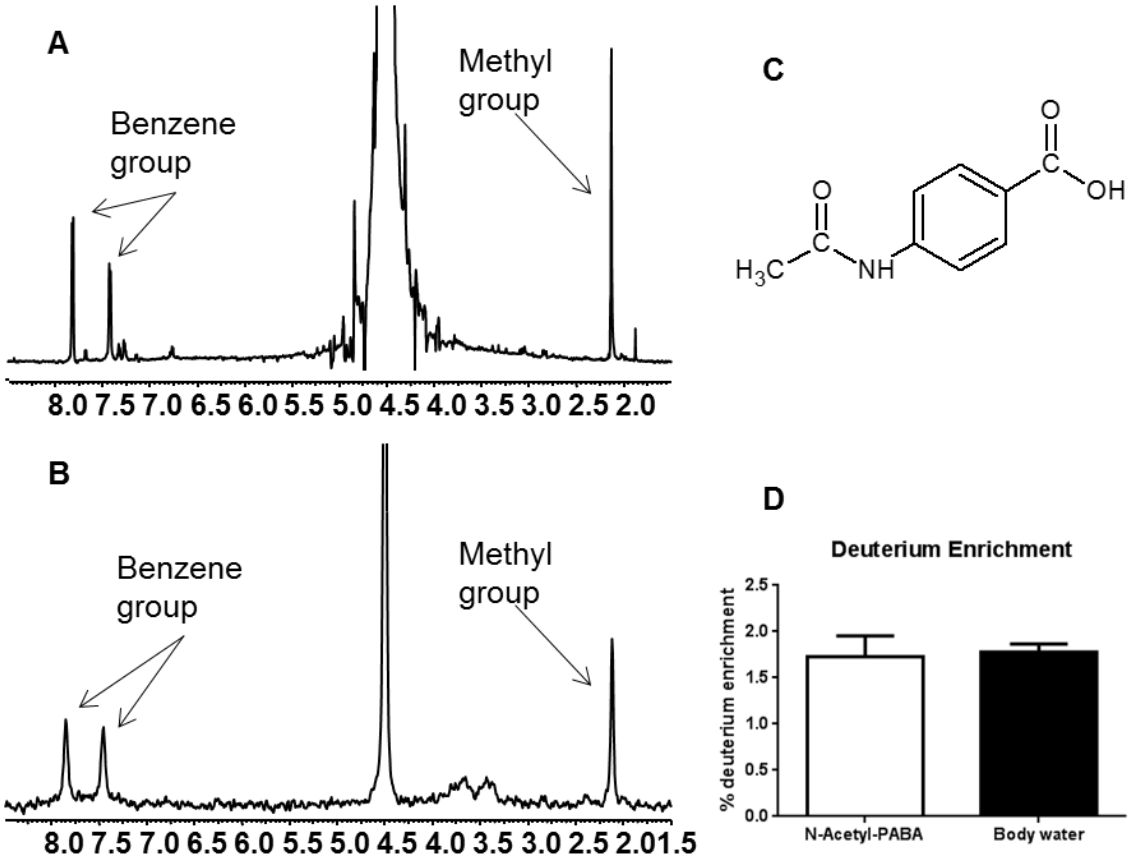

Figure 14: Xenobiotic sampling of liver acetyl-CoA indicates equal ^{2}H enrichment with body water. A) ^{1}H NMR spectra of N-Acetyl-PABA. B) ^{2}H NMR spectra of N-Acetyl-PABA. C) N-Acetyl-PABA molecule. D) Deuterium enrichment in N-Acetyl-PABA and in body water of mice injected with D_2O.

5.2 – General D_2O administration and tissue processing protocol for lipid biosynthesis analysis.

Mice were anesthetized with isoflurane and given a D_2O I.P. injection (27 µl/g) in order to achieve a total body enrichment of approximately 4%. If mice were treated with an agent by oral gavage (see below) they were injected with D_2O within 5 minutes of the last gavage. Mice were then returned to their cages and given *ad libitum* access to food and 4% D_2O drinking water for a period of 1 to 2 days. Mice were then anesthetized with isoflurane gas and blood was collected from the hepatic portal vein. Liver and adipose tissue were removed, immediately freeze clamped in liquid nitrogen and stored at -80ºC until further analysis. Tissues were homogenized and lipids were extracted via Folch extraction (57).

5.3 – General protocol for Nuclear Magnetic Resonance (NMR) analysis

Lipids were reconstituted in chloroform containing a pyrazine standard (4% D_5-pyrazine/ 96% pyrazine, 2 mg/ml). Spectra were obtained at 25°C with a Varian Inova 14.1 T spectrometer equipped with a standard 3 mm broadband probe. Proton NMR spectra were acquired using a 90º pulse, and a sweep width of 6000 Hz digitized into 1300 points, 2s acquisition time and 2s delay (4s repetition). Spectra were collected with 100 acquisitions (~6 minutes) and were processed by zero-filling the free-induction decay to 66000 points and applying 0.3 Hz of exponential multiplication. Proton-decoupled ^{2}H NMR spectra at 92.1 MHz were acquired with a 90° pulse and a sweep width of 920 Hz digitized into 1800 points, resulting in an acquisition time of 2 sec. A pulse delay of 2 sec was used between acquisitions (4 sec repetition time). Spectra were collected for 1 to 24 hours and were processed by zero-filling the free-induction decay to 8000 points and applying 0.5 Hz of exponential multiplication. Peak areas were analyzed using the curve-fitting routine supplied with the ACDLabs 1D NMR processor software. Peak assignment was performed by comparing to previously reported assignments in the literature (58, 59).

5.4 – Lipidomic profiling by ^{1}H nuclear magnetic resonance

Since the proton NMR spectra has different signals for the distinct moieties of fatty acids it is possible to determine the percentage of several fatty acid species within the samples.

5.4.1 – ω-3 fatty acids

It is possible to determine the % of ω-3 fatty acids since the terminal methyl group of the ω-3 fatty acids is slightly downfield of all the other terminal methyl groups (peak B in Figure 13). Therefore, the % of ω-3 fatty acids was determined as:

$$\%\ \text{of}\ \omega-3\ \text{fatty acids}\ = 100 \times \frac{B_{1Ha}}{B_{1Ha} + A_{1Ha}}\ (eq.4)$$

Where B_{1Ha} is the ^{1}H area of ω-3 fatty acids and A_{1Ha} is the ^{1}H area of non-ω-3 fatty acids.

5.4.2 – Poly- and mono-unsaturated fatty acids

The % of mono- and polyunsaturated fatty acids is given by:

$$\%\ PUFA = 100 \times \frac{(F_{1Ha} + H_{1Ha})}{(2 \times G_{1Ha}) + H_{1Ha}}\ (eq.5)$$

Where F_{1Ha} and H_{1Ha} are the ^1H areas of all polyunsaturated fatty acids, G_{1Ha} is the ^1H area of all fatty acid α2 protons and H_{1Ha} is the ^1H area of DHA α2 and α3 protons. Conjugated fatty acids, whose allylic protons appear between 5 and 6.5 ppm were not detected in these experiments. However, if conjugated fatty acids are present in the sample to a high extent, these extra resonances must be accounted in order to accurately determine total %PUFAS.

The percentage of MUFAS is given by:

$$\%\ MUFA = 100 \times \frac{E_{1Ha}}{(2 \times G_{1Ha}) + H_{1Ha}}\ (eq.6)$$

Where E_{1Ha} is the ^1H area of all monounsaturated fatty acids, G_{1Ha} is the ^1H area of all fatty acid α2 protons and H_{1Ha} is the ^1H area of DHA α2 and α3 protons. The % of unsaturated fatty acids is therefore:

$$\%\ unsaturated\ fatty\ acids = \%\ PUFAS + \%\ MUFAS (eq.7)$$

And the amount of saturated fatty acids is then:

$$\%\ saturated\ fatty\ acids = 100 -\ \%\ unsaturated\ fatty\ acids\ (eq.8)$$

5.4.3 – Calculation of average chain length and molecular weight

In order to calculate average fatty acid chain length, all fatty acids were considered polymers of a methylenic (CH_2) and/or an olefinic (HC=CH) subunit, i.e.: $^-OOC\text{-}(CH_2)_x\text{-}(HC{=}CH)_y\text{-}CH_3$. Therefore, the average number of protons (ANP) is given by:

$$ANP = x \times 2 + y \times 2 + 3 \ (eq. 9)$$

And the total number of carbons (ANC) is given by:

$$ANC = x + y \times 2 + 2 \ (eq. 10)$$

Since all olefinic protons are represented in peak N (Figure 13), the number of olefinic protons (y) is:

$$y = \frac{N_{1Ha}}{\frac{G_{1Ha}}{4} + \frac{H_{1Ha}}{8}} \ (eq. 11)$$

Where N_{1Ha} is the ^1H area of all olefinic protons. Additionally:

$$ANP = \frac{\sum_A^K (x_{1Ha})}{\frac{G_{1Ha}}{2} + \frac{H_{1Ha}}{4}} \ (eq. 12)$$

Where $\sum_A^K (x_{1Ha})$ is the sum of all corrected areas of peaks arising from the fatty acyl moieties, G_{1Ha} is the ^1H area of all fatty acid α2 protons and H_{1Ha} is the ^1H area of DHA α2 and α3 protons.

Using eq. 11 and eq. 12, eq. 9 for solves for x:

$$x = \frac{\sum_A^K (x_{1Ha})}{\frac{G_{1Ha}}{4} + \frac{H_{1Ha}}{8}} - \frac{N_{1Ha}}{\frac{G_{1Ha}}{4} + \frac{H_{1Ha}}{8}} - \frac{3}{2} \ (eq. 13)$$

Where $\sum_A^K (x_{1Ha})$ is the sum of all corrected areas of peaks arising from the fatty acyl moieties, N_{1Ha} is the ^1H area of all olefinic protons, G_{1Ha} is the ^1H area of all fatty acid α2 protons and H_{1Ha} is the ^1H area of DHA α2 and α3 protons. The x and y factors calculated in eq. 8 and 10 can then be applied in eq. 7 to yield the ANC.

These two calculations allow the determination of the average molecular weight (AMW) of the fatty acyl moieties:

$$AMW = ANP \times 1{,}00794 + ANC \times 12{,}0107 + 2 \times 15{,}9994 \; (eq.14)$$

5.4.4 – Linoleic and docosahexaenoic acid

Linoleic acid (18:2 n-6) and DHA (22:6 n-3) have resolved ^{1}H resonances. DHA α2 and α3 protons overlap and appear slightly upfield of the other α2 protons (peak H in Figure 13). Therefore, the % of DHA is given by:

$$\%\, DHA = \frac{\frac{H_{1Ha}}{2}}{G_{1Ha} + \frac{H_{1Ha}}{2}} \; (eq.15)$$

Where G_{1Ha} is the ^{1}H area of all fatty acid α2 protons and H_{1Ha} is the ^{1}H area of DHA α2 and α3 protons.

The bisallylic peaks arising from linoleic acid appear as a clearly defined triplet at around 2.76 ppm (peak J in Figure 13). Hence, the % of linoleic acid is given by:

$$\%\, linoleic\ acid = \frac{K_{1Ha}}{G_{1Ha} + \frac{H_{1Ha}}{2}} \; (eq.16)$$

Where K_{1Ha} is the ^{1}H area of oleic acids bisallylic protons, G_{1Ha} is the ^{1}H area of all fatty acid α2 protons and H_{1Ha} is the ^{1}H area of DHA α2 and α3 protons.

5.4.5 – Mass of lipid species

In order to convert the percentages referred to above into masses, an aliquot of tissue extract was assayed using a commercially available triglyceride detection kit (Sigma, St. Louis Mo). A calibration curve was prepared from various concentrations of triolein. Since the kit detects the TG-glycerol in solution, it is possible to convert the amount of each triolein sample used into its TG-glycerol equivalent, on the basis that the mass ratio of triolein:glycerol is 885.432:92.09. After calculating the amount of TG-glycerol in each sample, the amount of fatty acids (FA) per TG-glycerol is given by:

$$\text{FA/TG glycerol } = \frac{H_{1Ha} + 2 \times G_{1Ha}}{L_{1Ha}} \ (eq. 17)$$

Where L_{1Ha} is the ^{1}H area of triglyceride-glycerol C1 and C3 protons, G_{1Ha} is the ^{1}H area of all fatty acid α2 protons and H_{1Ha} is the ^{1}H area of DHA α2 and α3 protons. If a sample contains only triglycerides the theoretical value for FA/TG glycerol is 3. If there are free fatty acids present the value may be higher, and if diacyl- or monoacyl- glycerols are present the value may be lower.

The mass (in grams) of TG-FA present in the tissue was calculated by:

$$\text{FA (g)} = \text{FA/TG glyerol} \times \text{AMW} \times \frac{\text{TG glycerol amount (g)}}{92{,}09} \ (eq. 18)$$

The percentages of species calculated above may then be converted into their respective masses by multiplying the total fatty acid amounts. For example:

$$total\ linoleic\ acid\ (g) = FA(g) \times \%\ linoleic\ acid\ (eq. 19)$$

5.5 – Calculation of lipid biosynthetic fluxes.

5.5.1 –Determination of lipid methyl 2H enrichment:

Peak A represents the methyl hydrogens of non-ω-3 fatty acids. This signal is corrected for linoleic acid contribution, an essential fatty acid in mammals (60) which does not get labeled with deuterium and would otherwise lead to an underestimation of lipogenic flux. Since the % of linoleic acid present in the samples is calculated via eq. 1 the corrected methyl enrichment (A_{eC}) is given by:

$$A_{eC} = 100 \times \frac{A_{2Ha} \times \%\ 2HS \times P_{1Ha}}{(A_{2Ha} \times \%2HS \times P_{1Ha}) + \left(A_{1Ha} \times \left[1 - \times \frac{\%\ linoleic\ acid}{100}\right] \times \%1HS \times P_{2Ha}\right)} \ (eq. 20)$$

Where A_{1Ha} is the ^{1}H area of non ω-3 fatty acids terminal methyl, A_{2Ha} is the ^{2}H area of non ω-3 fatty acids terminal methyl, %2HS is the percentage of deuterium labeled standard (pyrazine), %1HS is the percentage of deuterium unlabeled standard

(pyrazine), P_{1Ha} is the ^{1}H area of the pyrazine standard and P_{2Ha} is the ^{2}H area of the pyrazine standard.

5.5.2 – De novo lipogenesis (DNL)

Fractional DNL is calculated as:

$$\%\ DNL = 100 \times \frac{A_{eC}}{\%\ body\ water\ enrichment}\ (eq.21)$$

Where A_{eC} is the corrected methyl enrichment calculated above.

The total mass of nonessential fatty acids is determined as:

$$Nonessential\ FA\ (g/g\ of\ tissue\ ) = All\ fatty\ acids\ (g/g\ of\ tissue\ ) - \omega 3\ fatty\ acids\ (g/g\ of\ tissue\ ) - linoleic\ acid\ (g/g\ of\ tissue\ )\ (eq.22)$$

The mass of lipids originating from DNL in 1 day of D_2O exposure is given by:

$$mass\ DNL\ (g/day/g\ of\ tissue) = \frac{\%DNL}{100} \times\ Nonessential\ fatty\ acids\ (g)\ (eq.23)$$

5.5.3 – Fatty acid elongation:

The α2 protons are enriched during either DNL or chain elongation. The first pathway involves the complete synthesis of a new fatty acid chain starting from acetyl-CoA while the second adds acetyl-CoA to preexisting fatty acid chains. Medium chain fatty acids pre-existing the treatment with D_2O will be unlabeled, but if these fatty acids are elongated during tracer exposure, the subsequently added methylene hydrogens will be labeled. Comparison of deuterium area at the terminal methyl end of the fatty acyl moieties with that of the α2 protons reports the percentage contribution of elongation to total lipid synthesis:

$$\%\ contribution\ of\ elongation\ to\ lipid\ synthesis = 100 \times \left(1 - \frac{A_{2H} \times 2}{H_{2H} \times 3}\right)\ (eq.24)$$

Where A_{2H} is the deuterium area of the terminal methyl group of fatty acids and H_{2H} is the deuterium area of the α2 protons of fatty acids.

After the % contribution of elongation to lipid synthesis is determined, the total percentage of elongation can be calculated via the equation:

$$\%\ total\ elongation = \frac{\%\ contribution\ of\ elongation\ to\ lipid\ synthesis\ \times \%\ DNL}{100 - \%\ contribution\ of\ elongation\ to\ lipid\ synthesis} (eq.25)$$

5.5.4 – Fatty acid desaturation:

Desaturase activity was determined in a similar fashion as lipogenic flux:

$$\%\ Desat.activity = 100 \times \frac{F_e}{\%\ body\ water\ enrichment}\ (eq.26)$$

Where F_e is the deuterium enrichment of the monounsaturated fatty acids' allylic protons.

The total mass of newly desaturated lipid which accumulated in during D_2O exposure is given by:

$$Desat\ mass\ (g/day/g\ of\ tissue) = \frac{\%SCD1\ activity}{100} \times Unsaturated\ fatty\ acids\ (g)\ (eq.27)$$

5.5.5. – Triglyceride bound glycerol synthesis:

The percentage of newly synthesized glycerol in triglyceride is given by:

$$\%\ glycerol\ synthesis\ = 100 \times \frac{L_e}{\%\ body\ water\ enrichment}\ (eq.28)$$

Where L_e is the deuterium enrichment of glycerol's C1 and C3 protons

The mass of newly synthesized glycerol in triglyceride formed during D_2O exposure is given by:

$$Mass\ of\ new\ glycerol\ (g/day/g\ of\ tissue) = \frac{\%\ glycerol\ synthesis}{100} \times TG - Glycerol\ (eq.29)$$

5.5.6 – Cholesterol Synthesis.

It is also possible to simultaneously determine the synthesis flux of cholesterol, as the protons of the methyl group attached to carbon 18 of the cholesterol molecule are sufficiently separated from the methyl groups of fatty acids to allow the accurate measurement of its peak area. Figure 15 shows a typical ^{1}H and ^{2}H NMR spectra of cholesterol. For this particular sample, cholesterol was purified using the method by Hamilton and Comai (54) before NMR analysis.

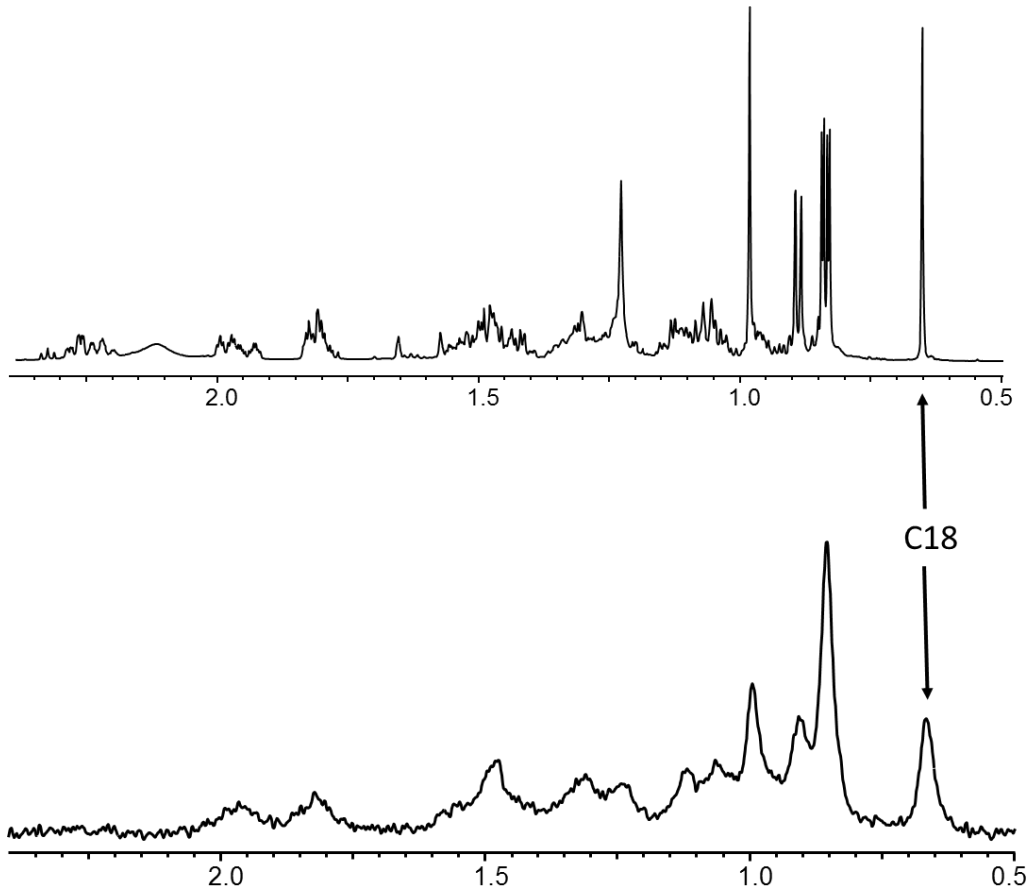

Figure 15: partial proton and deuterium NMR spectra of cholesterol, highlighting the position of the protons attached to carbon 18 of the molecule.

As previously mentioned the protons from the C18 methyl group of cholesterol are directly derived from acetyl-CoA (Figure 12) and, therefore, the same assumptions that were made for using the methyl group of fatty acids for the measurement can be used.

Therefore, assuming a complete equilibrium of acetyl-CoA enrichment with that of body water, the % cholesterol synthesis is calculated as:

$$\%\ Cholesterol\ Synthesis\ = 100 \times \frac{\%\ C18\ deuterium\ enrichment}{Body\ water\ enrichment}\ eq.(30)$$

And the total mass of newly made cholesterol is calculated as:

$$Mass\ of\ new\ cholesterol = total\ cholesterol\ \times \frac{\%\ Cholesterol\ Synthesis}{100}\ eq.(31)$$

5.6– Validation of measurement of de novo lipogenesis, cholesterol synthesis and triglyceride-glycerol synthesis using SREBP1a –TG mice

In order to validate the method's ability to measure DNL flux, this was measured in mice overexpressing a truncated and constitutively active form of SREBP-1a. As previously reported, these mice are incapable of downregulating lipogenic genes and therefore have elevated lipid synthesis (61). A robust increase in deuterium incorporation of all fatty acyl moieties was detected in the liver of SREBP-1a transgenic mice compared to controls (Figure 16).

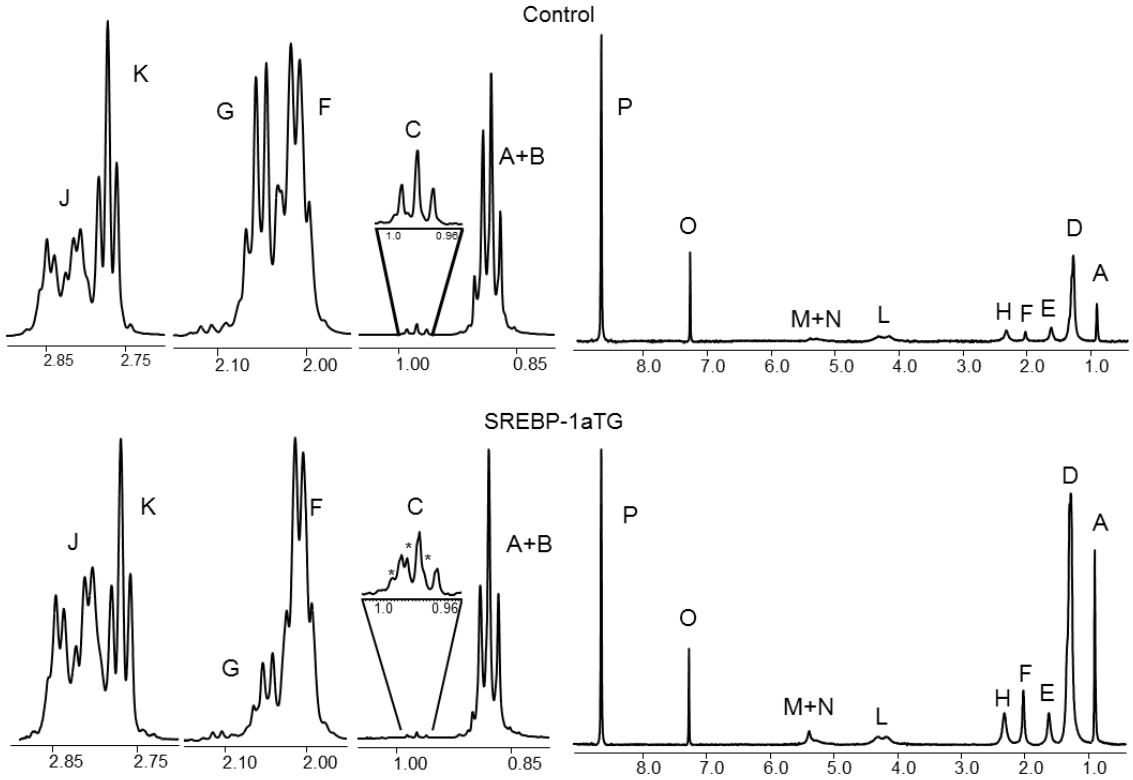

Figure 16: Comparison of key ^{1}H NMR peaks (left) and ^{2}H NMR spectra (right) of the triglyceride moieties of control and SREBP-1a transgenic animals. The peaks marked as * are natural abundance ^{13}C satellites of peak A.

This increased deuterium incorporation in SREBP-1a transgenic mice translated into a 2-fold increase in the % de novo lipogenesis and a 21-fold increase in the amount of newly synthesized lipids present in the liver (Table 1). Thus, NMR detection of ^{2}H incorporation in lipids detected fold changes in lipogenesis that were similar to values obtained by ^{3}H incorporation in these same mice (61). In conjunction with increased fatty acid synthesis, the amount of newly synthesized triglyceride-bound glycerol was also increased in SREBP-1a mice.

Table 1**:** Percent and mass of newly synthesis in SREBP1-a transgenic animals and respective controls.

	% Fluxes			mg new lipids		
	control	SREBP1-a transgenic	p value	control	SREBP1-a transgenic	p value
% De novo lipogenesis	14±1	32±1	<0.001	1.3±0.1	28±17	<0.001
Fraction of elongated lipid	0.25±0.04	0±0.02	<0.001	NA	NA	
% Total lipid elongation	4.6±0.7	0.7±0.7	<0.05	NA	NA	
% desaturation	3±1	14.1±0.5	<0.001	0.17±0.03	8.0±0.3	<0.001
% glycerol synthesis	31±3	27±2	NS	0.50±0.08	2.8±0.2	<0.001
SCD/DNL ratio				13±3	31.2±0.3	<0.001

Data are represented as the mean ± SE (n=5).

As expected SREBP-1a TG mice had significantly higher hepatic triglyceride content compared to controls, but they also had a substantially different lipid species profile (Figure 16). Transgenic mice had increased percent and total amount of unsaturated fatty acids, due largely to increased MUFA concentration (Table 2). In contrast, these mice had a decreased percentage of essential (linoleic acid), and conditionally essential fatty acids (ω-3 fatty acids and DHA) in triglycerides. This decrease probably occurs due to dilution by the larger pool of endogenously synthesized fatty acids.

Table 2**:** Percent and total amount of hepatic fatty acids types in SREBP1-a transgenic animals and respective controls.

	% fatty acids			Total fatty acids		
	control	SREBP1-a transgenic	p value	control	SREBP1-a transgenic	p value
ω-3 fatty acids	2.2±0.2	0.9±0.1	<0.001	0.3±0.1	0.8±0.1	<0.01
Other ω	71±1	79±1	<0.001	10±1	71±1	<0.001
Saturated	27±1	20±1	<0.001	4±1	18±1	<0.001
Monounsaturated	39±2	63±1	<0.001	5±1	57±2	<0.001
Polyunsaturated	34±1	17.3±0.4	<0.001	5±1	16±1	<0.001
Linoleic acid	26±1	9.9±0.2	<0.001	4±1	8.9±0.5	<0.001
Docohexaenoic acid	1.4±0.2	0.8±0.1	<0.05	0.20±0.04	0.70±0.07	<0.001
Average number of carbons per fatty acid	17.2±0.4	17.2±0.1	NS			
Average molecular weight of fatty acids	270±5	270±2	NS			

Data are represented as the mean ± SE (n=x5).

5.7 – Validation of SCD-1 activity measurement using an SCD-1 inhibitor

In addition to increased amounts of unsaturated lipids, SREBP-1a transgenic mice had increased deuterium incorporation at monounsaturated olefinic hydrogens. This finding indicates a ~3-fold increase in the percent of hepatic lipids undergoing desaturation and a ~40-fold increase in the mass of desaturated lipids formed during D_2O exposure (Table 1). These findings are consistent with a massive increase in the expression of sterol-CoA desaturase 1 (SCD-1) expression in the livers of these mice (61). To more explicitly confirm the method's ability to measure desaturation flux, we gavaged mice with the SCD-1 inhibitor A939572 (62, 63) in DMSO (5 mg/µl) at a dose of 10 mg/kg or with DMSO alone.

Although there was no substantial change in the concentration of unsaturated lipids over the course of the experiment, deuterium enrichment in olefinic protons was completely suppressed after treatment with the inhibitor (Figure 17), indicating a near absence of SCD-1 activity and desaturation flux.

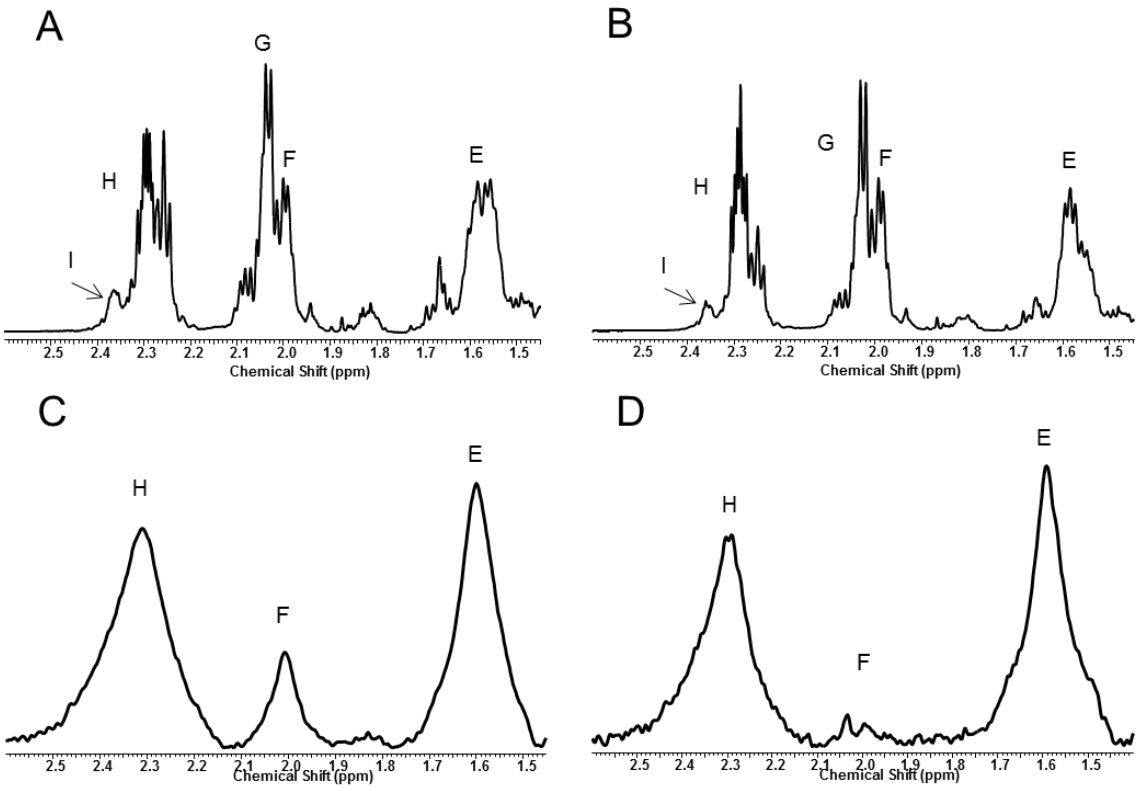

Figure 17: A) ^{1}H NMR of hepatic lipids from an animal gavaged with DMSO vehicle or B) DMSO plus SCD-1 inhibitor C) ^{2}H NMR of hepatic lipids from an animal gavaged with DMSO vehicle or D) DMSO plus SCD-1 inhibitor. Animals treated with inhibitor show no deuterium incorporation above natural abundance in their fatty acid olefinic protons (peak F), even though there is no change in the concentration of unsaturated lipid by ^{1}H NMR.

5.8 – Validation of measurement of fatty acid elongation using coconut oil

SREBP-1a livers had a near 2-fold increase in the percent of lipids that were elongated during D_2O exposure, consistent with the role of SREBP in the positive regulation of elongases (64). To examine whether the NMR method is able to discern more subtle activation of elongation flux, we treated mice with coconut oil, which reportedly contains a high amount of medium chain fatty acids. The composition of coconut oil was confirmed by MS/MS. Coconut oil was diluted 1:2000 in DCM:MeOH:IPA (1:1:1) with 10mM ammonium acetate. 300 µl of solution was injected on the AbSciex 5600 TripleTOF and data was collected for 5.5 minutes. TOF data was collected for 1.5min and MS/MS of all data was collected for 4 minutes. The elution solvent was DCM:MeOH:IPA (1:1:1). The MS/MS of all scan rate was 0.16 sec for the range of 200 amu to 1200 amu. The source temperature was set at 350 with a collision energy of 80. MS/MS of all data was analyzed using Multiquant (Ab Sciex).

MS-based analysis proves that the coconut oil contained a 59-fold medium chain to long chain free fatty acid ratio and a 1.5 fold medium chain to long chain triglyceride-fatty acid ratio (Figure 18A, Figure 18B). Despite a large dose of medium chain fatty acids, treated mice did not have a lower average chain length (rather it was very modestly increased from 18.01±0.04 to 18.40±0.11 carbons), which must have been facilitated by elongation of some of the exogenous medium chain fatty acids (Figure 18C). Comparison of deuterium incorporation at the terminal methyl of the fatty acyl moieties with that of the α2 protons confirmed that the % contribution of elongation to lipid synthesis was significantly increased in mice gavaged with oil (Figure 18D). These data indicate that the NMR approach was able to detect chain elongation.

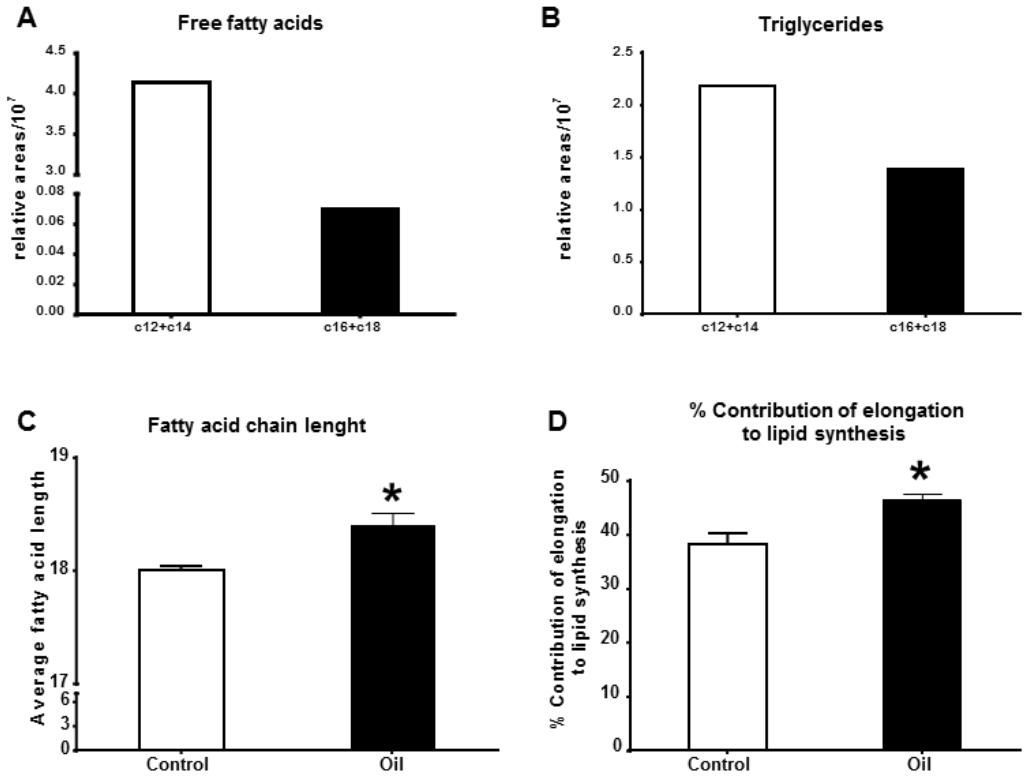

Figure 18: Short and medium chain length composition of hepatic (A) free fatty acids, (B) triglycerides, (C) chain length and (D) elongation in mice gavaged with vehicle or coconut oil.

5.9 – Validation of measurement of cholesterol synthesis.

SREBP-1a transgenic animals have markedly increased cholesterol synthesis and, therefore were also used to validate the NMR method's ability to accurately measure differences in the determination of cholesterol biosynthetic flux. Figure 19 shows that, even though there was no detectable change in the % new cholesterol synthesis in

control vs. SREBP-1a mice Figure 19A, there was a significant increase in the total amount of newly synthesized cholesterol Figure 19B, validating the NMR methods capacity to measure changes in cholesterol flux.

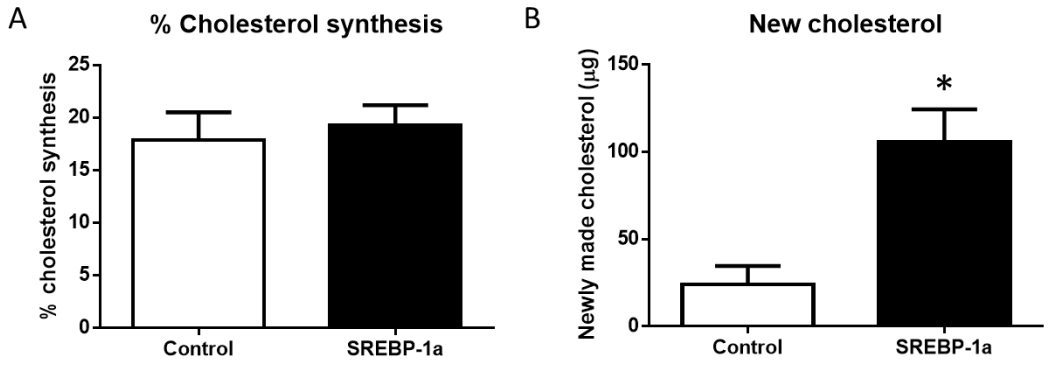

Figure 19: A) percentage of newly synthesized cholesterol and B) total mass of newly synthesized cholesterol in control vs. SREBP-1a transgenic mice.

6 – Discussion

It is the fact that both the source and position of the protons added in fatty acids are known that facilitates the determination of flux from positional enrichments of hydrogen isotopes (39). These different functional groups can be observed by ^{1}H NMR allowing an abbreviated lipodomic profile to be obtained. When deuterated water is administered, deuterium enrichment occurs proportionally to the synthesis rate, which ^{2}H NMR detects as stoichiometric peak intensities in the various functional groups of the lipid molecule. In other words, deuterium enrichment in the α2 position represents all lipid synthesis (including elongation), the methyl position represents only de novo lipogenesis and allylic positions represent new lipids that were also desaturated. The positional enrichment information provided by ^{2}H NMR eliminates the need to know the exact number of exchanging hydrogens in the entire fatty acid, and allows the straightforward determination of relative rates of desaturation, elongation and *de novo* lipogenesis. Although we focus this study on triglycerides of the liver and WAT, the methodology is equally applicable to any lipid species (e.g. cholesterol, bile acids, phospholipids) or any tissue which provides enough sample for analysis.

There are no gold standards for flux measurements. Therefore we tested the validity of the approach against model systems with known or predictable perturbations of *de novo* lipogenesis, desaturation and elongation. Mice expressing a constitutively active form of SREBP-1a were chosen because they have elevated lipid synthesis across all of these pathways. The massive increases of flux through these pathways in SREBP-1a TG mice were easily detected and consistent with rates reported earlier using $^{3}H_2O$ methods (61). The SCD-1 inhibitor has not been used extensively *in vivo*, but based on its in vitro efficacy (63), we predicted that it would suppress desaturation activity. Remarkably, this inhibitor rendered desaturase activity undetectable. Effects of in vivo SCD-1 inhibition are not known, but this result is consistent with the reduced adiposity, decreased lipogenesis and protection from hepatic steatosis in SCD-1 knockout mice (65, 66). Testing elongation was more difficult since inhibitors are not readily available or widely characterized. Genetic interventions, were excluded because manipulation of genes of elongation of very long chain (Elovl) fatty acids has broad effects on lipogenesis and related signaling pathways (64, 67, 68). We chose to administer coconut oil/myristic acid which is abundant in medium chain fatty acids. An increase in elongation was observed following coconut oil administration, although somewhat modestly, probably due to the propensity of medium chain fatty acids for oxidation. These results indicate that the novel methodology is capable of detecting changes in lipid synthesis flux.

We first consider several methodological issues related to measurements of lipogenesis. Previous studies measured either total increases in mass isotopes of select lipids following D_2O exposure or the mass isotopomer distribution analysis (MIDA) following ^{13}C-acetate exposure. Mass isotopomers M+1, M+2, M+3 incorporated into lipids following D_2O and these mass isotopomers can be used to determine new lipid synthesis, provided the number of exchangeable hydrogens are known for each lipid species of interest. For example the number of exchangeable hydrogens on palmitate varies between 17-22. While sometimes measured directly, more frequently it is set to a constant. This assumption is unnecessary for NMR analysis of positional deuterium enrichments since the methyl position arises from acetyl-CoA and its enrichment can be measured directly. The assumption that acetyl-CoA enrichment is the same as body water enrichment applies to both methods and this was verified here using xenobiotic conjugates of acetyl-CoA. MIDA approaches require a similar assumption regarding the homogeneity of acetate enrichment across the liver sinusoid.

Mass isotopomer analysis and NMR positional isotopomer analysis place slightly different constraints on the detection of lipogenesis versus chain elongation, and this could lead to interpretational differences about the extent of lipid synthesis. Elongation of fatty acids (C16) to very long chain fatty acids (C18 or longer) occurs through ELOVL mediated chain elongation. Mass detection distinguishes between *de novo* lipogenesis and elongation of C16 to C18 by fitting isotopomer pools to 3 distinct populations; unlabeled (i.e. preexisting lipids), label distributed equally (but not uniformly) across the 16 or 18 carbons (i.e. de novo lipogenesis) or label distributed only on 2 carbons (i.e. elongation of one acetyl unit). However, elongation may also include partially catabolized fatty acids that are recycled into the lipogenic pathway (69). The extent of such a futile cycle and whether it is effected by HFD or insulin resistance is unclear but would likely be detected as *de novo* lipogenesis by mass isotopomer analysis if elongation begins at carbons significantly lower than C16. On the other hand, NMR positional isotopomer analysis very strictly constrains *de novo* lipogenesis to the enrichment of the methyl hydrogens and detects elongation whenever the methyl enrichment is lower than the α2 carbon enrichment (which represents all forms of lipid synthesis). Thus, any degree of elongation, whether ELOVL mediated C16 to C18 elongation or a less conventional elongation, for instance C12 to C16 elongation, it would be detected separately from DNL.. However, since the α2 deuterium enrichment (total lipid synthesis, DNL + elongation) was still much lower, all forms of lipogenesis were reduced in mice on a HFD. Therefore we conclude that reduced versus increased lipogenesis after HFD is not caused by methodological differences.

7 – Conclusion

In summary, we have developed and validated a novel NMR-based method to calculate lipid biosynthetic flux as well as perform a partial lipidomic analysis. This method will be applied to multiple biological models, namely to study the effects of HFD-Induced obesity and diabetes on lipid metabolism (chapter 2 of this dissertation) and the effects of phosphoenolypyruvate carboxykinase (PEPCK) in the regulation of lipid metabolism (Chapter 3 of this dissertation).

CHAPTER 2

Lipid fluxes in a rodent model of type 2 diabetes model

1 – Introduction

In his review article “What if Minkowski had been ageusic? An alternative angle on diabetes” (70) McGarry highlights that, even though, partially due to an historical perspective of the disease, diabetes has been analyzed from a glucocentric perspective, insulin resistance and diabetes are diseases that not only alter carbohydrate metabolism but also have negative effects in lipid metabolism. In fact, though it is hard to provide one precise definition for the term “insulin resistance”, all definitions share three common metabolic changes: hyperinsulinemia, hyperglycemia and hypertriglyceridemia.

One key aspect of lipid metabolism in the pathology of insulin resistance is that there seems to be an apparent contradiction in the sense that even though insulin-mediated control of glucose metabolism is dysregulated, insulin-mediated control of lipid metabolism either remains responsive or is actually elevated. This is known as selective insulin resistance. Some molecular mechanism that explain this apparent contradiction in insulin signaling have been suggested. Since most of them are based on differential regulation of key molecules of the insulin receptor signaling pathway, this chapter will open with a brief introduction of the actions of insulin, focusing on key proteins that have been associated with selective insulin resistance. In the second half of this introduction some of the theories proposed to explain selective insulin resistance will be reviewed. Finally, the methodology described in chapter 1 of this dissertation will be applied to a murine model of HFD-induced diabetes to study the changes in whole body lipid fluxes.

2 – Insulin regulation of lipid metabolism

Insulin is arguably the most studied hormone in physiology as it is extremely important in metabolic homeostasis, promoting the accumulation of cellular energy by upregulating the production of glycogen, increasing lipogenesis and decreasing gluconeogenesis and lipolysis. The molecular mechanism of insulin action is complex involving numerous protein kinases transcription factors and in order to affect its actions in the regulation of glucose and lipid metabolism. Figure 20 shows some of the major mechanisms of insulin action, as well as the major metabolic pathways that are regulated by the hormone.

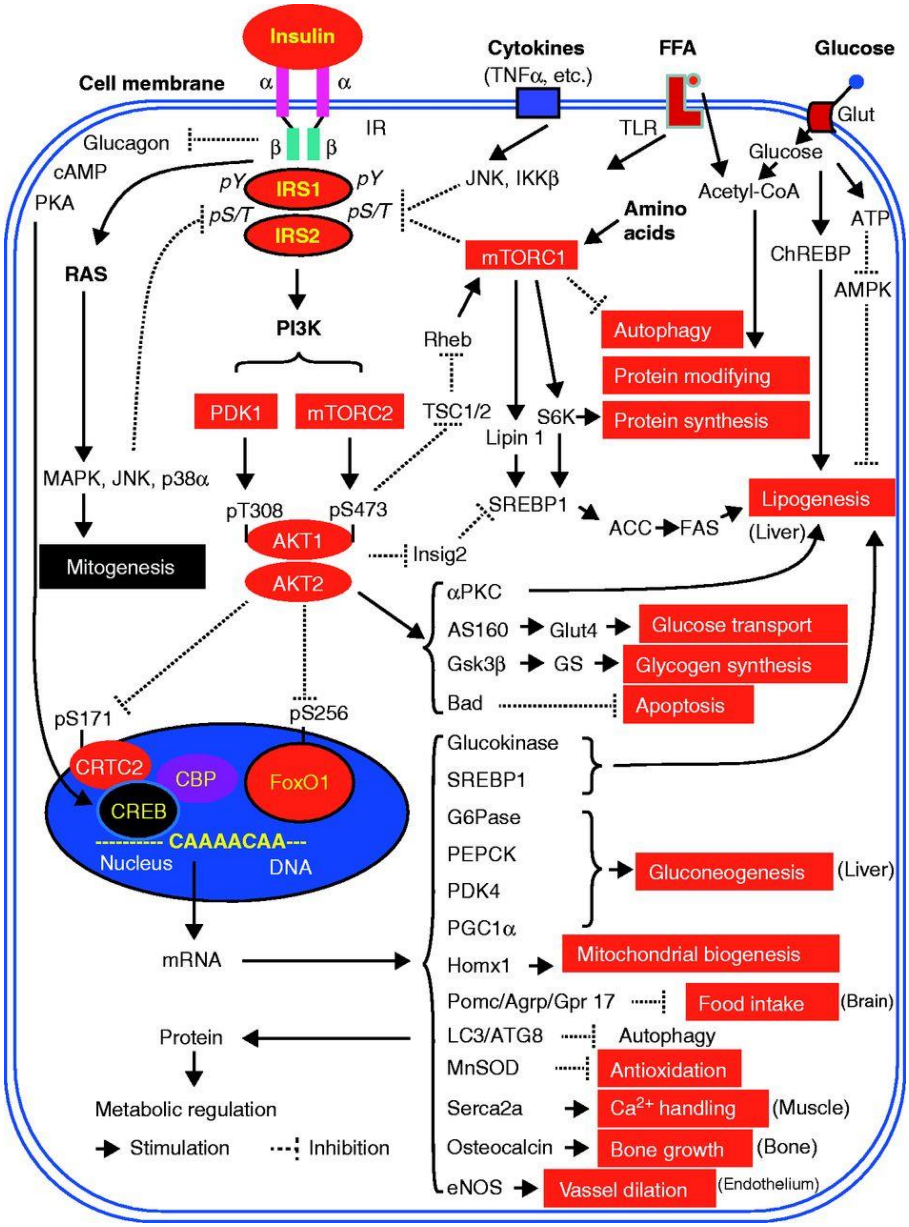

Figure 20: Molecular mechanisms of insulin action, highlighting the pathways that are affected in different tissues. Adapted from (71).

Whenever insulin binds to its receptor, it triggers a signaling cascade that starts with the phosphorylation of tyrosine residues in the cytosolic portion of the insulin receptor. Several other transcription factors and proteins are then phosphorylated and activated or deactivated in order to exert their metabolic function. Though a thorough review of these mechanisms of insulin signaling is beyond the scope of this introduction, a brief review of the role of some of the proteins that have been put forward as potential drivers of the selective insulin resistance will be made.

2.1 – Insulin receptor substrates (IRS)

The cellular effects of insulin are mediated by a host of protein kinases that work together to form the insulin signaling cascade. One of the key effectors of insulin signaling is the Insulin Receptor Substrate (IRS) which has 4 isoforms (IRS1-4), with IRS1 and IRS2 being the most prevalent. When the insulin receptor is activated by insulin and phosphorylated, IRS are recruited to the receptor and are phosphorylated as well. Phosphorylated IRS then activates Phosphatidylinositol-4,5-bisphosphate 3-kinase (PI3K) which converts Phosphatidylinositol 4,5-bisphosphate (PIP2) to Phosphatidylinositol (3,4,5)-triphosphate (PIP3). PIP3 then recruits and activates multiple proteins, namely protein kinase B (PKB) (also known as AKT) and 3-phosphoinositide- dependent protein kinase-1 (PDK1) further expanding the signaling cascade (Figure 20). Once activated, Akt phosphorylates targets that function to suppress gluconeogenesis and activate lipogenesis in the liver. Actions of Akt include, but are not limited to, activation of Foxo1 (which promotes the transcription of gluconeogenic genes), inhibition of GSK-3 (which phosphorylates and inactivates glycogen synthase), activation of Glut4 (Akt promotes the migration of Glut4 to the plasma membrane, promoting the entrance of glucose in the cell) and activation of mTOR (which regulates numerous metabolic pathways, such as protein production and lipid metabolism).

How insulin elicits differential effects on glucose and lipid production is an active area of research. RS1 and IRS2 have been identified as the main effectors of insulin action, as combined knockout of these proteins is a phenocopy of insulin receptor knockout in liver or muscle (72-75). Knockout of either IRS1 (76) or IRS2 (77) leads to peripheral insulin resistance, but only IRS2 KO mice developed overt diabetes, due to defects in β-cell. In a study using shRNA to knockdown either IRS1 or IRS2 it was verified that, after insulin stimulation, knockdown of IRS1 mainly increases the mRNA levels of

gluconeogenic enzymes (glucose-6 phosphatase and Phosphoenolpyruvate Carboxykinase) while mRNA levels of lipogenic enzymes do not differ from controls. In the same experiment, of IRS2 mainly increased the expression of SREBP-1c and fatty acid synthase without changing the mRNA levels of gluconeogenic enzymes (78). This study shows that IRS1 alone is sufficient to maintain the normal function of insulin in the regulation of lipid metabolism, while IRS2 alone helps maintain the insulin action on glucose metabolism physiological. A more thorough review on IRSs and their roles in regulation of metabolism can be found in (79).

2.2 – Mammalian target or rapamycin (mTOR)

Mammalian target or rapamycin (mTOR) is a serine/threonine kinase that regulates multiple metabolic pathways that intersects with many cell signaling pathways that include insulin signaling. mTOR forms two different types of multiprotein complexes: mTORC1 and mTORC2 (Figure 21). mTORC is a downstream target of Akt, which acts on intermediate kinases to activate it. mTORC complexes regulate multiple functions, such as protein synthesis, autophagy and nucleotide synthesis and lipogenesis (reviewed in (80)).

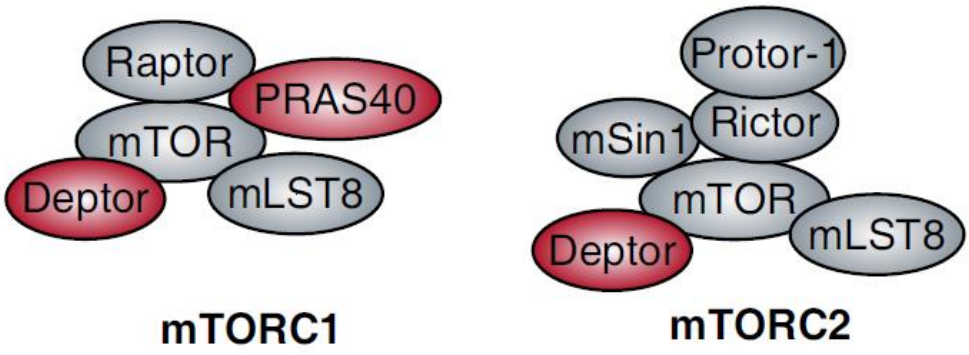

Figure 21: the two mTORC complexes. Adapted from (81).

There are two main ways that mTORC activates lipogenesis. mTORC1 can directly phosphorylate and inhibit Lipin1, which, under normal circumstances, prevents the

nuclear localization of SREBP-1c (82, 83). mTORC1 also directly increases the expression of SREBP-1c (84, 85). mTORC2 complex was also found to directly increase the expression of SREBP-1c (86, 87). A more thorough review on mTORC and its role in regulation of metabolism can be found in (81, 88, 89).

2.3 – Sterol Regulatory Element Binding Proteins (SREBP)

One of the main transcription factors involved in the translation of insulin signaling to lipid metabolism are the Sterol Regulatory Element Binding Proteins (SREBP). There are three SREBP isoforms: SREBP-1a, SREBP-1c (which are different transcripts of the same gene, but SREBP-1c is the most abundant hepatic isoform) and SREBP-2. SREBPs act at the transcriptional level, binding to Sterol Response Element (SRE) sites in the promoter of target genes, increasing their transcription. Each of the SREBP isoforms has slightly distinct specificity towards their targets, with SREBP-1a and mainly promote the translation of genes related to lipid synthesis. SREBP-1a induces the highest fold changes in mRNA of lipogenic genes of the two isoforms. SREBP-2a promoting the translation of genes related to cholesterol synthesis. Figure 22 summarizes genes whose transcription is upregulated by SREBP2 and SREBP-1c.

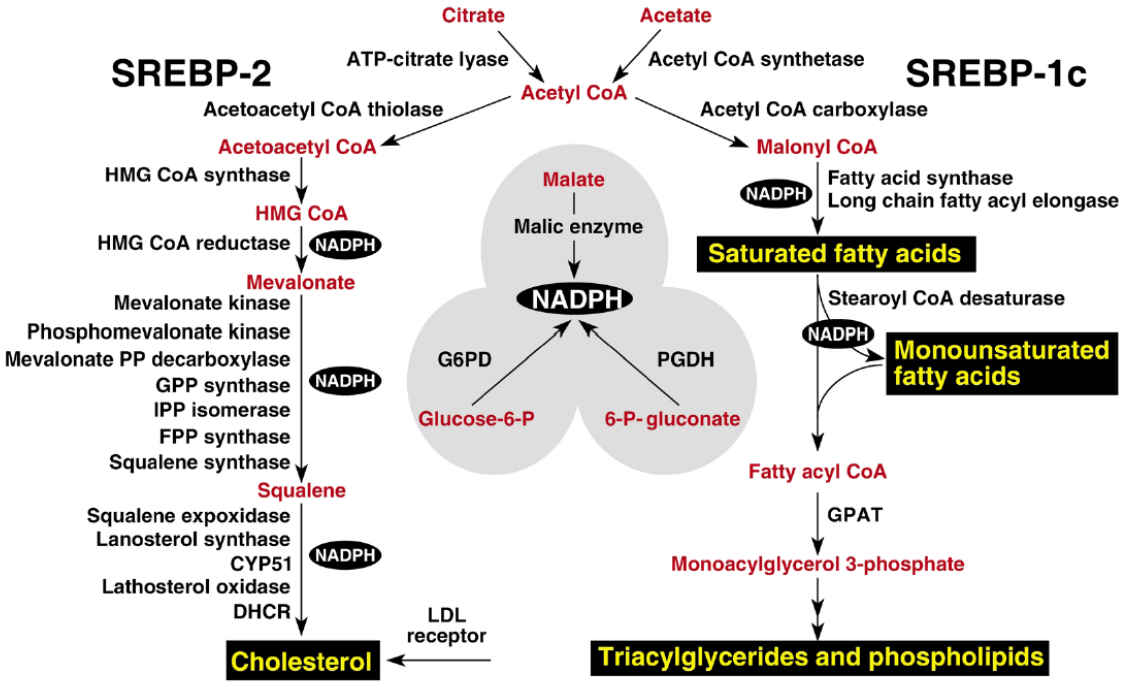

Figure 22: Genes whose translation is upregulated by SREBP-2 or SREBP-1c. Adapted from (90).

Insulin regulates SREBP through incompletely understood mechanisms but two general mechanisms are known. First, insulin activates the transcription of the SREBP gene (91). Secondly, insulin also regulates the activation of SREBP by promoting the proteolytic cleavage of the inactive SREBP precursor protein by SCAP (SREBP Cleavage Activating Protein), allowing the mature, active form SREBP to migrate to the nucleus and perform its physiological functions (92). SREBP levels have a direct effect in the regulation of metabolic fluxes. Several studies determined the rates of de novo lipogenesis and cholesterol synthesis in mice constitutively active forms of SREBP. DNL was increased 26 fold and cholesterol synthesis was increased 5 fold in SREB-1a transgenic mice (61, 93) and DNL was increased 4 fold in SREBP-1c transgenic mice (93, 94) while SREBP-2 transgenic mice showed an 4 fold increase in DNL and a 28 fold increase in cholesterol synthesis (93). A more thorough review on SREBPs and their roles in regulation of metabolism can be found in (90, 95).

2.4 – NADPH Oxidase (NOX)

NADPH oxidases (NOX) are enzymes that catalyze the production of superoxide ions from NADPH. There are 7 isoforms (NOX1-5 and DUOX1-2) (96). In adipocytes, NOX4 in particular is activated by insulin and is associated with the propagation of insulin signaling, as the superoxide produced inhibits protein tyrosine phosphatases, such as PTEN and PTP1B which normally dephosphorylate the insulin receptor and IRSs, terminating the insulin signaling cascade (97-99). A more thorough review on NADPH oxidases and their roles in regulation of metabolism can be found in (96, 100).

3 – Selective insulin resistance

Insulin has several actions in different tissues and alters distinct metabolic pathways within those same tissues. In the liver, for example, insulin suppresses gluconeogenesis, increases glycogen production and stimulates glucose oxidation (101) In the muscle and white adipose tissues, it regulates the translocation of GLUT4 to the plasma membrane, increasing glucose uptake (102). Insulin also regulates lipid metabolism in liver by promoting hepatic DNL, while inhibiting its packaging and release in VLDL (101) (Figure 23A). Paradoxically insulin resistance impairs insulin's actions over glucose metabolism, *i.e.*, glucose production is increased and glucose storage as glycogen is decreased, but its actions on lipid metabolism remain intact, *i.e.*, lipogenesis is elevated. This phenomenon is known as selective or mixed insulin resistance (Figure 23B).

Animal models of total hepatic insulin resistance, namely the Liver-Specific Insulin Receptor Knockout (LIRKO) mice (73), are hyperglycemic and hyperinulinemic (73), but have decreased circulating triglycerides, due, in part, to a decrease in hepatic VLDL export (103) (Figure 23C). Thus selective insulin resistance occurs from defects downstream of the insulin receptor. Though the precise mechanism is unknown, several models have been developed to explain selective insulin resistance, some of which will be explored in following section

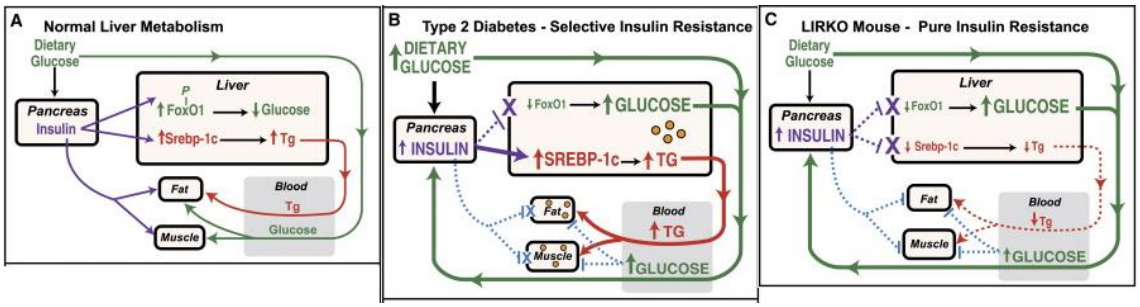

Figure 23: effects of insulin in a physiological state (A), selective insulin resistance (type 2 diabetes) (B) and partial insulin resistance (LIRKO) mice (C) adapted from (104).

3.1 – IRS hypothesis

One hypothesis to explain the phenotype of selective insulin resistance was described by Shimomura et al. (105) using *ob*/*ob* mice, which do not produce leptin (a satiety hormone produced by adipose tissue) becoming obese due to hyperphagia, eventually developing hyperinsulinemia and diabetes. In both *ob*/*ob* mice and in lipodystrophic mice, the levels of IRS-2 where significantly lower than IRS-1. The authors then performed multiple experiments with isolated mouse hepatocytes, discovering that, when insulin was added to the culture medium, there was a significant decrease in IRS-2 mRNA and protein levels, without changes in IRS-1 levels. Indicating that chronic hyperinsulinemia, such as observed in diabetes, is capable of selectively alter the expression of IRS-2 but not IRS-1 or SREBP-1c which remain active, leading to selective insulin resistance (Figure 24).

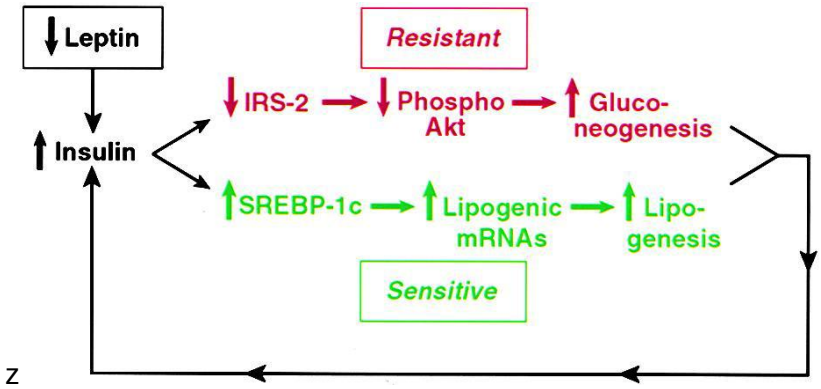

Figure 24: The IRS-2 model of selective insulin resistance. Adapted from (105).

3.2 – mTORC1 hypothesis

Li *et al* (106) have suggested that selective insulin resistance occurs due to a bifurcation in the insulin signaling pathways. This model focuses on analysis of the expression of multiple transcription factors, namely FoxO1 and SREBP-1c. The general idea is that FoxO1 is the one of the main mediators of the insulin regulated increase in expression of the PEPCK and glucose-6-phosphate genes and, therefore one of the main drivers of insulin-mediated increased gluconeogenesis (107). In the same way, SREBP-1c is considered the main driver behind insulin-induced increase in expression of hepatic genes related to lipogenesis, namely ACC, FAS and glycerol-3-phophate acyltransferase (90, 108).

Using specific inhibitors for the kinases of the insulin receptor-mediated signaling cascade (Figure 25) in cultured hepatocytes Li *et al* (106) discovered that inhibition of either PI3K or Akt led to both a decrease in the induction of SREBP-1c mRNA levels in response to insulin and a failure to reduce PEPCK mRNA levels in the same condition. This mimics the complete insulin resistance phenotype and, therefore, if the condition of selective insulin resistance is caused by a bifurcation in insulin resistance, it must necessarily lie downstream of Akt. This is also supported by other work that shows that Akt2 is required for hepatic lipid accumulation in models of insulin resistance (109). When these hepatocytes where treated with rapamycin, a selective inhibitor of the mTORC1 complex, SREBP-1c mRNA levels did not increase in response to insulin but PEPCK mRNA levels where decreased, suggesting that mTORC1 is a potential target for the point of bifurcation in insulin signaling that leads to the pathology of insulin resistance (Figure 25). In this experiment selective inhibitors for GSK3β and MEK where using as controls.

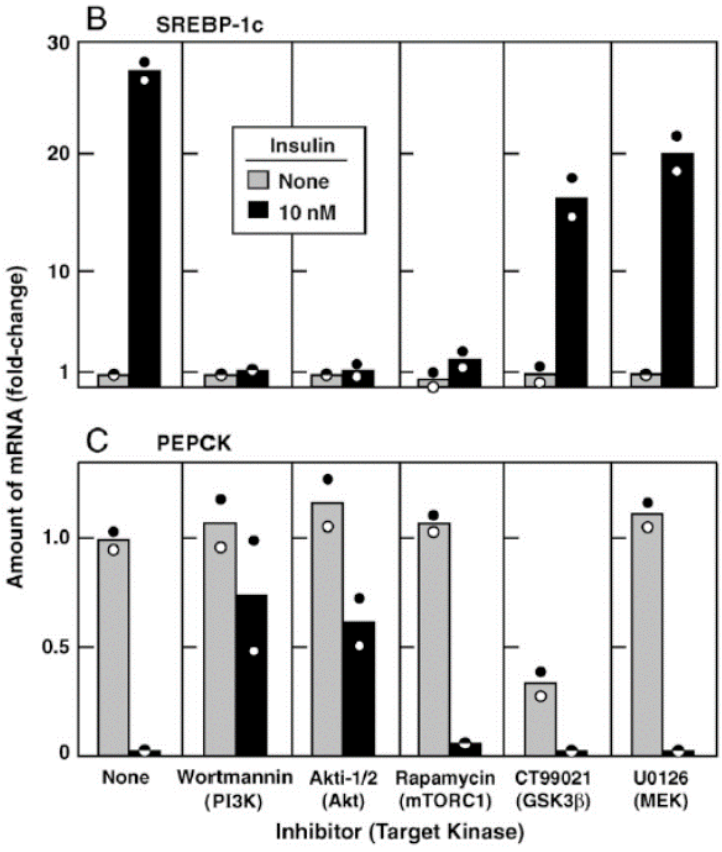

Figure 25: Effects of specific protein kinase inhibitors on the expressions of SREBP-1c and PEPCK in isolated hepatocytes treated with or without insulin. Adapted from (106).

Li *et al* (106) then performed rapamycin treatments *in vivo* in rats and analyzed the response of mRNA levels in response to a fast-refeeding protocol, showing that the increase in SREBP-1c, FAS and SCD-1 mRNA levels was severely blunted in rats treated with rapamycin but the reduction in PEPCK mRNA levels remained unchanged. This once again suggests that mTORC1 is at least partially responsible for the signaling cascade events that lead to the pathology of selective insulin resistance. Figure 26 shows a simplified version of the proposed signaling cascade model.

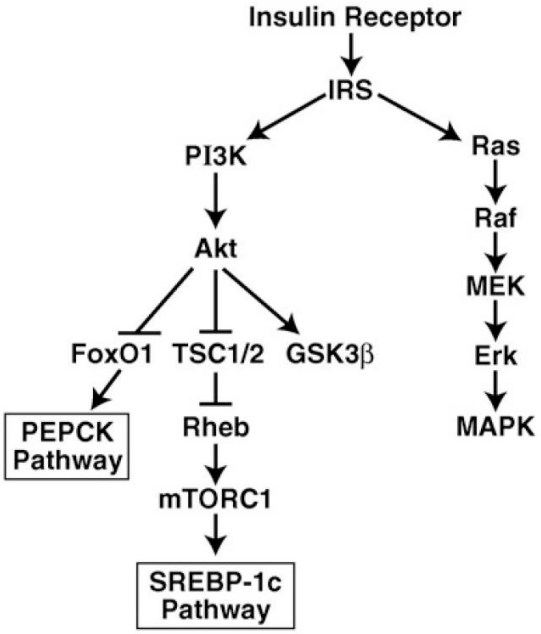

Figure 26: Map of the insulin activated protein kinase signaling cascade. Adapted from (106).

3.3 – Endoplasmic reticulum stress hypothesis

Ferré *et al.* (110) suggest that another possible mechanism for the development of selective insulin resistance involves the endoplasmic reticulum (ER). The ER is an organelle with multiple roles, such as the synthesis of secretory proteins and the maintenance of cell calcium homeostasis. The ER is also capable of initiating a process denominated unfolded protein response (UPR) which, through a series of signaling cascades, activates the degradation of unfolded proteins. One of the key proteins in mediating UPR – XBP1 – has been directly correlated with lipogenesis (111). The authors suggest that, in obesity, through mechanisms yet unknown, there is an increase

in ER stress that triggers the activation of SREBP-1C independently of insulin action (112) (Figure 27).

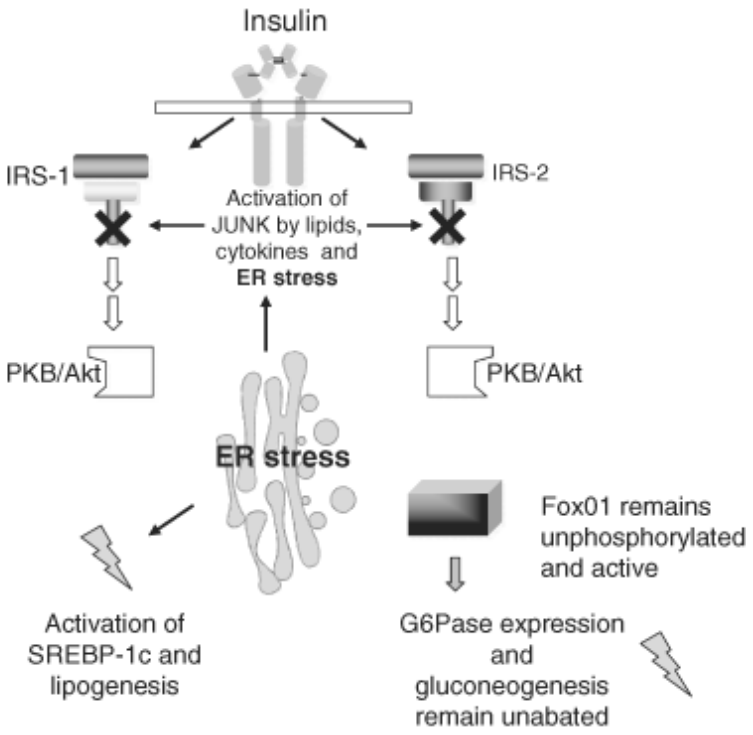

Figure 27 The ER stress model of selective insulin resistance. Adapted from (112)

3.4 – NOX4 hypothesis

Another possible mechanism that explains development of selective insulin resistance involves NOX4. Wu *et al.* (113) verified that, in db/db mice (which do not express the leptin receptor and have a similar phenotype to ob/ob mice) there was a distinct phosphorylation pattern on different positions of Akt, with serine 473 (S473) showing impaired phosphorylation capacity in response to insulin, while threonine 308 (T308) remained fully insulin responsive. These phosphorylation results were recapitulated in isolated hepatocytes in which NOX4 had been knocked out using NOX4 siRNA. Hepatocytes that did not express NOX4 showed significant impairment of FOXO-1 phosphorylation, while phosphorylation of ACC and GSK3β remained responsive. When hepatocytes were treated with diphenyleneiodonium (DPI) the insulin response in the downregulation of Pepck mRNA levels was blunted (Figure 28A), while SREBP-1C levels, though not as responsive to insulin as vehicle treated animals, remained high (Figure 28B). It was also observed that glucose uptake by hepatocytes treated with

NOX4 siRNA had significantly reduced basal and insulin-stimulated glucose uptake Figure 28C, recapitulating the pathology of selective insulin resistance.

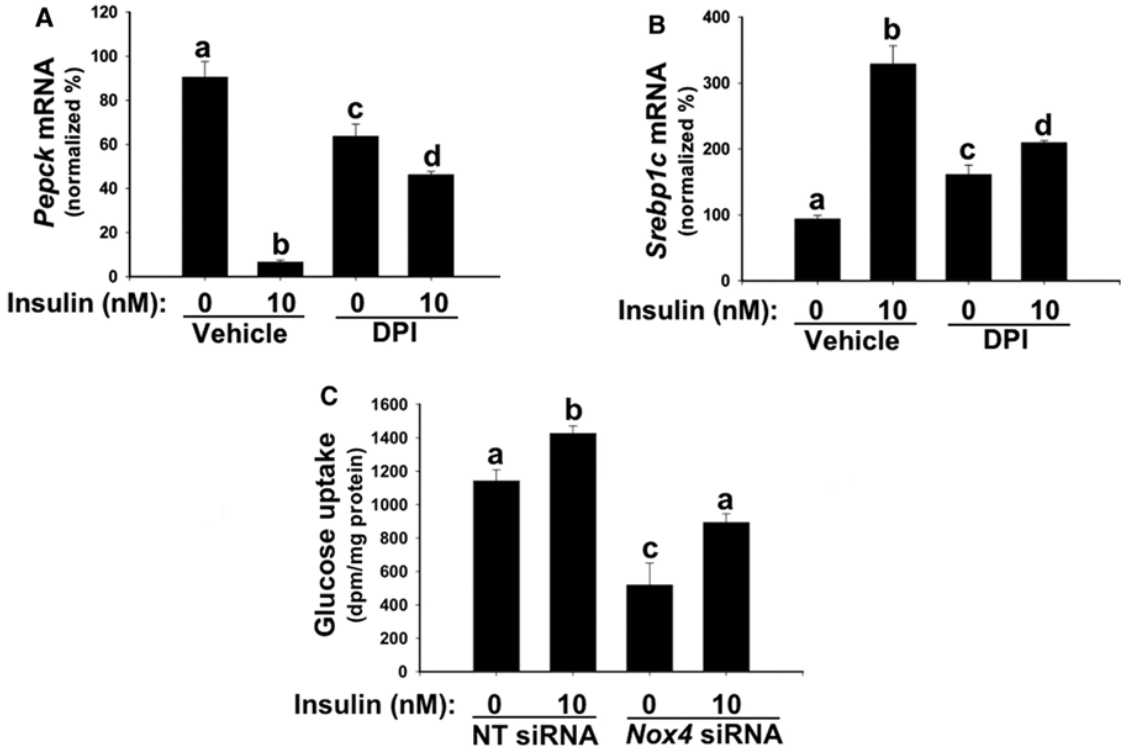

Figure 28: Changes in mRNA expression of Peck (A) and Srebp1c (B) in hepatocytes treated with an inhibitor of NOX4. (C) Decreased basal and insulin-stimulated glucose uptake in hepatocytes treated with either Nox4 siRNA vs. control RNA. Adapted from (113).

3.5 – Flux hypothesis

One very important point to bear in mind is that analysis of mRNA levels of enzymes of a pathway cannot be taken as a definite measure of flux through that pathway, as there are multiple post-transcriptional points of regulation of enzymatic activity, such as protein degradation, allosteric regulation and substrate availability. In fact, Turner *et al* (114) show that, in an *ob/ob* mouse model, there as about a 3-fold increase in FAS mRNA levels when these mice where treated with leptin compared with untreated *ob/ob* mice, which would suggest that leptin-treated animals had increased lipogenesis. However, stable isotope tracer analysis showed that, in fact, lipogenic flux was significantly decreased in *ob/ob* mice treated with leptin.

Otero *et al* suggests that selective insulin resistance might occur due to a combination of insulin resistance in the glucose metabolism signaling branch which alters metabolic fluxes, leading to an increase in lipogenesis that is independent of differential

insulin signaling (101). The general idea is that, by selectively decreasing the liver's ability to use produce glycogen, there is a compensatory, insulin independent increase in hepatic lipogenesis. This is supported by studies showing that, inhibition of glucose-6-phosphate translocator (115) or glucose-6-phosphatase (116) or knockout of glycogen synthase (117) lead to an increase in DNL. There have also been recent reports of Akt independent activation of the lipogenic machinery, namely via mTORC2 (87), which could bypass insulin signaling.

Overall, this data suggests that mRNA levels alone are not enough to inform about changed flux through a pathway. In chapter we will apply the NMR based method described in chapter 1 of this dissertation to understand the metabolic flux changes that occur in the context of high-fat diet induced obesity and diabetes.

4 - Methods

HFD studies were performed on BDF1 mice (Charles Rivers) (n=5). Since the effect of HFD on lipogenesis in C57Bl6 mice has been previously studied (38, 109, 118, 119), we examined BDF1 mice, a strain suggested to be more susceptible to diet induced diabetes than the C57Bl6 (120, 121). Mice were fed either a control semi-synthetic diet (10% fat calories; Teklad diet TD06416; Harlan Laboratories) or a high-fat diet (60% fat calories; Teklad diet TD06414; Harlan Laboratories) for a period of 35 weeks. These animals were weighted regularly. Fed and fasted blood samples were collected via tail vein at several timepoints during the experiment for measurement of plasma glucose levels and insulin. Four days before the end of the feeding protocol, animals were injected with 27 µl/g of 99.9% D_2O saline solution, and returned to their cages with their regular drinking water replaced by a 4% D_2O solution. At the end of the 35 weeks time period mice were anesthetized using isoflurane and sacrificed via exsanguination. Their livers and epidydimal fat pads were quickly excised and rapidly frozen in liquid nitrogen. Tissues were then stored in -80ºC. Tissues were processed and analyzed for analysis of lipid biosynthetic fluxes as described in chapter 1 of this dissertation.

5 – Application of 1H/2H hybrid NMR technique for the measurement of lipid flux in diabetic animals

To determine how type 2 diabetes changed lipid metabolism a High Fat Diet (HFD) model was studied using the methodology developed in chapter 1. BDF1 mice on a HFD were significantly heavier than mice on the low fat diet (LFD) after week 4 (Figure 29A) and continued diverging throughout the study period. Fasted glucose concentration was slightly elevated after one week (Figure 29E) and fed glucose concentration increased after 14 weeks of HFD (Figure 29D). Both fasting and fed hyperglycemia were most prominent between 16 and 30 weeks. Fasted insulin was significantly elevated after 1 week (Figure 29C) and fed state insulin (Figure 29B) concentration was ~30-fold increased by 25 weeks of HFD. Although declining insulin (i.e. β-cell dysfunction) was previously described in BDF1 mice (120, 121), this condition was not reached by 35 weeks at which time flux experiments were carried out.

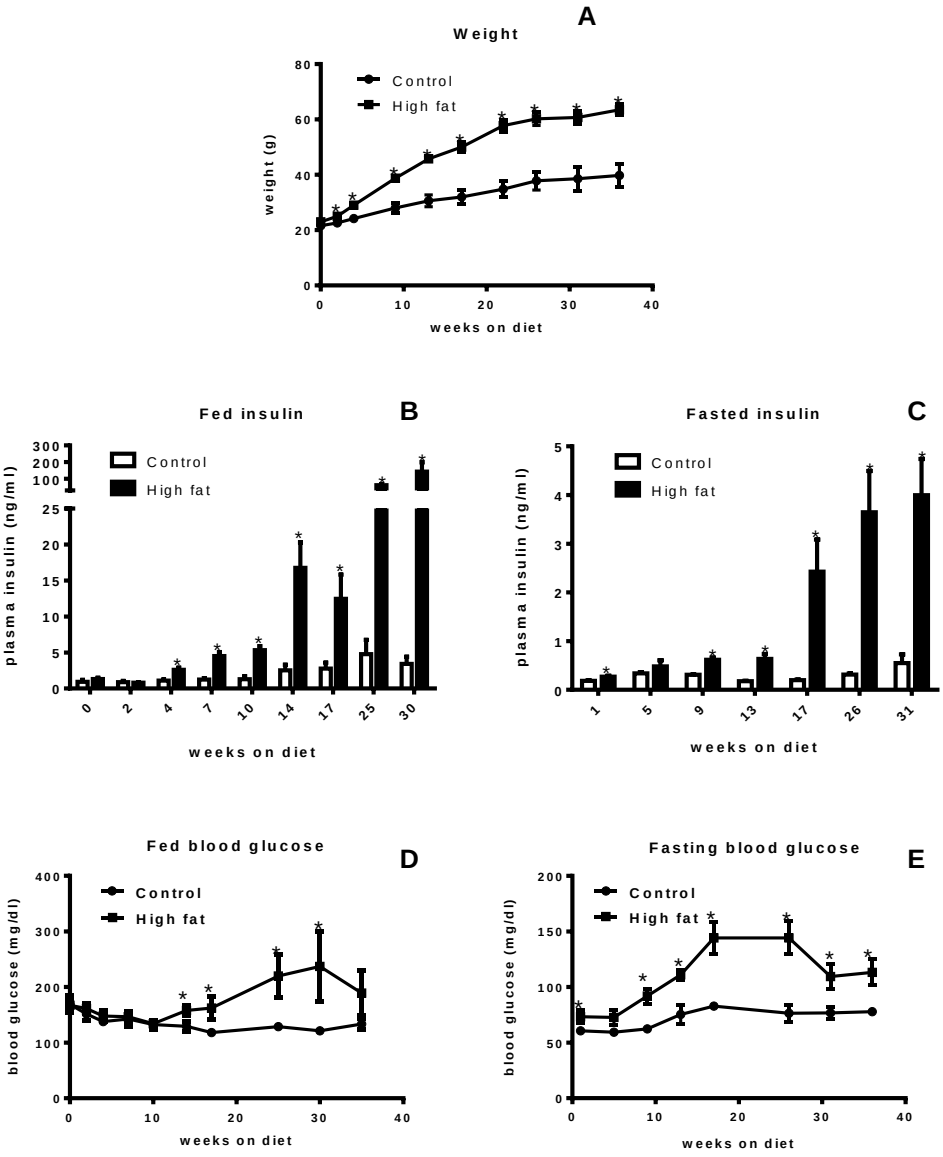

Figure 29: HFD-induced insulin resistance in BDF1mice. (A), body weight changes in control and HFD mice. (B) and (C), fasted and fed glucose levels throughout the study, respectively. (D) and (E), fasted and fed insulin levels of insulin during the duration of the study. Data are presented as the mean ± SE (n=5).

As expected, hepatic triglyceride content was increased in HFD mice compare to controls (Table 3). Although basal liver fat was lower than previously reported in C57Bl6 under the same conditions (122), the fold increase in response to HFD was similar. This elevated triglyceride content occurred with increased percent polyunsaturated, linoleic acid, DHA and ω-3 fatty acids in liver. In contrast there was a decrease in percent MUFAS in liver (Table 4).

Table 3: Hepatic and WAT triglycerides in HFD and control non-fasted BDF1 mice.

	Liver			White adipose tissue		
	Control	High fat diet	p value	Control	High fat diet	p value
Fatty acid per glycerol unit	3.04±0.02	3.05±0.01	NS	3.2±0.3	2.93±0.02	NS
Hepatic glycerol concentration (mg/g liver)	2.96±0.20	4.65±0.20	<0.05	38±8	46±4	NS
Fatty acid concentration (mg/g tissue)	27±2	41±2	<0.05	320±63	396±31	NS

Data are represented as the mean ± SE (n=5).

Table 4: Percentage of fatty acid types in HFD and control BDF1 mice.

	% fatty acids					
	Liver			White Adipose tissue		
	Control	High fat diet	p value	Control	High fat diet	p value
ω-3 fatty acids	0.8±0.1	1.9±0.3	<0.01	1.04±0.09	0.52±0.04	<0.01
Other ω	70±1	71±1	NS	75±1	78±1	NS
Saturated	29±1	27±1	NS	24±1	21±1	NS
Monounsaturated	58±1	46±1	<0.001	60±1	60.4±0.8	NS
Polyunsaturated	13±1	28±1	<0.001	16.1±0.2	18.6±0.4	<0.001
Linoleic acid	10±1	18±1	<0.001	15±1	19.0±0.3	<0.05
Docohexaenoic acid	0.24±0.03	1.6±0.3	<0.001	0.02±0.01	0.03±0.01	NS
Average number of carbons per FA	17.4±0.4	16.9±0.1	NS	15.7±1	17.1±0.12	NS
Average molecular weight of fatty acids	273±5	267±1	NS	249±13	268.46±1	NS

Data are represented as the mean ± SE (n=5).

Changes in the constituents of adipose triglyceride species were less conspicuous, though polyunsaturated and linoleic acids were modestly increased. Differences in dietary constituents of the LFD (29% saturated, 37% monounsaturated, 34% polyunsaturated) and HFD (HFD - 37% saturated, 47% monounsaturated, 16% polyunsaturated) could not account for all changes in tissue lipid species, particularly with regard to polyunsaturated lipids. The total amounts of all measured fatty acid classes except monounsaturated fatty acids were significantly higher in HFD mice compared to control (Table 5).

Table 5: total of fatty acid types in HFD and control BDF1 mice.

Total fatty acids (mg/g of liver)						
	Liver			White adipose tissue		
	Control		p value	Control	HFD	p value
ω-3 fatty acids	0.21±0.03	0.76±0.08	<0.001	3.3±0.7	2.1±0.2	NS
Other ω	19±2	29±2	<0.01	316±63	394±31	NS
Saturated	8±1	11±1	NS	74±13	83±8	NS
Monounsaturated	15±1	19±1	NS	194±40	240±20	NS
Polyunsaturated	3.6±0.4	11.4±0.3	<0.001	52±10	74±6	NS
Linoleic acid	2.6±0.3	7.6±0.3	<0.001	49±11	75±5	NS
DHA	0.06±0.01	0.64±0.08	<0.001	0.08±0.03	0.14±0.06	NS

Data are represented as the mean ± SE (n=5) HFD: High Fat Diet. DHA: Docosohexaenoic acid.

To examine the nature of lipid synthesis in diet induced obese BDF1 mice, they were given D_2O in drinking water so that DNL, desaturation and elongation could be measured by the described NMR method (Table 6). A HFD significantly decreased percentage (Table 6) and total new mass of lipids and newly desaturated lipids in liver (Table 7). Similar findings were made in the white adipose tissue. The desaturated/DNL flux ratio was also lower in HFD BDF1 mice, suggesting that the reduction in desaturation

was even more severe than the reduction in DNL. The finding of reduced DNL was surprising inasmuch as insulin resistance is thought to activate lipid synthesis in liver. However, in keeping with this effect, we found that chain elongation was doubled in HFD mice. The important distinction in the context of this method is that DNL is detected only when the initial 2 carbon unit is synthesized from acetyl-CoA during deuterium exposure (i.e. the methyl hydrogens are labeled); while elongation is detected when *at least* the first two carbon unit was pre-existing (i.e. the α2 hydrogens are labeled but the methyl hydrogens are not). The mass of newly synthesized glycerol was increased, consistent with the expected increase in gluconeogenesis, glyceroneogenesis and re-esterification of lipids (38, 122). Thus, these findings indicate that HFD promotes fatty acid elongation and esterification but suppresses DNL in BDF1 mice.

Table 6: Percent fluxes in HFD and control BDF1 mice.

% De novo synthesis						
	Liver			White adipose tissue		
	Control	High fat diet	p value	Control	High fat diet	p value
% De novo lipogenesis	13.8±1.6	2.2±0.4	<0.001	0.8±0.1	0.21±0.04	<0.01
Fraction of elongated lipid	0.21±0.05	0.62±0.04	<0.001			
% Total lipid elongation	2.9±0.7	2.9±0.8	NS	NA	NA	
% desaturation activity	6.4±0.8	0.4±0.2	<0.001	0.07±0.02	0±0	<0.05
% glycerol synthesis	25±2	24±4	NS	7±1	10±0.6	<0.05

Data are represented as the mean ± SE (n=5).

Table 7: mass of new lipids in HFD and control BDF1 mice.

	Amount of new lipids (mg/ g of tissue)					
	Liver			White adipose tissue		
	Control	High fat diet	p value	Control	High fat diet	p value
De novo lipogenesis	3.2±0.3	0.7±0.1	<0.001	25±3	7±2	<0.001
Desaturation activity	0.97±0.13	0.07±0.03	<0.001	1.6±0.5	0±0	<0.05
Desaturation/ DNL ratio	0.30±0.01	0.08±0.03	<0.01	0.06±0.01	0±0	<0.01
glycerol synthesis	0.73±0.05	1.1±0.2	<0.05	26±4	50±5	<0.01

Data are represented as the mean ± SE (n=5).

6 – Discussion

We tested whether flux through several lipid metabolism pathways were altered by high fat diet induced obesity. Obesity causes “mixed insulin resistance” in liver, such that insulin’s suppressive actions on gluconeogenesis are impaired but its propensity to stimulate SREBP mediated lipid synthesis is paradoxically maintained (106). For instance, in agreement with prior studies (38), we observed an increase in the amount of new glycerol in liver and adipose triglycerides after HFD. The new synthesis of glycerol occurs mainly via glyceroneogenesis from dihydroxyacetone phosphate produced by the gluconeogenic pathway, which is increased during insulin resistance. However, studies of lipogenic flux in diet induced and genetically obese models have produced variable results. Genetically obese rodents have increased lipogenesis (37), but high fat diet induced obesity confers changes in lipogenesis that are apparently more complex. Studies of rodents on a HFD have revealed increased (119), no change (118) and dramatically reduced *de novo* lipogenesis (38, 53, 119). The variability of these findings is relevant to role of mixed insulin resistance in the accumulation of lipid during NAFLD.

To clarify this issue, we examined BDF1 mice fed a HFD because this strain was reported to develop a more severe form of diet induced diabetes than C57Bl6 mice (120, 121). In previous studies, BDF1 mice fed a 64% HFD became insulin resistant by 8 weeks and had fed plasma glucose levels of 335 mg/dl after 14 weeks on the diet (121). Here we used a 60% fat diet and observed profound hyperinsulinemia but hyperglycemia was mild. Overall, the insulin and glycemic phenotype was reminiscent of our experience with C57Bl6 mice on this diet (123). However, despite fat accumulation in liver we found a dramatic decrease in both the percent lipogenesis and total hepatic fat derived from lipogenesis. Inasmuch as this finding contrasts the expectation that insulin resistance causes increased lipogenesis, it is worth considering the factors that dictate the outcomes of lipogenesis during high fat feeding.

We first consider several methodological issues related to measurements of lipogenesis. Previous studies measured either total increases in mass isotopes of select lipids following D_2O exposure or the mass isotopomer distribution analysis (MIDA) following ^{13}C-acetate exposure. Mass isotopomers M+1, M+2, M+3 etc incorporate into lipids following D_2O and these mass isotopomers can be used to determine new lipid synthesis, provided the number of exchangeable hydrogens are known for each lipid species of interest. For example the number of exchangeable hydrogens on palmitate varies between 17-22. While sometimes measured directly, more frequently it is set to a constant. This assumption is unnecessary for NMR analysis of positional deuterium enrichments since the methyl position arises from acetyl-CoA and its enrichment can be

measured directly. Multiple approaches have been applied to lipogenesis in HFD mice with variable results; MIDA found no change (118), ^{2}H NMR found a decrease (53) and ^{2}H mass isotopomers reported an increase and decrease in different studies (38, 119). Although these methods require unique assumptions, there is no obvious reason why they would provide systematically higher or lower flux during a HFD.

Mass isotopomer analysis and NMR positional isotopomer analysis place slightly different constraints on the detection of lipogenesis versus chain elongation, and this could lead to interpretational differences about the extent of lipid synthesis. Elongation of fatty acids (C16) to very long chain fatty acids (C18 or longer) occurs through ELOVL mediated chain elongation. Mass detection distinguishes between *de novo* lipogenesis and elongation of C16 to C18 by fitting isotopomer pools to 3 distinct populations; unlabeled (i.e. preexisting lipids), label distributed equally (but not uniformly) across the 16 or 18 carbons (i.e. de novo lipogenesis) or label distributed only on 2 carbons (i.e. elongation of one acetyl unit). HFD induces the expression of ELOVL1, 2, 5 and 6 in mice (124) and indeed Oosterveer and colleagues found that a HFD induced the elongation of C16 to C18:1 but not de novo synthesis of C16 using mass isotopomers (118). However, elongation may also include partially catabolized fatty acids that are recycled into the lipogenic pathway (69). The extent of such a futile cycle and whether it is effected by HFD or insulin resistance is unclear but would likely be detected as *de novo* lipogenesis by mass isotopomer analysis if elongation begins at carbons significantly lower than C16. On the other hand, NMR positional isotopomer analysis very strictly constrains *de novo* lipogenesis to the enrichment of the methyl hydrogens and detects elongation whenever the methyl enrichment is lower than the α2 carbon enrichment (which represents all forms of lipid synthesis). Thus, any degree of elongation, whether ELOVL mediated C16 to C18 elongation or a less conventional elongation, for instance C12 to C16 elongation, it would be detected separately from DNL. Indeed, compared to LFD mice, HFD mice had double the percentage of hepatic lipid derived from chain elongation. However, since the α2 deuterium enrichment (total lipid synthesis, DNL + elongation) was still much lower, all forms of lipogenesis were reduced in mice on a HFD. Therefore we conclude that reduced versus increased lipogenesis after HFD is not caused by methodological differences.

Next we consider several procedural differences that cause biological variations in lipogenesis independent of methodology. Mice in our study were kept on a HFD for a longer duration than previous studies, and this could have caused a more complete degree of insulin resistance (i.e. nullifying mixed insulin resistance). Although, we did not examine the cell signaling pathways necessary to specifically address this possibility, the relatively mild hyperglycemia of the model leads us to believe that this is an unlikely

factor. Another possibility may relate to the rather wide variety of “high fat” and “control” diet formulations used in various studies. For instance, Leavens and colleagues used a hydrogenated coconut oil (58 kcal% or 334 g/kg) diet, and found a 2-fold increase in the amount of newly synthesized hepatic lipid (109). Oosterveer and colleagues found no change in lipogenesis after 6 weeks of a lard diet (344 g/kg) (118). Delgado et al. and Lee et al. found a large decrease in lipogenesis, after feeding rats with a lard diet (230 g/kg) for 5 weeks and (120 g/kg) 2 weeks (37, 53) respectively. In all cases sucrose was the major carbohydrate source, and standard laboratory chow was used as the control diet. We used a lard based diet (60 kcal% or 330 g/kg from fat) and a semi-synthetic control diet (10 kcal% or 40 g/kg from fat) whose carbohydrate component was sucrose (i.e. same as the HFD). We observed much lower lipogenesis in the HFD compared to control, which is consistent with previous MS studies using similar dietary formulations (38, 119). Thus, we cannot rule out macronutrient components of the diets as factors determining whether lipogenesis is increased or decreased during high fat diet induced obesity, but there is no obvious pattern in the literature.

The timing of tracer exposure is another procedural factor that affects measurements of lipogenesis. Generally, lipogenesis is measured in either the postabsorptive state (e.g. 4-5 hours after removal of food) and sample is collected within hours of administration, or tracer is given over several days of *ad libitum* feeding. The two approaches have clear physiological consequences, and test two distinct aspects of lipid biology. In the first case, lipid synthesis is measured at a time when lipogenesis is down-regulated. To the extent that insulin resistance constitutively activates signaling pathways that promote lipogenesis, this is a relevant experiment because it tests whether lipogenesis has been appropriately suppressed. Indeed, under these conditions, Leavens and colleagues found that lipogenesis was increased in mice on a HFD (109). In the latter approach, tracer accumulates in lipids over one or more feeding cycles, providing an average lipogenesis that includes prandial contributions. Inasmuch as lipogenesis predominates in the prandial/postprandial state, this approach provides important insight into lipogenic regulation and its impact on lipid accumulation. In the four instances discussed here, where animals were exposed to tracer across at least one feeding cycle, lipogenesis was reduced following a HFD (37, 38, 53, 119). Thus, the effect of insulin resistance to stimulate lipogenesis may be a postabsorptive phenomenon inasmuch as dietary fat suppresses lipogenesis even in the setting of insulin resistance.

A complication of providing tracer across meals arises because at long time scales other lipid fluxes, such as dietary absorption, triglyceride export and oxidation also contribute to lipid homeostasis in liver. Indeed, linoleic acid can only be derived from the

diet, accumulated in both tissues of HFD mice. Reasoning that excessive newly synthesized lipids could have been diluted by diet and exported, we also examined their incorporation into adipose tissue. Mice on the LFD had roughly the same mass of new lipid in adipose and liver, but HFD mice had twice as much new lipid in adipose as liver, consistent with increased export of new lipid from the liver. However, the total amount of new lipid was still 3-fold higher in the adipose of LFD mice, suggesting that dietary dilution and export is not masking high DNL in HFD mice.

7 - Conclusion

We used a novel $^{1}H/^{2}H$ NMR method to investigate lipid synthesis and applied it in mice with HFD induced insulin resistance. Together, our data indicate that lipogenesis is suppressed by HFD, even during insulin resistance, when examined across feeding periods. However, there is an increase in elongation flux and

CHAPTER 3

Role of cytosolic Phosphoenolpyruvate Carboxykinase (PEPCK-C) in the regulation of lipid metabolism

1 – Introduction:

Phosphoenolpyruvate Carboxykinase (PEPCK) is considered an important regulatory enzyme of GNG but may also play a lesser understood role in lipid metabolism. PEPCK-C catalyzes the conversion of oxaloacetate into phosphoenolpyruvate and carbon dioxide, which is the second irreversible enzymatic reaction of gluconeogenesis (GNG). There are two isoforms of PEPCK, PEPCK-C and PEPCK-M, located in the cytosol and the mitochondria, respectively. Each species possesses different ratios of these two isoforms. Humans have about 50% of each form, rodents have about 90% PEPCK-C and birds have almost exclusively PEPCK-M. PEPCK-C has been assumed to be one of the rate controlling enzymes of GNG since at least 1979, when DiTullio et al (125) determined, that the use of mercaptopicolinate, an inhibitor of PECK, reduced gluconeogenic output in rat hepatocytes. The acceptance of PEPCK-C as the main rate controlling enzyme of GNG has become so well established, that PEPCK-C mRNA levels are often used as a surrogate for gluconeogenic capacity.

Despite the canonical view that PEPCK-C is the rate controlling enzyme of GNG, metabolic studies indicate it plays a subtle, if not sophisticated, role in metabolism. First, the control coefficient for every enzyme of the gluconeogenic pathway has been determined (126). Pyruvate carboxylase (PCX) had the highest influence on gluconeogenic activity with a control coefficient over GNG that was approximately ten-fold higher than that of PEPCK-C. Second, a more recent study by Burgess *et al.* (127) proved, using a mouse genetics and a tracer approach that the metabolic control coefficient of PEPCK-C over GNG was just 0.18 out of a maximal value of 1, Hence PEPCK-C seems to have a smaller role in regulating GNG flux than typically assumed.

Faced with the array of control mechanisms for PEPCK-C transcription (reviewed in (128)) one question arises: if PEPCK-C is not the main rate controlling enzyme of GNG, what is its metabolic role? It seems unlikely that such comprehensive regulation mechanisms would be in place to regulate an enzyme with a negligible role in metabolic activity.

The fact that both isoforms of PEPCK are present in non-gluconeogenic tissues such as adipose tissue, brain, muscle and muscle further underscore the notion that this

enzyme must have other important roles besides GNG. Importantly, brown adipose tissue has higher PEPCK activity per gram of protein than liver (129), suggesting that PEPCK-C might have an important effect in the regulation of lipid metabolism. One such proposed role of PEPCK is the regulation of glycerol production via the pathway known as glyceroneogenesis (GlyNG), a truncated form of GNG that produces glycerol-3-phosphate necessary for the synthesis of triacylglycerides as well as diversity of structural and signaling lipids. PEPCK-C also regulates cataplerosis, *i.e.*, the removal of TCA cycle intermediates from the mitochondria. Since the lipogeneic enzymes are located in the cytosol, it is important to export citrate from the mitochondria to the cytosol, where it is converted by ATP-citrate lyase to oxaloacetate and acetyl-CoA, the latter then used for the synthesis of fatty acids. Few studies have analyzed the direct role of PEPCK-C on lipid metabolism, but mice with a liver specific deletion of PEPCK show pronounced steatosis after an overnight fast (130), suggesting that this enzyme might also play a role in the regulation of hepatic lipid metabolism.

In this chapter, the methodological approaches described in chapter 1 where applied to mice expressing different levels of PEPCK-C in order to determine the influence of this enzyme in lipid homeostasis, focusing on the liver and adipose tissue. The rates of triglyceride disposal from the liver, either as release of VLDL-bound triglycerides or via hepatic β-oxidation were measured. Since one of the key steps of lipogenesis is the export of citrate from the mitochondria into the cytosol where lipogenic enzymes are located, functional shuttling of metabolites and reducing equivalents between mitochondria and cytosol is mandatory. To determine if alterations in intracellular metabolite distributions secondary to manipulation of PEPCK-C expression informed the lipid phenotype, a partial metabolomics analysis on isolated hepatic cytosolic and mitochondrial fractions was also performed.

2 –Glyceroneogenesis

As mentioned in chapter 1 of this dissertation, the glycerol-3-phosphate precursor for the synthesis of triacylglycerides can be synthesized via 3 distinct pathways: 1) glycolysis, 2) glycerol kinase and 3) glyceroneogenesis. Glyceroneogenesis (GlyNG) is essentially a truncated form of gluconeogenesis (GNG), in the sense that they share the same enzymatic reactions but glyceraldehyde phosphate is converted to glycerol-3-phosphate by glycerol phosphate dehydrogenase. This pathway is of particular importance in adipose tissue, as it only has residual glycerol kinase activity (131). In the post prandial state, when meal lipid absorption and insulin are high, the liver produces and exports triglycerides in the form of Very Low Density Lipoproteins (VLDL). When VLDL reaches target tissues, such as the adipose tissue, extracellular lipoprotein lipase (LPL) cleaves triglycerides into free glycerol and fatty acids. Due to the low activity of glycerol kinase in adipose tissue, the majority of free glycerol is returned to the circulation and metabolized by the other tissues. Thus, in order to esterify the absorbed free fatty acids into triacylglycerols, glycerol-3-phosphate needs to be synthesized *in situ*.

Several studies have attempted to determine the relative contribution of GlyNG to glycerol-3-phosphate production both in the liver and in the adipose tissue. Chen *et al.* (27) determined the relative contributions of GlyNG and in adipose tissue of mice that were fed either a high-carbohydrate, low carbohydrate or high-carbohydrate supplemented with rosiglitazone were 17%, 50% and 53%, respectively. However, this study assumes that the circulating glucose contributing to Gly3P is unlabeled. To the extent that this glucose pool is previously labeled with deuterium, for example via gluconeogenesis, it would cause an artificial increase in the contribution of glycolysis to Gly3P. This was addressed by Bederman *et al.* (132) who, using a double tracer approach determined the contributions of GlyNG to Gly3P synthesis to be 31% and 72% in mice fed a high-carbohydrate and carbohydrate-free diet, respectively. Another study by Nye *et al.* (133) determined that, in the epididymal adipose tissue GlyNG contributed to about 90% to Gly3P production in fed rats and almost 100% in 48h fasted rats. In rats fed with fructose GlyNG was approximately 86% of total Gly3P production. This study also determined that GlyNG accounts for almost 100% and 60% liver and muscle, respectively.

Glyceroneogenesis is also an active metabolic pathway in the liver. Martins-Santos *et al.*(134) determined the contributions of glucose, pyruvate and glycerol to glycerol-3-phosphate production in liver slices of fed, fasted and STZ-induced diabetic

rats, via administration of radioactive-labeled substrates. Since the different labeled substrates were not administered simultaneously it was not possible to determine the relative contribution of each pathway for a given metabolic state, but it was possible to determine how these states altered the absolute contributions of each substrate to Gly3P production. When the animals were fasted, the contribution of glucose to Gly3P was decreased by about 26%, the contribution of pyruvate increased by about 70% while the contribution of glycerol remained constant. A similar result was observed in STZ-induced diabetic mice, where the contribution of glucose was reduced by about 36%, the contribution of pyruvate increased by 36% and the contribution of free glycerol remained unchanged. GlyNG is also important in humans, as exemplified in a study by Kalham *et al.* (135) where the contribution of GlyNG to plasma VLDL-derived triglycerides in patients with type 2 diabetes was determined to be approximately 54%, a value that remained constant even after the patient underwent diet and behavior modifications that led to an increase in their insulin sensitivity.

These studies highlight the importance of GlyNG as the major source of glycerol-3-phosphate synthesis, but a questions remains: what exactly is the role of PEPCK in the regulation of GlyNG in any of these tissues? Franckhauser *et al.*(136) overexpressed PEPCK-C in the adipose tissue of mice, leading to about a 12-fold and 5-fold increase in PEPCK-C mRNA expression in white and brown adipose tissue, respectively. These mice had an increase in the incorporation of label from ^{14}C labeled pyruvate into glycerol as well as an increased rate of fatty acid reesterification, leading to an increase in adipocyte weight and size. However, these mice did not show any of the negative effects associated with increased adiposity, such as impaired glucose tolerance. Another study, by Olswang *et al.*(137) determined that animals where PEPCK-C expression had been ablated in adipose tissue had reduced adiposity and some of the animals even became lipodystrophic. In order to indirectly determine the role of GlyNG, adipocytes from these animals were incubated with or without pyruvate and the amount of free fatty acids released to the media was analyzed. In control animals, when pyruvate was added to the media, there was a significant decrease in the amount of fatty acids released to the media, but, for PEPCK-C knockout adipocytes, there was a higher basal release of fatty acids and there was no response when pyruvate was added to the media. These data, though not a direct measurement of GlyNG, highlights the importance of PEPCK-C in the maintenance of regular adipose tissue homeostasis.

The direct role of PEPCK-C in the regulation of hepatic glyceroneogenesis and lipid metabolism is not well studied, as most studies have hitherto focused on the gluconeogenic role of hepatic PEPCK. One study demonstrated that liver specific

PEPCK KO mice (130) developed severe hepatosteatosis in response to an overnight fast even though the expression of enzymes related to the degradation of fatty acids were significantly elevated. This suggests that hepatic PEPCK-C is required for proper homeostasis of hepatic lipid metabolism. In this chapter the methodology described in chapter 1 of this dissertation will be applied to mice expressing varying levels of PEPCK-C in order to determine the influence of this enzyme in overall lipid metabolism, focusing on the liver and the adipose tissue.

3 – Cataplerosis

Lipid synthesis occurs in the cytosol and requires acetyl-CoA as an obligatory substrate. Since there are no acetyl-CoA transporters in the mitochondria, mitochondrial acetyl-CoA is first converted to citrate which can be transferred to the mitochondria via the citrate carrier (CIC), encoded by the SLC25A1 gene, where it can be converted to oxaloacetate and acetyl-CoA by ATP-citrate lyase (ACL). The oxaloacetate formed this way can then be converted to malate by malate dehydrogenase which transported back to the mitochondria via the dicarboxylate carrier or can be further converted to pyruvate by malic enzyme, generating NADPH in the process. Cytosolic pyruvate can then be transported back to the mitochondria via the mitochondrial pyruvate transporter. This process is known as the citrate/malate/pyruvate cycle (Figure 30). An alternative shuttle involves the exchange of cytosolic malate with mitochondrial isocitrate. The cytosolic isocitrate can then be converted to oxaloacetate (with production of NADPH) and this oxaloacetate exchanges with mitochondrial malate via the Oxoglutarate Carrier protein (OGC). These cycles allow the transfer of acetyl-CoA and NADPH from the cytosol to the mitochondria, allowing lipogenesis to occur.

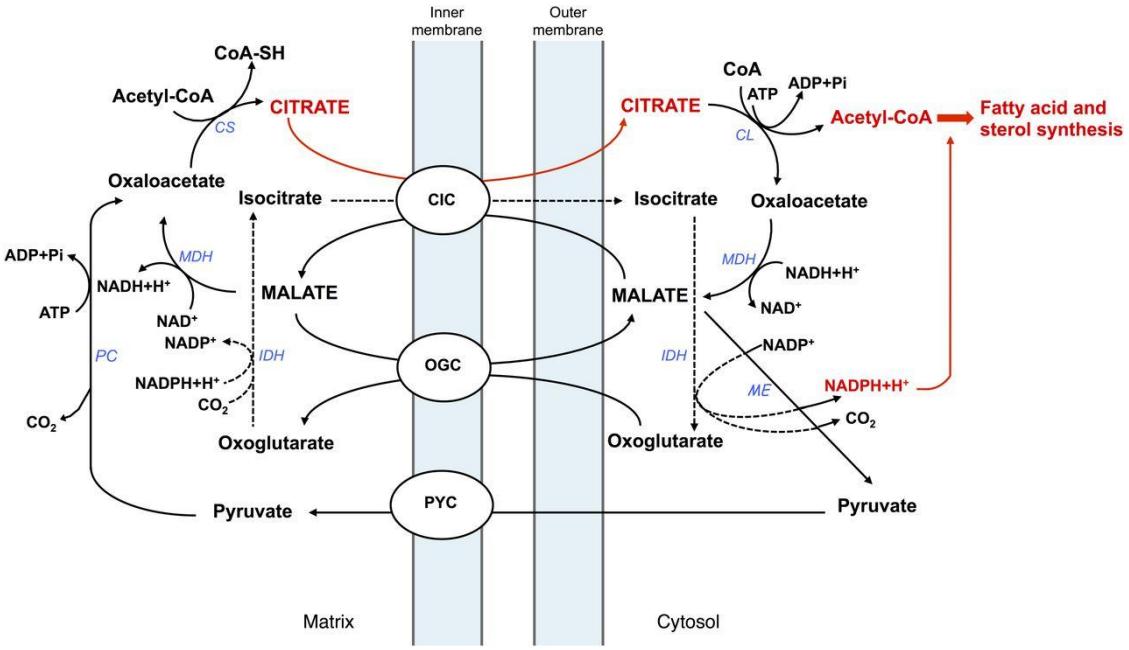

Figure 30 Hepatic mitochondrial shuttles and their involvement in lipogenesis. Adapted from (138)

Citrate is also a metabolite of the tricarboxylic acid (TCA) cycle, which is one of the central mitochondrial metabolic pathways that exists in all cells (with the exception of red blood cells, which do not possess mitochondria). Citrate is, therefore a metabolite at the intersection of mitochondrial energy metabolism and cytosolic lipogenesis and, therefore, it is important to maintain its concentration (and, consequently, the concentration of other TCA cycle metabolites) balanced. In order to achieve this balance, there are chemical reactions that increase the concentration of TCA cycle intermediates (anaplerotic reactions) to balance reactions that decrease their concentration (cataplerotic reactions). The major anaplerotic reaction is catalyzed by pyruvate carboxylase, which converts pyruvate to oxaloacetate, while the major cataplerotic reaction is catalyzed by PEPCK. There are other enzymes that can function as cataplerotic or anaplerotic reactions, by virtue of being reversible. These include glutamate dehydrogenase (which converts glutamate to α-ketoglutarate) and aspartate transaminase (that converts aspartate and α-ketoglutarate to oxaloacetate and glutamate) (Figure 31)

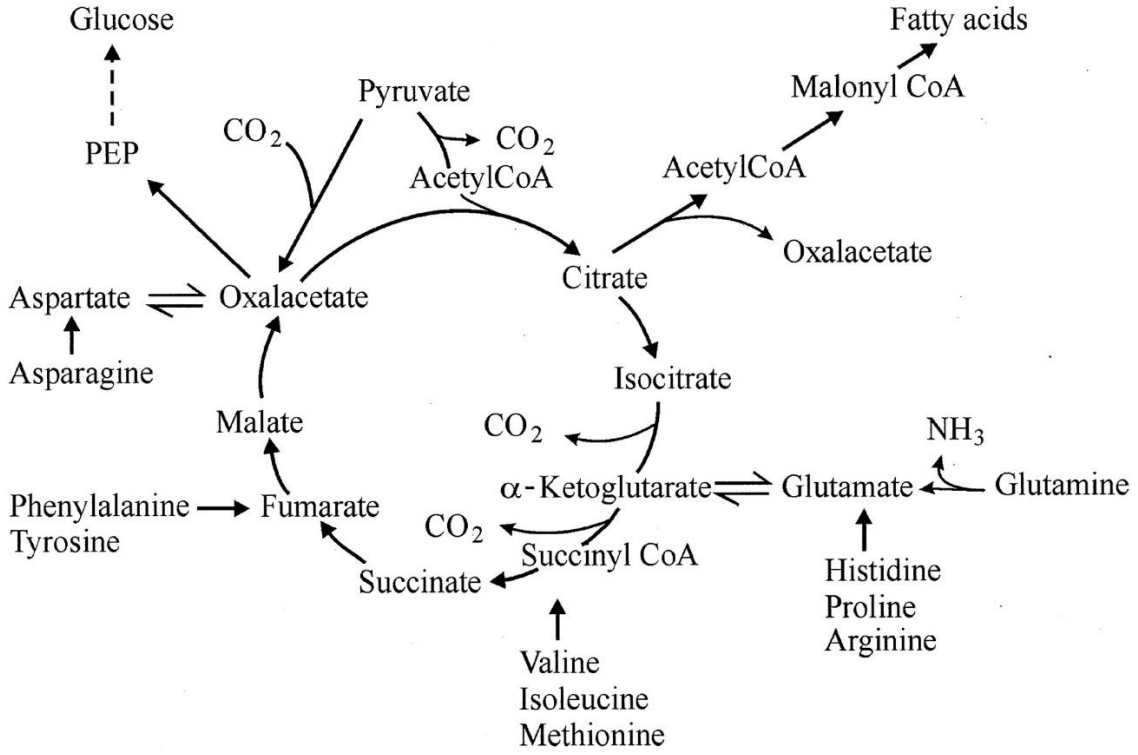

Figure 31: Anaplerotic and cataplerotic reactions of the TCA cycle. Adapted from (139)

PEPCK-C, being the major irreversible cataplerotic reaction, plays a significant role in the maintenance of TCA cycle activity. In fact, animals with whole-body knockout of PEPCK-C die two days after birth through a yet unknown mechanism (140). These animals are hypoglycemic and have elevated levels of plasma triglycerides, ammonia, lactate and β-hydroxybutyrate as well as increased levels of hepatic triglyceride, lactate and malate (140). The lethality of PEPCK-C whole body KO makes it difficult to probe its metabolic role. However, liver-specific KO mice have been created using Flox/Cre technology and these mice are viable (130). Surprisingly, they are able to maintain normal glucose and insulin levels, even after an overnight fast. However, after a 24h fast they have increased plasma FFA and triglycerides as well as increased hepatic triglyceride and malate levels. Since liver-specific PEPCK-KO mice have little to no glycogen after a 24h fast (130) there is significant interest in determining exactly how glycaemia is maintained. Another study (141) used ^{13}C and ^{2}H NMR isotope based techniques to show that liver-specific PEPCK-C KO mice only slightly decreased total production of glucose from TCA cycle intermediates. These data suggest that there is a compensatory increase in gluconeogenesis in extra-hepatic tissues, such as the kidney. Lastly, in a study where^{13}C and ^{2}H NMR isotope based flux analysis was performed in isolated perfused liver of liver-specific PEPCK-C KO mice (127) PEPCK-C was found to have a bigger influence in regulating TCA cycle activity than in the regulation of gluconeogenesis, with TCA cycle activity being robustly suppressed possibly due to the disruption of GNG and cataplerosis. These data further highlight the role of PEPCK-C in the control of cataplerosis and maintenance of mitochondrial metabolism and, therefore, partially determines the concentration of TCA cycle intermediates as evidenced by the increased malate concentration in PEPCK-C KO mice. If PEPCK-C expression also induces changes in other TCA cycle intermediates, those changes could lead to a dysregulated mitochondrial metabolic shuttling and, therefore, with decreased lipogenesis. To test this hypothesis, the hepatic cytosolic and mitochondrial fractions of mice expressing different levels of PEPCK-C were isolated and the concentration of TCA cycle intermediates was determined in both fractions.

4 – Methods

4.1 – Lipid metabolism

In order to determine the influence of PEPCK-C on lipid metabolism the methods described in chapter 1 of this dissertation were applied to mice expressing different levels of hepatic PEPCK-C. Briefly, 4 mice types were used 1) $pck^{flox/flox}$ mice that express normal levels of 2) PEPCK-C, $pck^{lox/neo}$ mice with about 30% of normal hepatic PEPCK-C expression, 3) $pck^{lox+\ neo/del}$ mice, with about 10% of normal hepatic PEPCK-C expression and 4) $pck^{flox/flox}$ +Alb-cre mice which do not express PEPCK-C in the liver. For simplicity, these mice lines will be referred to as Lox/Lox, Neo/Neo, Neo/Del and LKO for the remainder of this chapter.

Three different protocols were applied in the measurement of lipid metabolism in these mice. In all experiments, animals were I.P. injected with 27 µl/g body weight of 99.9% D_2O-saline and returned to their respective cages. Their drinking water was then supplemented with D_2O to match the target loading dose enrichment of 4%.

In the first protocol, mice were maintained on the deuterium enriched water for 4 days, having been given *ad libitum* access to food. These mice were then sacrificed in the morning of the 5th day. The goal of this experiment was to determine the role of PEPCK-C in the regulation of lipid metabolism on a whole body level. Since the lipid pool is much larger in adipose tissue compared to liver, the WAT lipid pool has a slower turnover and, therefore, a longer exposure time is required to be sure there is adequate incorporation of deuterium label in both lipid pools. In the second labeling protocol the deuterium labeling period was about 16h, and mice had *ad libitum* access to food. This shorter labeling period allows the determination of hepatic lipogenic flux without much influence from the adipose tissue. In the third protocol, mice were fasted for four hours prior to the bolus injection of D_2O, after which time they were returned to cages without food and with false bottoms to trap feces and prevent coprophagia. The labeling period for these mice was also 16h, for a total fasting period of about 20h. This protocol was used to study the effects of PEPCK-C on lipid synthesis in the fasted state, when the steatotic phenotype is more pronounced. In all protocols, at the end of the labeling period, mice were anesthetized and their livers and adipose tissue were quickly excised and snap frozen in liquid nitrogen until further analysis. The livers were processed for lipid analysis as described in chapter 1 of this dissertation.

4.2 – Determination of metabolic control coefficients

The flux control coefficient (FCC) of an enzyme over a pathway is, essentially a measure of the relative importance of flux through that enzyme relative to the overall pathway flux. FCC values range from 0 to 1, the former indicates that the enzyme has no influence on the pathway in question while the latter informs that a small change in the activity of the enzyme leads to significant changes in whole pathway flux. FCC was determined by plotting the total pathway flux versus the activity of the enzyme in question as previously described (127). If the graph thus obtained is an exponential function, the FCC can be determined by taking the natural logarithm of both variables and performing a linear regression analysis. The slope is defined as the FCC.

4.3 – Determination of metabolite concentrations

Metabolite concentrations were determined using commercially available enzymatic detection kits. Mouse ultrasensitive insulin kit was purchased from Alpco Diagnostics, Salem, NH. Triglyceride and glycerol assay kits were purchased from Cayman Chemicals, Ann Arbor, MI. FFA and ketone kits were purchased from WAKO diagnostics, Richmond, Va. Free cholesterol and cholesterol ester assay kits were purchased from Abcam, Cambridge, MA. Glucose levels were monitored using an Accu-Chek Aviva glucometer.

4.4 – Determination of tissue glycerol and fatty acid content.

Tissues were weighed and lipid were extracted using a modified version of the Folch extraction protocol (57). Briefly, 20ml of a mixture of 2:1 chloroform/methanol was added per gram of tissue (WAT or liver). Tissues were homogenized and shaken for approximately 30 min to promote the extraction of lipids. Saline was then added to the samples at a ratio of 4 ml per gram of tissue initially used. Samples were thoroughly mixed and then centrifuged at 1000 rpm for 10 min to promote phase separation. The lower phase containing the lipid fraction was collected into a 5ml volumetric flask and the total volume was adjusted to 5 ml with pure chloroform. After at least 4h, the remaining aqueous fraction was removed from the volumetric flasks and the volume once again adjusted to 5 ml with pure chloroform. 200 µl were collected for the determination of tissue triglyceride levels with the rest of the solution being dried down for NMR analysis,

as described in chapter 1. To determine hepatic glycerol and triglycerides, the aliquoted samples were dried down and reconstituted in 120µl of tert-butanol and 80µl of a 1:1 mix of triton X-100/methanol. 20µl of this mix were then used with a commercially available kit (Sigma-Aldrich) to determine the tissue contents of glycerol and triglycerides.

4.5 – Triglyceride export experiments

In order to determine the effects of PEPCK-C on hepatic triglyceride clearance, mice were fasted for either 4h or 16h, after which they were I.P. injected with poloxamer 407 (142), at a dose of 1 mg/g body weight as described. Blood samples were collected before the injection and at 1h, 2h, 4h, 6h and 20h post injection. Plasma triglycerides were assayed in plasma samples using a commercially available enzymatic detection kit (Cayman Chemical). Poloxamer 407 inactivates capillary lipoprotein lipase preventing triglycerides released as VLDL from being absorbed by extrahepatic tissues. VLDL production rate can be measured as the rate of appearance of triglycerides in plasma over time after the administration of Poloxamer 407.

4.6 –Ex vivo hepatic β-oxidation

In vitro oxidation of palmitate was performed as described by Dohm et al. (143) with few modifications. Briefly, overnight (16 h) fasted animals were anesthetized by Isoflourane and blood was collected by cardiac puncture into syringes containing EDTA. Liver was excised and submerged into ice cold reaction buffer (2 mM ATP, 0.05 mM CoASH, 1 mM dithiotreitol, 0.1 mM NAD^+, 1 mM DL-carnitine, 0.1 mM malate, 1 mM $MgCl_2$, 0.072 mM fatty acid free BSA, 100 mM sucrose, 10 mM K_2HPO_4, 80 mM KCl, 0.1 mM EDTA, 100 mM HEPES pH 7.3). ~500 mg of liver was homogenized in 2.5 ml of reaction buffer by 11 strokes of hand-operated Potter-Elvehjem homogenizer. Reaction was started by adding 3 ml of [1-^{14}C] palmitate (0.3 mCi, final 25 mM; PerkinElmer, Waltham, MA) to 200 ml of homogenate and the tube was immediately inserted into a vial with silicone septa containing filter paper soaked in hyamine hydroxide to capture $^{14}CO_2$. Reactions were incubated at 37°C for 4, 5, 6, and 7 min (duplicate for each time point) and terminated by injecting 100 ml of 7% (v/v) $HClO_4$. To ensure complete capture of $^{14}CO_2$, vials were left at 4°C overnight. Next day, reaction tube was centrifuged at 15,000 x *g* for 10 min. 200 ml of supernatant as well as filter paper were counted for incorporation of ^{14}C into acid soluble molecules and $^{14}CO_2$ in 6 ml of scintillation liquid.

After conversion to DPM and correction for scintillation counter efficiency, oxidation rate was calculated as picomoles of oxidized palmitate per minute per milligram of tissue.

4.7 – Metabolomic analysis of mitochondrial and cytosolic extracts

In order to determine if PEPCK-C knockdown dysregulates the equilibrium of mitochondrial shuttle mechanisms, mitochondria were isolated from livers of Lox/Lox, Neo/Neo, Neo/Del and LKO mice. Briefly, mice where either sacrificed after an overnight (16h fast) or with *ad libitum* access to food. Livers were quickly removed and a portion was cut and placed in an ice-cold solution of mitochondrial isolation buffer (25. mM sucrose, 10 mM Tris-HCl and 1 mM EGTA, pH 7.4), livers were washed 3 times to remove blood and weighed. The samples were then transferred to a Potter-Elvehjem homogenizer containing mitochondrial isolation buffer (1 ml/100 mg of tissue used). Samples were homogenized by hand with an average of 20-25 strokes per sample. The homogenizer was placed in an ice-filled container throughout the process to keep the sample chilled. The homogenate was placed in a chilled centrifuge tube and centrifuged at 700g for 5 minutes. The pellet was discarded and the supernatant was placed in a new pre-chilled centrifuge tube and centrifuged at 7500g for 10 minutes. The supernatant, which contains the cytosolic fraction of the liver was collected and stored at -80ºC until further analysis. The pellet, which contains the mitochondrial fraction, was resuspended in 10 ml of mitochondrial isolation buffer and centrifuged at 7500 for 10 min, and the supernatant was discarded. In order to minimize cross contamination of mitochondrial and cytosolic metabolites, mitochondria were once again resuspended in 10 ml of mitochondrial isolation buffer and centrifuged at 7500 for 10 min, with the supernatant being discarded. The remaining mitochondrial fraction was then resuspended in water (150 µl/g of initial tissue used) and sonicated to lyze mitochondrial membranes and release intramitochondrial metabolites to solution. The mitochondrial fraction was then stored in -80º C until further analysis.

4.8 – GC/MS determination of organic acid concentrations

Determination of the concentrations of organic acids was performed based on the method described by Des Rosiers et al (144) with some changes. Briefly, 20µL internal standard mix (U-^{13}C, U-^{2}H labeled lactate, pyruvate succinate, fumarate, citrate and α-ketoglutarate), 350 µL of 8% sulfosalicylic acid and 50 µL of 5M hydroxylamine-HCl were

added to the 50 µl isolated cytosolic or mitochondrial fraction. Samples were then centrifuged at 3000 RPM for 15 minutes at 4ºC and the supernatant was collected. The supernatant was then neutralized to pH 6-7 using 2N KOH and incubated for 60 minutes at 65 ºC. The sample was then acidified to pH 2.0 with 1M HCl. 250 mg of NaCl was then added to the solution. The solution was extracted twice with 2 ml of ethyl acetate. The ethylacetate phase was then evaporated to dryness and reacted with 80ul of mixture of N-methyl-N-(t-butyldimethylsilyl)trifluoroacetamide and acetonitrile (1:1 ratio) at 60 ºC for 60 minutes.

Analysis of organic acids was performed via GC/MS (Agilent 5975C), using a HP-5MS capillary column (non-polar) with 0.25 mm ID, 30m length and 0.25 µm film thickness. The temperature gradient used was as follows: Initial temperature 150 ºC, increase to 205 at 5 ºC/min, followed by increase to 250 ºC at 50 ºC/min for 1 minute and increase to 275 ºC at 25 ºC/min for 2 minutes.

Ions monitored were m/z 261-264 (lactate and labeled lactate I.S), 274-277 (pyruvate and labeled pyruvate I.S), 289-293 (succinate and labeled succinate I.S), 287-291 (fumarate and labeled fumarate I.S), 419 (malate), 432-436 (oxaloacetate), 446-450 (α-ketoglutarate and labeled α-ketoglutarate I.S), and 459-465 (citrate and labeled citrate I.S).

4.9 – Gene expression analysis

Total RNA was extracted from tissues with RNA Stat-60 reagent (Tel-Test, Friendswood, TX). cDNA was synthesized from 4 µg of RNA treated with 0.2 U DNase (Qaigen, Valencia, CA) using High Capacity cDNA Reverse Transcription Kit (Applied Biosystems, Carlsbad, CA). Quantitative real-time PCR was run in triplicates using SYBR GreenER™ qPCR SuperMix for ABI PRISM® instrument (Invitrogen, Carlsbad, CA) and ABI PRISM 7900HT Fast Real-Time PCR System (Applied Biosystems). Gene expression was normalized to cyclophilin b (Ppib).

5 – Results

5.1 – Plasma metabolite levels in fed PEPCK-C KD mice

Plasma metabolite profiles of fed PEPCK-C KD mice (Table 8) show that Neo/Del mice have 20% higher levels of blood glucose and 47% higher insulin levels compared to controls, suggesting the that these mice were more insulin resistant than controls. Triglyceride levels were significantly decreased 32% and 48% in Neo/Del and LKO animals, respectively and glycerol levels were reduced by 38% in LKO mice. This was accompanied by a significant decrease in free fatty acids in all PEPCK-C KD mice (38%, 33% and 25% in Neo/Neo, Neo/Del and LKO mice, respectively). There were no changes in ketones and free cholesterol but cholesterol esters were significantly increased by 53% in LKO mice (Table 8).

Table 8: Plasma metabolite levels of mice expressing different levels of PEPCK-C. * p value < 0.05 vs Lox/Lox. Data is presented as average ± SEM.

Plasma metabolites	Lox/Lox	Neo/Neo	Neo/Del	LKO
Glucose (mg/dl)	126±9	130±4	154±5*	141±7
Insulin (ng/ml)	0.16±0.02	0.21±0.05	0.33±0.05*	0.21±0.05
Triglycerides (mg/dl)	47±6	37±4	32±3*	25±3*
Glycerol (mg/L)	3.1±0.4	2.7±0.3	2.7±0.5	1.9±0.3*
Free fatty acids (mEq/L)	0.62±0.04	0.39±0.07*	0.41±0.03*	0.47±0.05*
Total ketones (µmol/L)	212±41	204±30	225±24	223±52
Free cholesterol (mg/dl)	17±3	12±2	14±1	16±1
Cholesterol esters (mg/dl)	48±4	32±7	52±5	71±3*

5.2 – Tissue triglyceride levels.

To determine the effects of PEPCK-C on tissue lipids, the levels of glycerol and triglycerides in both the white adipose tissue and the liver of *ad libitum* fed PEPCK-C animals were measured (Figure 32). In the fed state, there were no significant differences in either triglyceride associated glycerol (TG-Gly) or fatty acids (TG-FA) in either liver (Figure 32A-B) or white adipose tissue (Figure 32C-D), even though the amount of WAT TG-Gly and TG-FA tended to be higher in LKO mice (p value = 0.06 and 0.07 vs control, respectively).

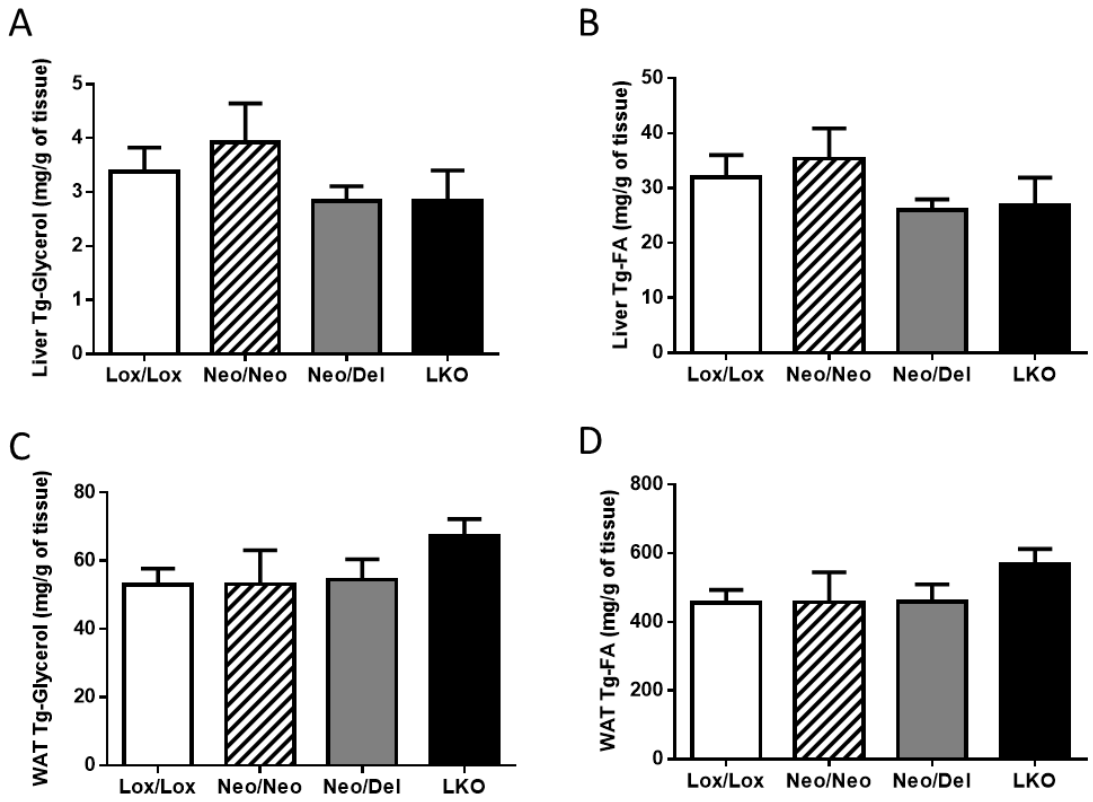

Figure 32. Levels of A) hepatic Tg-Glycerol, B) hepatic Tg-FA, C) WAT Tg-Glycerol and D) WAT Tg-FA in control and PEPCK-C transgenic mice. Error bars represent SEM.

5.3 – VLDL export

To verify if triglyceride export from the liver was altered in PEPCK-C KD mice, these animals were treated with poloxamer 407. Up to 6h post injection there is no significant difference in VLDL release to the bloodstream in all 4 genotypes. (Figure 33).

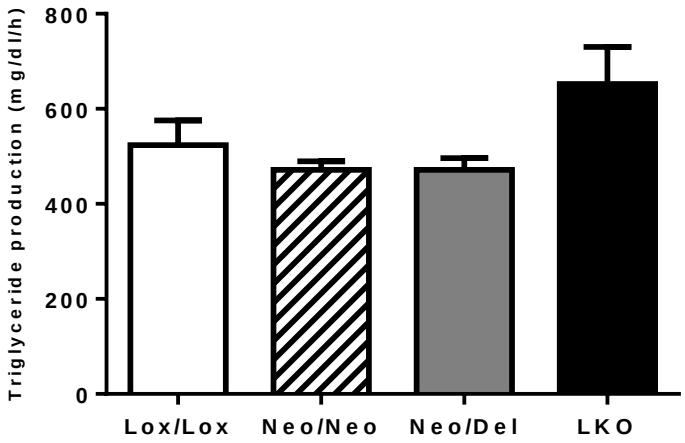

Figure 33: Rates of VLDL excursion in Lox/Lox, Neo/Neo, Neo/Del and LKO mice 4 hours after injection of poloxamer 407.

To further investigate the effects of fasting time on VLDL export a second poloxamer experiment was performed. In this experiment, mice were fasted overnight for 16h before injection of poloxamer 407. This experiment also serves the purpose of measuring VLDL export in a metabolic condition where LKO mice are overtly hepatosteatotic. In this experiment blood was collected before the injection and 1h, 2h, 4h and 6h later, and the samples were treated as described above. Under these conditions, there are no differences in VLDL release in any of the PEPCK-C KD mice (Figure 34).

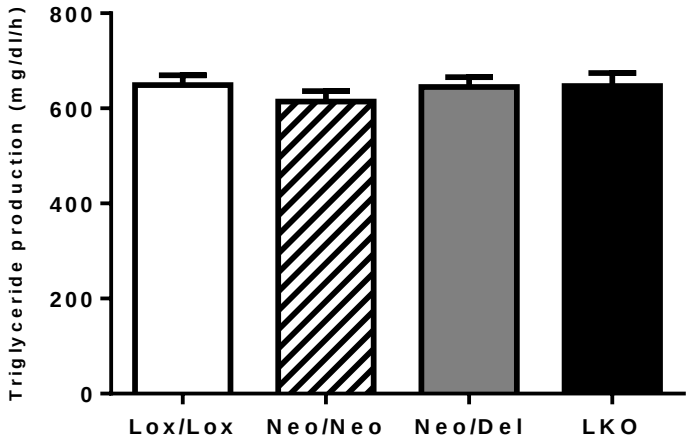

Figure 34: Rates of VLDL excursion in Lox/Lox, Neo/Neo, Neo/Del and LKO mice injected with poloxamer after a 16h fast

5.4 – Hepatic β-oxidation

In order to test whether the β-oxidation pathway in livers of PEPCK-C mice remained responsive, [1-^{14}C]palmitate was administered to liver homogenates from PEPCK-C mice. When this tracer undergoes β-oxidation, it forms [1-^{14}C] acetyl-CoA, which can enter the TCA cycle. In the second turn of the cycle, the labelled carbon is released as CO_2 during the conversion of isocitrate to α-ketoglutarate (catalyzed by isocitrate dehydrogenase). Another possible fate for the acetyl-CoA is the synthesis of ketone bodies, which will remain in the homogenate fraction. The total amount of detected radioactivity was significantly decreased in Neo/Neo and Neo/Del animals, but unchanged in LKO animals (Figure 35). When analyzing the different sources of radioactivity, it becomes clear that, in all PEPCK-C animals there is a clear reduction in the contribution of CO_2 to total detected radioactivity. Radioactivity in the acid soluble fraction was significantly elevated in LKO mice, but unchanged in Neo/Neo or Neo/Del mice (Figure 35). These data suggest that β-oxidation is decreased in Neo/Neo and Neo/Del mice while LKO mice have normal β-oxidation. This data also informs about the fate of the acetyl-CoA generated through oxidation of the labeled fatty acids. In all PEPCK-C mice there was a significant decrease in the total amount of radioactivity detected as CO_2. This correlates well with previous reports (127) where PEPCK-C levels were found to positively correlate with hepatic TCA cycle, as decreased TCA cycle activity would reduce the amount of CO_2 released. The radioactive activity detected in the acid soluble fraction in Neo/Neo and Neo/Del mice was not different from control,

albeit being increased in LKO mice, which could be suggestive of an accumulation of radioactive label in TCA cycle intermediates or other compounds such as ketone bodies (Figure 35).

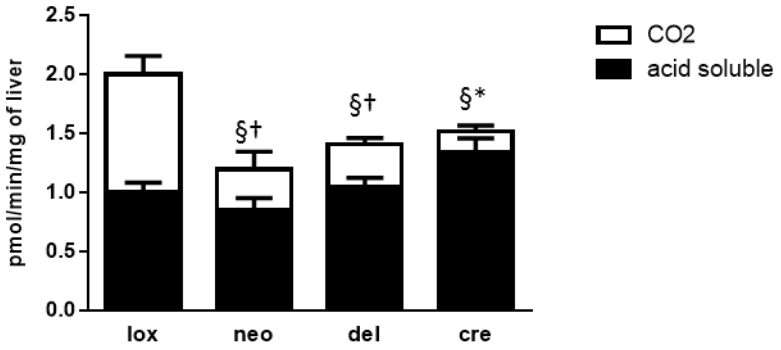

Figure 35: Relative radioactive counts in CO_2 and acid soluble fraction of liver homogenates of PEPCK-C mice per mg of tissue used. Error bar represent SEM. * $p<0.05$ for radioactivity in acid soluble fraction vs Lox/Lox. § $p<0.05$ for radioactivity in CO_2 fraction vs Lox/Lox. † $p<0.05$ for total radioactivity.

5.5- Whole body lipid biosynthetic fluxes in PEPCK-C transgenic mice: 4 day D_2O exposure

In order to determine the effect of liver knockdown on liver and adipose PEPCK-C, mRNA was quantified in both tissues. PEPCK-C mRNA was significantly decreased in the livers of all PEPCK-C KD mice, and in the adipose of Neo/Neo and Neo/Del mice (Figure 36). PEPCK-C levels were not different from control mice in the adipose tissue of LKO mice.

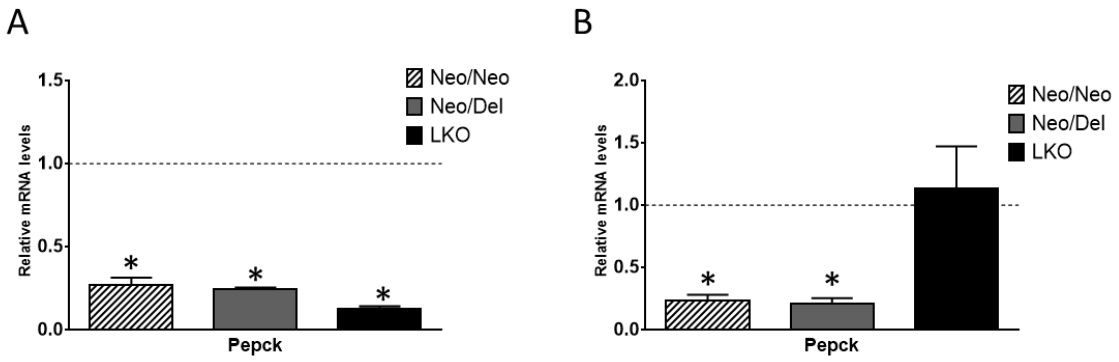

Figure 36: PEPCK-C mRNA levels in A) Liver and B) White adipose tissue of ad libitum fed mice. Dashed line represents the relative amount of mRNA in control mice. Bars are SEM. * $p<0.05$ vs Lox/Lox mice.

To measure lipid metabolism in these animals, lipid synthesis was determined in Lox/Lox, Neo/Neo Neo/Del and LKO mice. After 4 days of D_2O exposure, a significant decrease in hepatic FA synthesis was observed in the livers of Neo/Neo and Neo/Del mice (both in relative contribution and mass of new lipids made during the labeling period). However, there was no significant difference in LKO mice compared to controls (Figure 37A-B). The differences in total glycerol synthesis were less striking, as only Neo/Del mice showed a significant decrease in glycerol production (Figure 37C-D). Hepatic unsaturated fatty acid production was significantly reduced in both Neo/Neo and Neo/Del mice but unchanged in LKO mice (Figure 37E-F). There was an increase in the contribution of fatty acid elongation to total fatty acid synthesis in all knockdown mice (Figure 37G). The total amount of elongated fatty acids also followed this trend, but there was no statistical power to reach significance in any of the 3 transgenic mice. This data indicates that PEPCK-C knockdown in the liver significantly changes hepatic lipid fluxes, but animals with complete liver-specific knockdown of this enzyme were not different from controls.

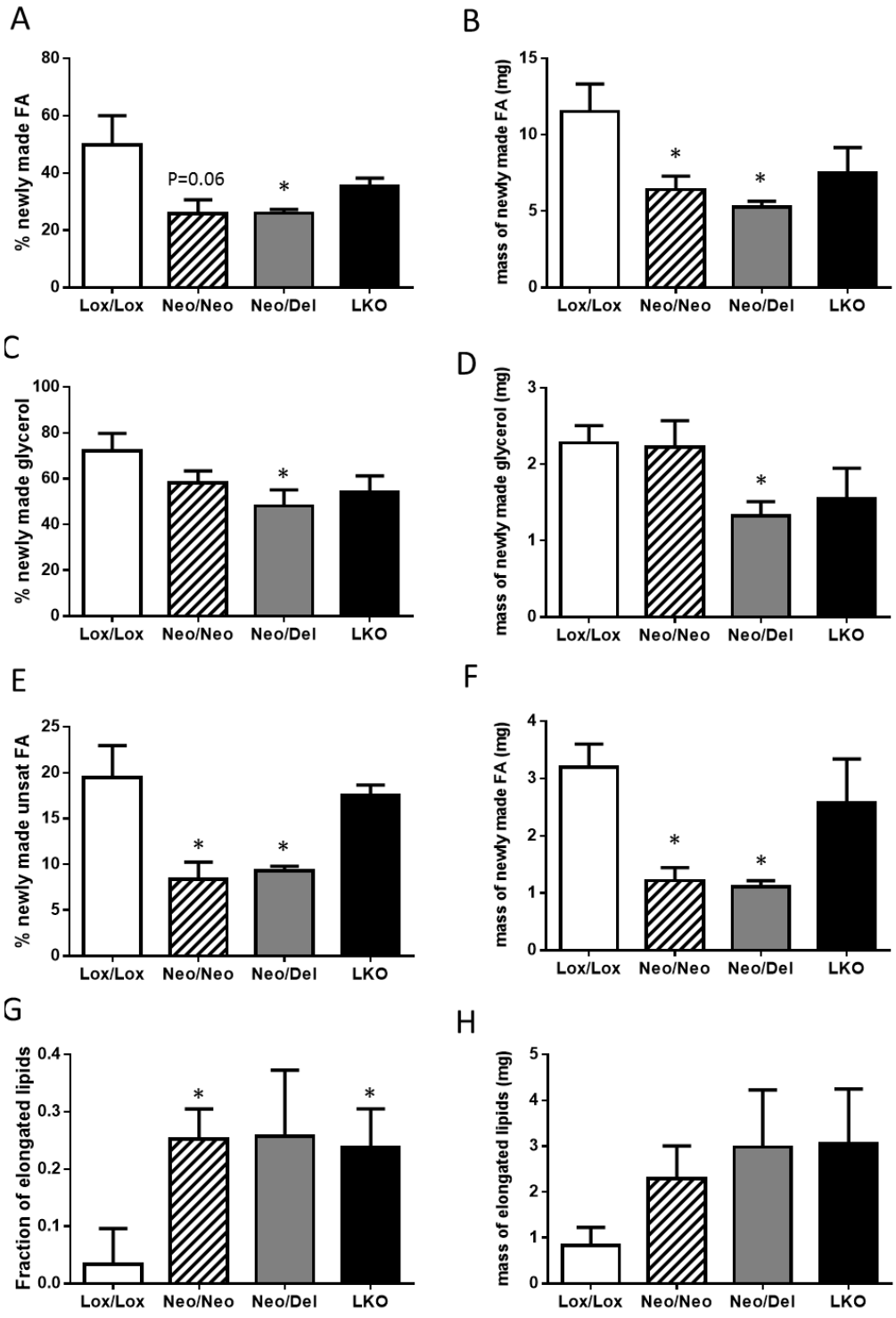

Figure 37: Hepatic lipid biosynthetic fluxes in fed mice: A) percent contribution of DNL to total fatty acid synthesis. B) Percent of newly made triglyceride-associated fatty acids during the labeling period. C) Percent contribution of de novo synthesis to glycerol production D) Total mass of newly made glycerol. E) Percent contribution of desaturation to the synthesis of unsaturated fatty acids. F) Total mass of newly made unsaturated fatty acids during the labeling period. G) Fraction and H) mass of lipids that underwent chain elongation. Error bars represent SEM. * p value < 0.05 vs Lox/Lox mice.

In white adipose tissue, both the contribution of DNL to fatty acid synthesis and the amount of newly made fatty acids were significantly increased in the white adipose tissue (Figure 38A-B). Though the relative contribution of DNL to FA synthesis in Neo/Neo and Neo/Del mice was not statistically different, the total amount of newly made lipid was significantly reduced in both of these animals while LKO mice a compensatory increase in DNL º (Figure 38A-B). The same pattern was found for the synthesis of unsaturated fatty acids, with LKO animals showing increased percent synthesis and mass of newly made lipids, while Neo/Neo and Neo/Del animals had a decreased total mass of newly made lipids. Only LKO animals had a difference in glycerol synthesis, having significantly increased % and total new glycerol (Figure 38C-D). There was no detectable elongation in the WAT of any of the four groups of mice (data not shown). This data suggests that PEPCK-C also plays an important role in the maintenance of adipose tissue lipid homeostasis, with a reduction in PEPCK-C levels leading to a reduction in fatty acid synthesis. Also, liver-specific knockout animals have significantly higher production of fatty acids in their adipose tissue, possibly in order to compensate for deficient hepatic lipid synthesis.

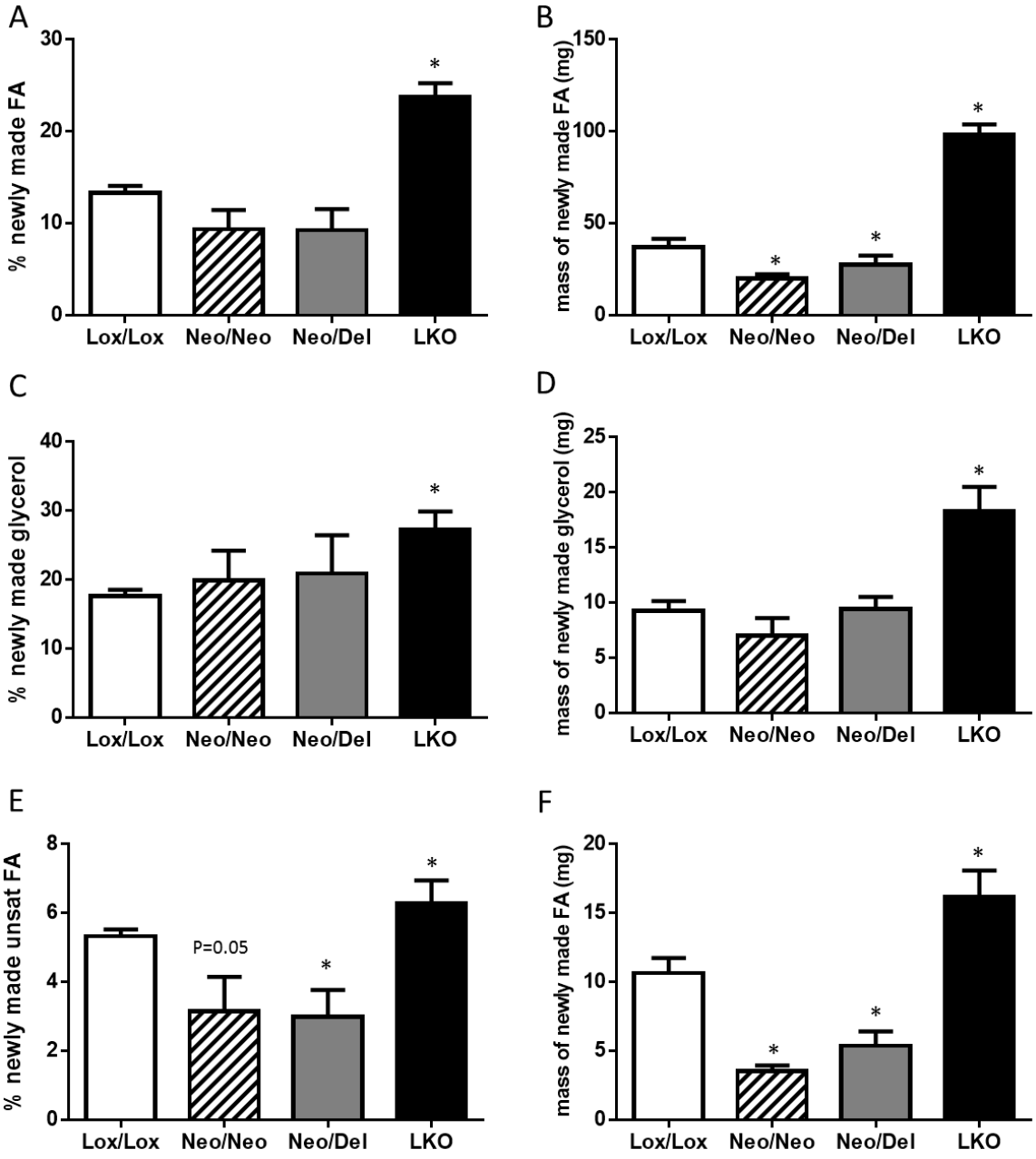

Figure 38: WAT lipid biosynthetic fluxes in fed mice: A) percent contribution of DNL to total fatty acid synthesis. B) Percent of newly made triglyceride-associated fatty acids during the labeling period. C) Percent contribution of de novo synthesis to glycerol production D) Total mass of newly made glycerol. E) Percent contribution of desaturation to the synthesis of unsaturated fatty acids. F) Total mass of newly made unsaturated fatty acids during the labeling period. Error bars represent SEM. * p value < 0.05 vs Lox/Lox mice.

To further understand how PEPCK-C acts on lipid metabolism, mRNA levels of enzymes related to lipid synthesis were measured. Neo/Neo, Neo/Del and LKO mice had decreased mRNA levels of Acl (ATP-citrate lyase), Acc1 (acetyl-CoA carboxylase),

Fasn (fatty acid synthase) and Scd-1 (stearoyl-CoA desaturase) in animals, concomitant with the reduction of hepatic fatty acid synthesis in these animals. In contrast, Elovl5 mRNA was significantly increased in the liver of Neo/Neo and Neo/Del animals while Elvol6 mRNA was significantly decreased in Neo/Del and LKO animals. Elvol5 mainly elongates essential fatty acids derived from the diet, while Elovl6 uses palmitate as the preferred substrate, suggesting that detected increase in hepatic elongation flux might be due the preferential elongation of diet-derived fatty acids. There were no significant differences in the mRNA levels of Acl, Acc1, Fasn and Scd-1 in the adipose tissue of Neo/Neo or Neo/Del mice, but were all of these enzymes were significantly upregulated in the WAT in LKO animals, helping to bolster the idea that there is a compensatory increase in fatty acid production in these animals to compensate the decrease in fatty acid synthesis of the liver.

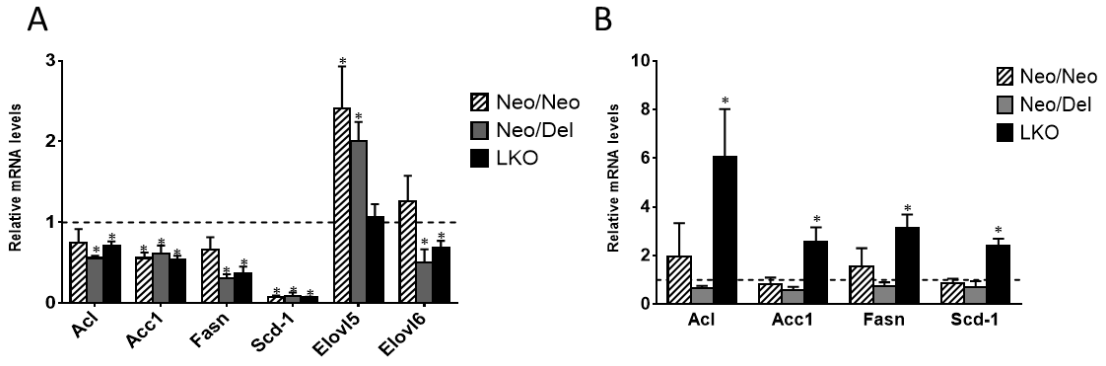

Figure 39: Relative mRNA levels of genes related to lipid metabolism in A) Liver and B) White adipose tissue of ad libitum fed mice. Dashed line represents the relative amount of mRNA in control mice. Bars are SEM. * $p<0.05$ vs Lox/Lox mice. Acl, ATP citrate lyase; ACC1, acetyl-CoA carboxylase 1; Fasn, Fatty acid synthase; SCD-1: Stearoyl-CoA Desaturase 1; ELOVL, Elongation of very long chain fatty acids.

5.5- Hepatic lipid biosynthetic fluxes in PEPCK-C KD mice: overnight D_2O exposure

To more specifically target the rates of hepatic lipid biosynthetic fluxes, PEPCK-C transgenic mice were administered with D_2O for a period of approximately 16h. Mice had *ad libitum* access to food or where fasted overnight. There were no observable differences in the fed state but, as previously reported (130), there was a significant increase in the amount of hepatic glycerol in livers of fasted LKO mice. A similar trend

was observed for hepatic fatty acids, with a significant increase being observed in the livers of fasted LKO mice (Figure 40).

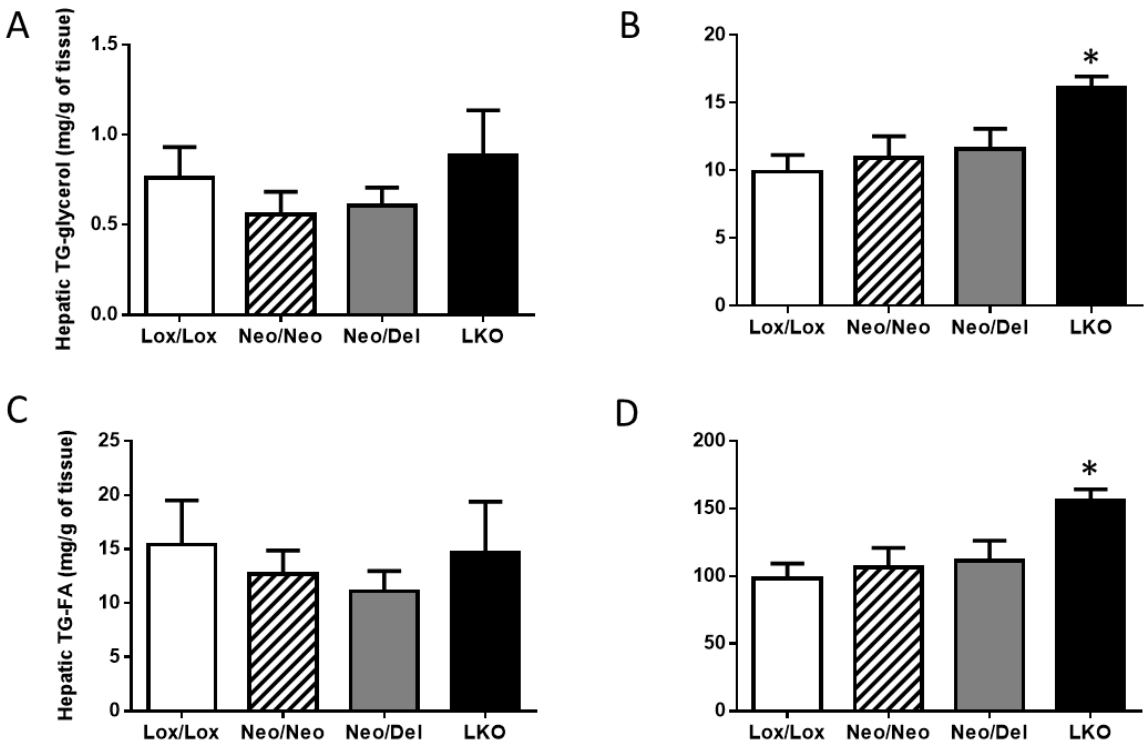

Figure 40: Hepatic glycerol levels in fed mice (A) and fasted mice (B). Hepatic fatty acids in fed mice (C) and fasted mice (D).

Contributions of de novo lipogenesis to the hepatic fatty acid pool were reduced in Neo/Neo mice but were not in Neo/Del and LKO mice (Figure 41A). The total amount of newly made fatty acids follows a pattern similar to that observed in the livers of fed mice administered D_2O for 4 days, as there was a tendency for all the genotypes to have a decreased amount of newly made fatty acids, (Figure 41B). The same trend was observed for glycerol synthesis, with both Neo/Neo and LKO mice having a significantly reduced contribution of de novo synthesis to the glycerol pool (Figure 41C), and a tendency for the total amount of newly made glycerol to be reduced (Figure 41D). The percentage contribution of new synthesis to unsaturated fatty acids was similar in all animals (Figure 41E) but the total amount of newly made unsaturated fatty acids tended to be lower in both Neo/Neo and Neo/Del animals. Finally, though all mice had a significant increase in the ratio of lipids that underwent elongation (Figure 41F), the total mass of elongated lipids wasn't different between the genotypes (Figure 41G).

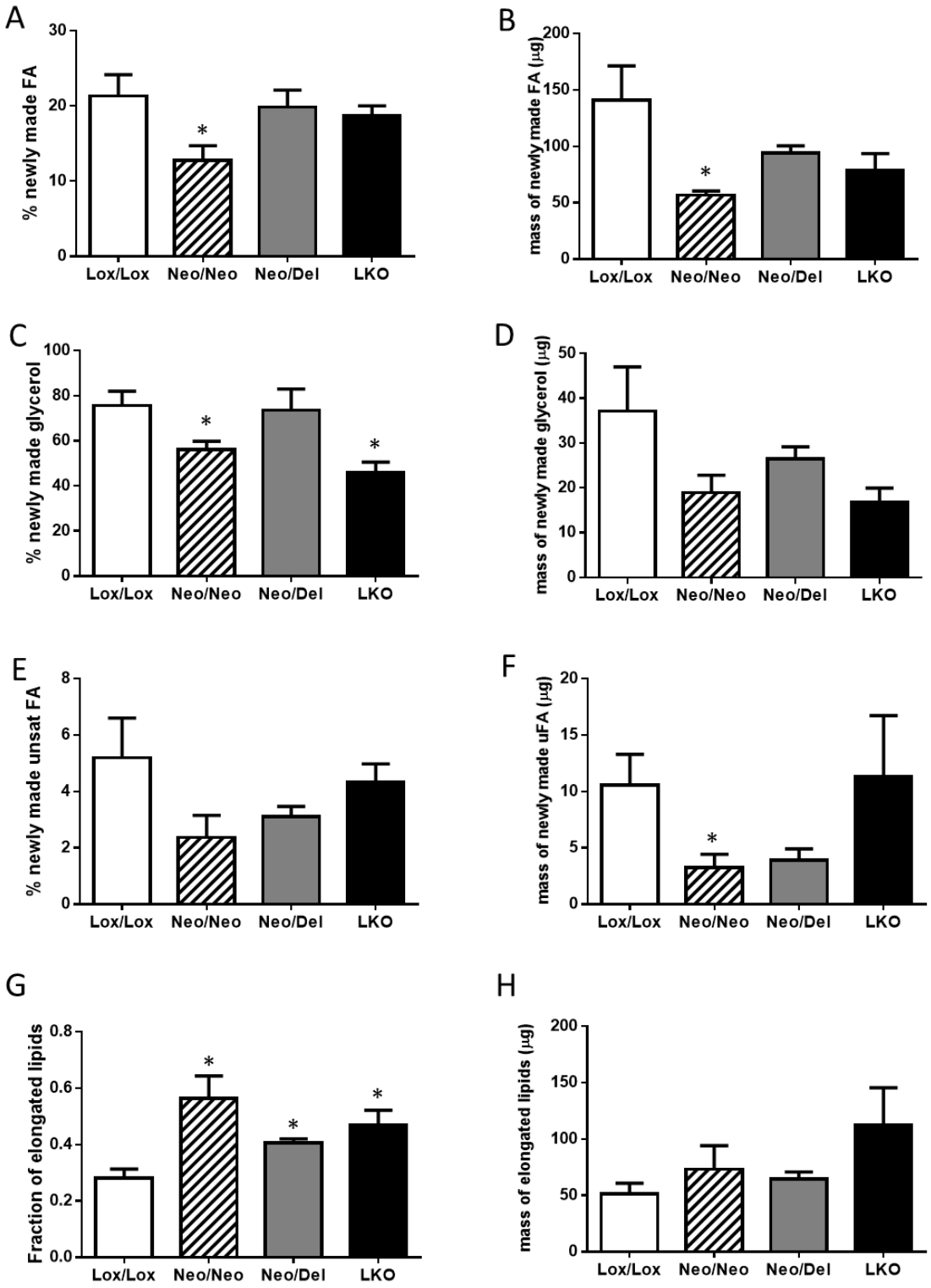

Figure 41: lipid biosynthetic fluxes in fed mice after overnight exposure to D_2O: A) percentage contribution of DNL to total fatty acid synthesis. B) Percentage of newly made triglyceride-associated fatty acids during the labeling period. C) Percentage contribution of de novo synthesis to glycerol production D) Total mass of newly made glycerol. E) Percentage contribution of desaturation to the synthesis of unsaturated fatty acids. F) Total mass of newly made unsaturated fatty acids during the labeling period. Error bars represent SEM. * p value < 0.05 vs Lox/Lox mice.

Since LKO animals develop hepatic steatosis after an overnight fast, we examined if defective regulation of fasting lipid metabolism could be a contributing factor to the steatotic phenotype by measuring lipid fluxes in fasted PEPCK-C KD animals. There was a significant increase in the contribution of DNL to FA (Figure 42A) and the total amount (Figure 42B) of newly made fatty acids, with the latter being elevated by approximately 50% and 400% in Neo/Del and LKO mice, respectively. There was a tendency for this value to be higher in Neo/Neo mice as well. The contribution of new synthesis to the total glycerol pool was unchanged in Neo/Neo and Neo/Del mice, but was reduced by nearly half in LKO animals (Figure 42C). However, there was no differences in the total amount of newly made glycerol (Figure 42D). Synthesis of new unsaturated fatty acids tended to be elevated in Neo/Neo mice, while in LKO mice there was approximately a 300% increase in this value (Figure 42E). The total mass of newly made unsaturated fatty acids was similar, with Neo/Neo mice showing a tendency for this value to be elevated and LKO mice have almost 800% more newly made unsaturated fatty acids (Figure 42F). Finally, though the fraction of elongated lipids was similar in all animals (Figure 42G), the mass of lipids that underwent elongation was elevated by 200% and 300% in Neo/Del and LKO mice, respectively. These data suggest that PEPCK-C is an important enzyme in the regulation of the metabolic changes that occur in the transition from the fed to the fasted state. It also suggests that increased fatty acid synthesis in the fasted state is a contributing factor for the development of hepatic steatosis in LKO mice which, surprisingly, produce more hepatic fatty acids during in the fasted state than in the fed state.

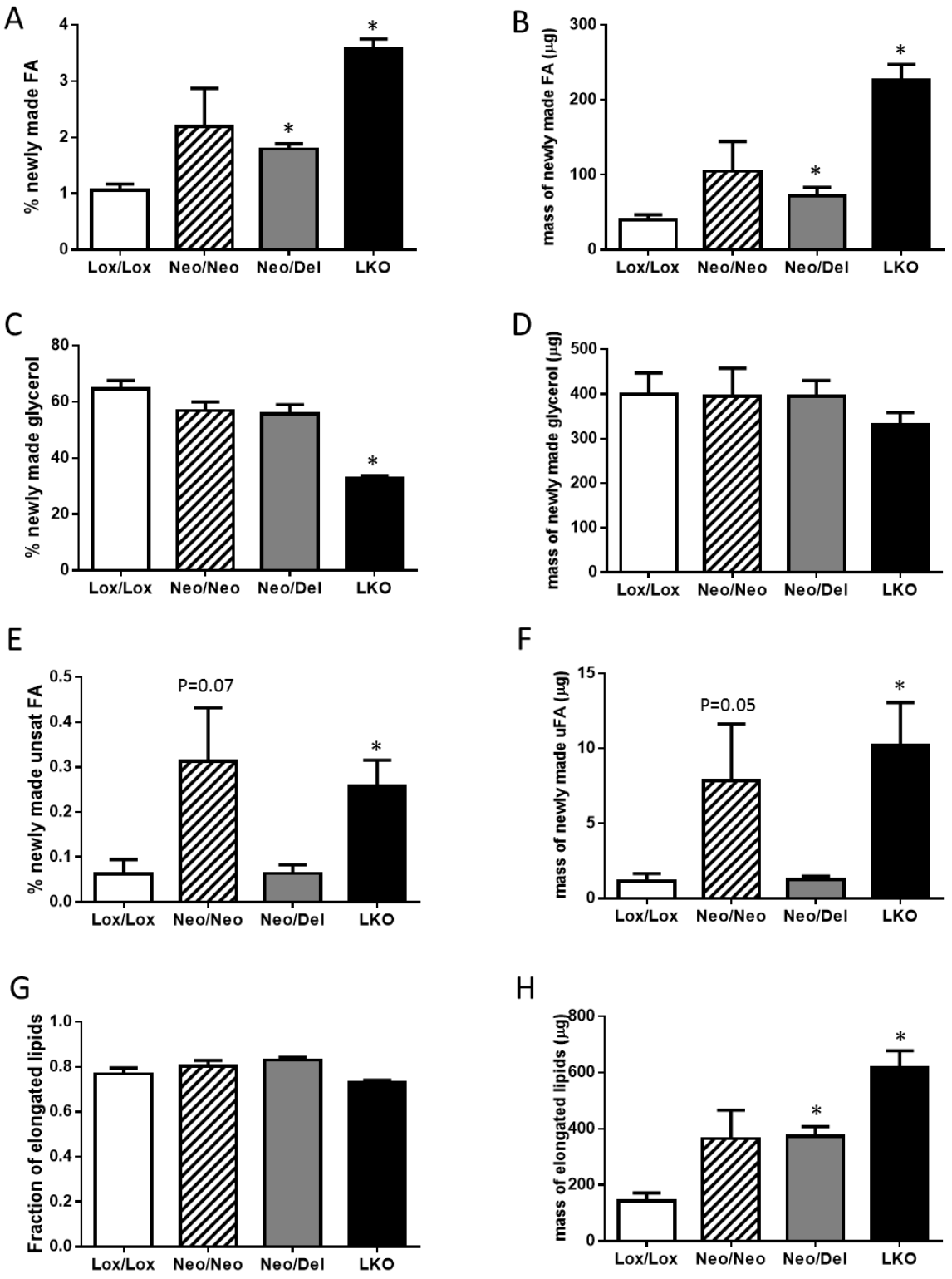

Figure 42: lipid biosynthetic fluxes in fasted mice after overnight exposure to D_2O: A) percent contribution of DNL to total fatty acid synthesis. B) Percent of newly made triglyceride-associated fatty acids during the labeling period. C) Percent contribution of de novo synthesis to glycerol production D) Total mass of newly made glycerol. E) Percent contribution of desaturation to the synthesis of unsaturated fatty acids. F) Total mass of newly made unsaturated fatty acids during the labeling period. Error bars represent SEM. * p value < 0.05 vs Lox/Lox mice.

5.6 – Flux control coefficient determination

For each experiment where lipid fluxes were calculated in the liver, the Flux Control Coefficient (FCC) was calculated by plotting the total mass of newly made lipids vs the total amount of hepatic PEPCK-C protein. It was assumed that PEPCK-C protein amounts followed the trend described by Burgess *et al.* (127). Table 9 shows the calculated values of FCC for each of the fluxes, as well as the goodness-of-fit, indicated by the R^2 value of the slope.

Table 9: Calculated slope and R^2 of the linear regression for the effects of PEPCK-C on lipid biosynthetic fluxes in each of the D_2O labeling protocols. Grey shades indicate experiments with an R^2 above 0.85.

	4 day experiment		**16h experiment**			
Fed metabolites	**Liver - Fed**		**Liver - Fed**		**Liver- Fasted**	
	FCC	R^2	FCC	R^2	FCC	R^2
Fatty acids	**-0.33**	**0.9035**	0.14	0.2204	**0.37**	**0.9053**
Glycerol	**-0.25**	**0.8739**	0.1	0.1267	0.01	0.0398
Unsat Fatty acids	-0.46	0.7672	0.51	0.6525	0.17	0.0491
Elongation	0.19	0.7914	-0.08	0.3753	**0.47**	**0.8751**

5.7 – Hepatic mitochondrial and cytosolic metabolite levels.

The maintenance of a concentration gradient between cytosol and mitochondria is essential for metabolic shuttling between the two compartments. A key point in the synthesis of lipids involves the export of citrate from the mitochondria into the cytosol, where all the lipogenic enzymes are located. In order to determine if the observed lipid phenotypes could be attributed to dysregulation of the of metabolite shuttling between the cytosol and the mitochondria of PEPCK-C mice, hepatic mitochondria and their respective cytosolic fraction were isolated and a partial metabolomics analysis was performed on these fractions, focusing on the determination of the concentration of organic acids. Table 10 shows the concentrations of organic acids in mitochondria and cytosol of mice with ad libitum access to food and Table 11 shows the same

measurements performed in mice that had been fasted overnight for 16h prior to the livers being collected.

Table 10: Metabolite concentration of hepatic cytosol and mitochondria from fed PEPCK-C mice. Data is expressed as average±SEM. * p<0.05 vs Lox/Lox. † 0.05 < p < 0.08.

Fed metabolites	Cytosol (µg/g of liver)				Mitochondria (µg/g of liver)			
	Lox/Lox	Neo/Neo	Neo/Del	LKO	Lox/Lox	Neo/Neo	Neo/Del	LKO
Lactate	125±17	93±10	102±13	111±13	8.8±0.6	7.3±0.4	8.1±0.4	8.5±0.5
Pyruvate	49±7	47±2	45±4	54±5	7.3±0.5	7.4±0.4	7±1	7.0±0.5
Succinate	22.8±0.2	23.4±0.3	23.7±0.4	23.3±0.2	3.74±0.04	3.8±0.1	3.66±0.03	3.74±0.06
Fumarate	18±7	36±0.3	42±7*	31±8	1.9±0.2	2.9±0.2*	3.0±0.2*	2.7±0.5
Malate	72±10	91±3†	101±7*	89±8	11.2±0.3	11.3±0.3	11.4±0.3	12.6±0.8
Oxaloacetate	37±15	2158±512*	2426±550*	1801±933	86±5	303±69*	206±72*	205±63*
α-ketoglutarate	18±6	39±7†	30±6	26±7†	3±1	6±1	4.9±1.3	2.7±0.6
Citrate	55±1	57±1	55±1	54.4±0.4	8.8±0.1	9.4±0.2*	9.1±0.2*	8.9±0.2

Table 11: Metabolite concentration of hepatic cytosol and mitochondria from fasted PEPCK-C mice. Data is expressed as average±SEM. * p<0.05 vs Lox/Lox.

Fasted metabolites	Cytosol (µg/g of liver)				Mitochondria (µg/g of liver)			
	Lox/Lox	Neo/Neo	Neo/Del	LKO	Lox/Lox	Neo/Neo	Neo/Del	LKO
Lactate	87±7	58±5*	57±3*	72±3	8.3±0.4	7.2±0.4	7.8±0.3	8.3±0.1
Pyruvate	41±2	37±1†	37±1*	50±5	6.8±0.2	6.2±0.1*	46.8±0.5	7.1±0.3
Succinate	22.8±0.1	22.5±0.1	23±3	23.5±0.2*	3.68±0.02	3.64±0.02	3.66±0.02	3.68±0.03
Fumarate	10.1±0.6	19±3*	27±2*	66±4*	1.53±0.04	2.3±0.2*	2.6±0.1*	3.5±0.3*
Malate	62.2±0.7	73±2*	82±2*	137±8*	9.8±0.1	10±0.2*	11.0±0.1*	712.1±0.3*
Oxaloacetate	168±40	517±179	1592±286*	3215±789*	142±29	66±11*	385±9†	348±127
α-ketoglutarate	19±5	28±8	38±5*	107±4*	4.7±0.4	2.0±0.4*	4.7.±1.0	6.9±0.5*
Citrate	56.5±0.3	57±1	58±2	58±1	8.6±0.1	9.4±0.1*	9.7±0.4*	9.4±0.3*

Since the ratio between mitochondrial and cytosolic metabolite levels is essential in the regulation of mitochondrial shuttling, Figure 43 shows the concentration ratios of metabolites in PEPCK-C mice.

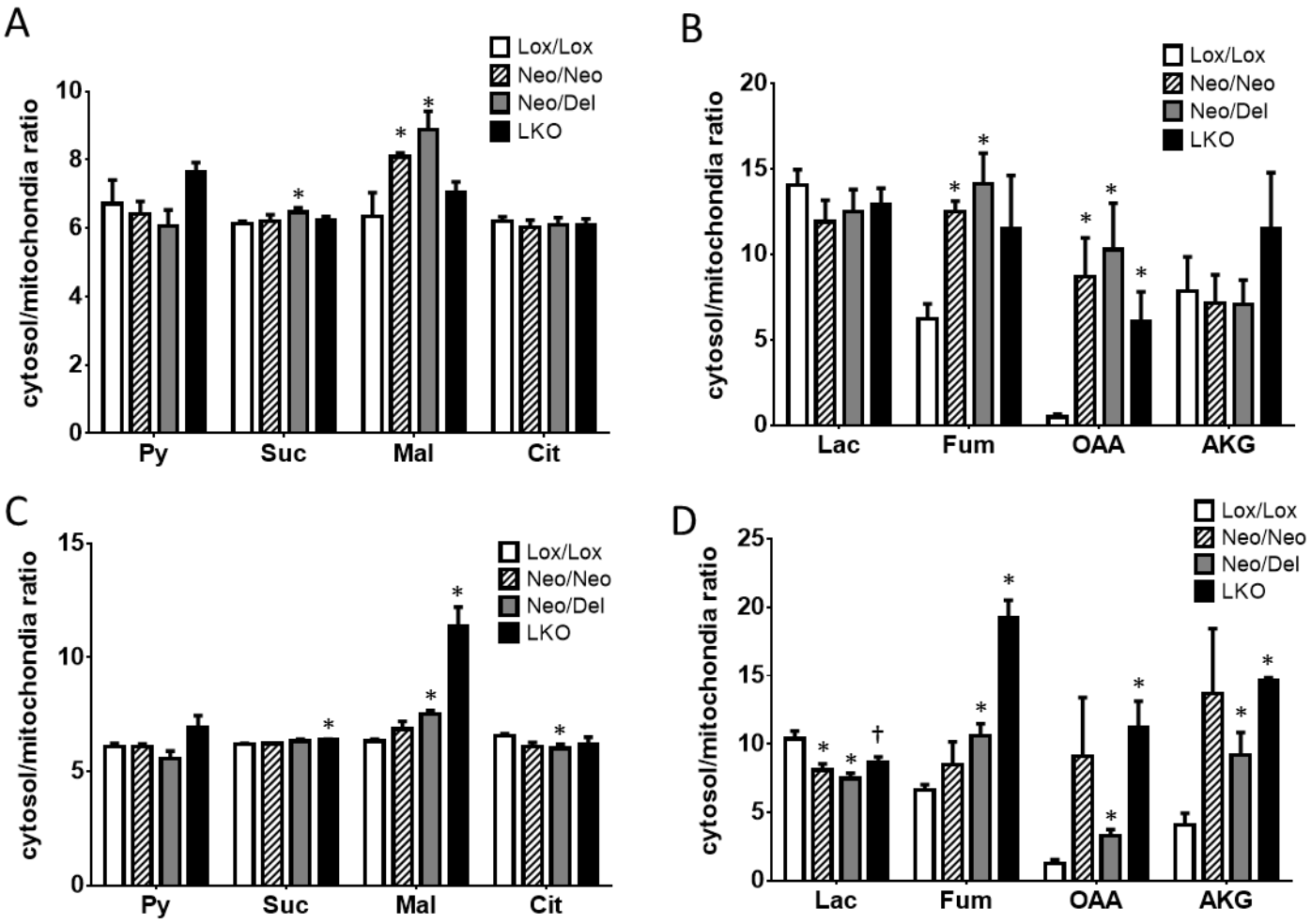

Figure 43: Ratios of hepatic cytosolic and mitochondrial concentrations of several metabolites in the livers of fed (A and B) and fasted mice (C and D). Py, pyruvate; Suc, succinate; Mal, malate; Cit, citrate; Lac, lactate; Fum, fumarate; OAA, oxaloacetate; AKG, α-ketoglutarate. * $p<0.05$ vs Lox/Lox mice. † $p=0.05$ vs Lox/Lox mice.

In the fed state, fumarate concentrations were almost doubled in the cytosol of Neo/Neo, Neo/Del and LKO mice, but only partially increased in the mitochondria of these same animals, leading to a big increase in the concentration ratio. Oxaloacetate ratios were also vastly increased (about 20-fold) in Neo/Neo, Neo/Del and LKO mice. This was mainly driven by an accumulation of oxaloacetate in the cytosol, though the concentration of mitochondrial oxaloacetate was also increased. Malate concentrations were slightly increased in the cytosol of Neo/Neo and Neo/Del mice but the mitochondrial concentrations remained unchanged, leading to a slightly increased concentration ration between these two. There was a tendency for an increase in the concentration ratio of α-ketoglutarate in LKO mice, but it did not reach statistical significance.

The metabolic differences were more prevalent in the fasted state, where there is a significant decrease in lactate concentrations ratios consequence of the decrease of cytosolic lactate concentration in Neo/Neo and Neo/Del mice. There also was increased fumarate, both in the cytosol and the mitochondria of Neo/Neo, Neo/Del and LKO mice, though the increase was more prevalent in the cytosol, leading to an increase in the concentration ratio. Malate followed the same trend, being elevated in both the cytosol and mitochondria of Neo/Neo, Neo/Del and LKO animals when compared to control, but more so in the cytosol, leading to an increase in the concentration ratio. Both oxaloacetate and α-ketoglutarate concentration ratios were vastly increased across the board, mainly due to an increase in their cytosolic concentrations.

To further clarify the molecular mechanisms of the effects of PEPCK-C on mitochondrial shuttles, QPCR for several key genes was performed in livers of fed PEPCK-C KD mice (Figure 44). Neo/Neo Neo/Del and LKO mice all showed increased Mdh1 levels, possibly as compensation for the accumulation of oxaloacetate in the cytosol of these animals. Slc25a10, the mitochondrial dicarboxylate channel that facilitates the mitochondrial transport of malate was significantly increased in Neo/Del mice. Finally, mRNA of Slc25a1, the mitochondrial citrate carrier, was slightly but significantly reduced in Neo/Neo and LKO mice, helping to explain the small accumulation of citrate in the mitochondria of these animals. Overall both this data informs that, either in the fed or fasted state, there is a profound imbalance of the concentration of organic acids in liver of PEPCK-C animals, as well as their ability to maintain the appropriate concentration gradients between the mitochondria and the cytosol, required for mitochondrial shuttles to work properly.

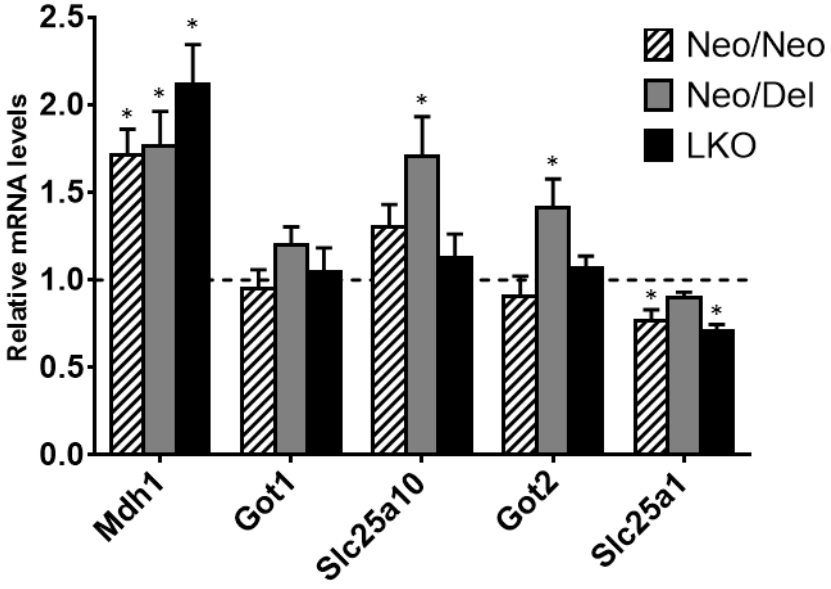

Figure 44: Relative mRNA levels of enzymes related to lipid metabolism in A) Liver and B) White adipose tissue of ad libitum fed mice. Dashed line represents the relative amount of mRNA in control mice. Bars are SEM. * $p<0.05$ vs Lox/Lox mice. Mdh1, cytosolic malate dehydrogenase; Got1, cytosolic aspartate transaminase; Slc25a10, mitochondrial dicarboxylate carrier; Got2 mitochondrial aspartate transaminase; Slc25a1, mitochondrial citrate carrier.

6 - Discussion

Our results establish that PEPCK-C has a high control over production of fatty acids in the fed and fasted state. In fed mice, PEPCK-C knockdown lead to a decrease in hepatic fatty acid production, but complete removal of this enzyme from the liver elicited a compensatory response in the adipose tissue which produced more fatty acids. In the fasted state, knockdown of PEPCK-C leads to an inability to reduce DNL, with liver specific knockout mice being the most affected. PEPCK-C knockdown animals also seem to have problems performing complete β-oxidation. PEPCK-C was also shown to have a significant impact in the metabolism of glycerol, although it was not possible to establish if this involved changes in glyceroneogenesis or other pathways of glycerol production. Finally, it was observed that these mice have significant derangements in the maintenance of hepatic metabolite distributions between the mitochondria and the cytosol, which might reduce the amount of citrate and/or NADPH available for the production of lipids in the cytosol.

Several studies (127, 130, 140, 141, 145) have demonstrated that PEPCK-C has a broader role in the regulation of other key aspects of metabolism besides GNG. PEPCK-C has been associated with both dysregulated lipid metabolism and cataplerosis. As PEPCK-C liver specific knockout mice develop hepatic steatosis after an overnight fast (130) and whole body PEPCK-C KO mice, though only alive for about 2 days after birth, already show significant accumulation of hepatic lipids (140). The goal of this study was to further define the mechanisms through which PEPCK-C impinges on lipid metabolism. There are four possible causes for the changes in lipid content: 1) Increased production, 2) Decreased oxidation, 3) Decreased export or 4) Increased absorption. The first 3 points were analyzed in mice expressing various levels of hepatic PEPCK-C in an attempt to better understand the mechanisms through which PEPCK-C regulates lipid metabolism

In order to see if hepatic steatosis could be partially explained by a defect in clearance of triglycerides from the liver, hepatic VLDL production was measured by using poloxamer 407 (P407). However, there were no observable differences in VLDL production in any of the PEPCK-C KD mice in any of the protocols used, so the development of steatosis does not seem to be driven by defects in hepatic triglyceride export.

Another possible way for fat accumulation in the liver is by having a reduced rate of hepatic β-oxidation. LKO mice were reported to have increased mRNA levels of enzymes related to β-oxidation and a 16% increase in β-oxidation of labelled palmitate (130). However, the rates of β-oxidation in Neo/Neo and Neo/Del mice were not measured. Here both Neo/Neo and Neo/Del mice had a significant decrease in total radioactivity detected, suggesting an impairment in the regulation of β-oxidation in these animals (Figure 35). Furthermore, the amount of radioactive CO_2 detected in Neo/Neo and Neo/Del mice was significantly lower than that of control animals. LKO animals, on the other hand, had total levels of radioactivity that were similar to those of control mice, but the amount of radioactivity in the acid soluble fraction was significantly elevated in these animals, while the fraction of radioactive CO_2 was the smallest in all of the mice models used, being significantly different from that of Lox/Lox mice. This suggests that, though β-oxidation seems to remain intact in these animals, the fate of the acetyl-CoA units generated during β-oxidation is significantly altered. A likely explanation is that these mice have decreased TCA cycle activity (127), which prevents radioactive carbon from being released during the isocitrate dehydrogenase complex, leading to the accumulation of activity in TCA cycle intermediates and, possibly, ketone bodies.

In contrast to gluconeogenesis and TCA cycle functions, little is known about the role of PEPCK-C in lipid metabolism. In experiments designed to measure global lipid synthesis (i.e. 4 days of D_2O exposure) PEPCK-C KD mice, but not LKO had significantly decreased rates of hepatic fatty acid production (Figure 37). This apparent contradiction is in part explained by the fact that LKO mice also had substantially increased fatty acid synthesis in their WAT, where PEPCK-C protein levels are unchanged. In contrast, Neo/Neo and Neo/Del mice, which are whole body knockdown animals, also had a decrease in the synthesis of WAT fatty acids (Figure 38). Thus there is a compensatory increase in the production of fatty acids in the WAT of LKO animals. In fact, the amount of fatty acids tended to be higher in the WAT of these animals, but did not reach statistical significance (Figure 32). LKO mice also had a reduction in plasma levels of free fatty acids, triglycerides and glycerol (Table 8), which could be associated with an increase in uptake of these metabolites, though more experiments are required to verify this hypothesis. The mechanism by which white adipose tissue upregulates lipid synthesis in LKO mice is unknown.

A possible mechanism by which PEPCK-C's influence on lipid metabolism is through the synthesis of glycerol phosphate via the pathway of GlyNG. Total hepatic glycerol production remained largely unchanged in Neo/Neo mice (Figure 37). Neo/Del animals, however, had a significant reduction in total hepatic glycerol production. Hepatic

glycerol production in LKO mice did not differ from control but there was a compensatory increase in the amount of total glycerol produced in the adipose tissue, being about twice as high as Lox/Lox control animals (Figure 38). WAT production of glycerol was unchanged for Neo/Neo and Neo/Del mice (Figure 38). Since the calculated flux control coefficient of PEPCK-C over total glycerol production was found to be higher than that previously determined for GNG (127) (Table 9) it is clear that PEPCK-C has a bigger role in regulating glycerol production than glucose production. This might be due to a decrease in GlyNG in PEPCK-C KD mice, though the NMR method we applied cannot directly analyze GlyNG. Another possibility is that PEPCK-C might have a flux control coefficient over GlyNG similar to that of GNG but PEPCK-C knockdown leads to a decrease in the other sources of hepatic glycerol-3-phosphate production (glycolysis and glycerol kinase), leading to a synergistic decrease in the total production of glycerol-3-phosphate. In order to address this question, it is imperative to be able to distinguish the contributions of GlyNG, glycolysis and glycerol kinase to the production of glycerol-3-phosphate. PEPCK-C might also regulate glycerol-3-phosphate via changes in the redox state. Glycerol-3-phosphate dehydrogenase (GPD), catalyzes the reversible conversion of dihydroxyacetone phosphate to glycerol-3-phosphate and the direction of the reaction is partially controlled by the cytosolic NADH/NAD^+ ratio. PEPCK-C LKO mice are known to have significantly altered ratio of mitochondrial NADH/NAD^+ ratio (145) though it is unknown if the cytosolic ratio is also altered. If the cytosolic NADH/NAD^+ is significantly decreased in PEPCK-C mice, it might decrease the amount of glycerol-3-phopshate produced by GPD, which would affect the production of glycerol-3-phosphate from both GlyNG and glycolysis. Another possibility is that, since GNG has a higher number of reactions (including the irreversible dephosphorylation of glucose-6-phosphate) than GlyNG, the control of GNG is more dispersed through these extra enzymes, when compared to GlyNG, leading to a smaller flux control coefficient of PEPCK-C over GNG.

Another important piece of information that relates to glycerol production can be derived from the lipid fluxes determined in fasted PEPCK-C KD mice. Neither Neo/Neo nor Neo/Del mice showed any differences in the fraction of newly synthesized glycerol or the mass of newly synthesized glycerol, with LKO animals having only a slight decrease in the fraction of newly made glycerol (about 50% vs. Lox/Lox) but no decrease in the total amount of new glycerol produced. Since the pathways of glyceroneogenesis and gluconeogenesis share the same enzymes up to the production of triose phosphates and it has been previously published that LKO mice have negligible gluconeogenesis from TCA cycle intermediates (127), LKO mice must derive their newly made glycerol from alternative pathways, such as glycerol kinase or glycolysis. It is also important to

note that the absence of changes in Neo/Neo and Neo/Del mice's glycerol production might be due to a combination of compensation by alternative pathways and due to a low control of PEPCK-C over gluconeogenic flux (and therefore, potentially, also over glyceroneogenic flux) in the fasted state. In order to fully answer this question the different sources of glycerol production need to be better resolved.

In experiments designed to measure hepatic fatty acid synthesis (i.e. 16h D_2O exposure), fatty acid synthesis was significantly decreased in Neo/Neo mice and tended to be decreased in Neo/Del and LKO mice. Thus, this data indicates that adipose tissue might be the main driver of the lipid phenotype observed in the protocol that measured global lipid synthesis. When the 16h D_2O exposure protocol was applied in fasted mice. The contribution of de novo lipogenesis to the total lipid pool was vastly decreased in Lox/Lox control mice, when compared to the fed state (~20% vs ~1%, respectively). However, PEPCK-C KD mice were unable to shut down lipogenesis to the same extent as Lox/Lox mice, with LKO mice having about a 3% production of fatty acids even in the fasted state (Figure 42). The mechanism through which PEPCK-C KD animals fail to donwnregulate their lipogenic flux is unknown.

The combination of fed and fasted experiments indicates that PEPCK-C is essential in regulating the transition from fed to fasted state fatty acid metabolism. This suggests the possibility of PEPCK-C acting as a metabolic switch that coordinates the metabolic changes of the fed-fasted transitions. Furthermore, when analyzing the flux control coefficients of PEPCK-C, it is apparent that PEPCK-C strongly controls fatty acid synthesis to a similar extent for both fed and fasted states, leading to the surprising revelation that PEPCK-C has a higher control over the non-canonical pathway of lipogenesis than it does over gluconeogenesis (Table 9). (FCC values of -0.33 in fed mice and 0.37 in fasted mice). In the fed state there also was a strong correlation between PEPCK-C levels and glycerol production with PEPCK-C KD mice showing a marked decrease in total glycerol production, perhaps via regulation of glyceroneogenesis. Finally, PEPCK-C had a surprising and strong correlation with fatty acid elongation in the fasted state.

It is unclear how PEPCK-C could regulate lipogenesis but it might involve secondary metabolic effects. In order for lipogenesis to occur, acetyl-CoA and NADPH must be present in the cytosol, where lipogenic enzymes are located. This is partly achieved by the transport of citrate from the mitochondria via the citrate-malate shuttle. Essentially, citrate leaves the mitochondria through the CIC and, once in the cytosol it is converted to acetyl-CoA and oxaloacetate. Oxaloacetate is converted to malate via

malate dehydrogenase (consuming one NADH molecule), Cytosolic malate has two possible fates 1) it is transferred back to the mitochondria via the dicarboxylate transporter or 2) is converted to pyruvate via the malic enzyme and the pyruvate then enters the mitochondria via the pyruvate transporter. The reaction of malic enzyme also produces NADPH, which is an essential cofactor for fatty acid synthesis. Metabolomic analysis of hepatic cytosolic and mitochondrial from PEPCK-C KD mice revealed that there are significant changes in the concentration of organic acids in both compartments. Additionally, the concentration ratios between the cytosol and the mitochondria were also significantly altered, suggesting that transport of metabolites from the mitochondria to the cytosol and vice versa might be impaired. There are two possible mechanisms through which these changes might affect lipid metabolism. First, the excessive accumulation of oxaloacetate in the cytosol might impair the activity of ATP-citrate lyase, reducing this enzymes ability to produce the necessary acetyl-CoA required for lipid synthesis. Alternatively, any potential changes in shuttling efficiency could result in an altered NAD(P)H/NAD(P)$^+$ ratio. If NADPH levels are sufficiently low, it might limit the rate of lipogenesis. LKO mice have been previously reported to have altered NADH/NAD$^+$ balance in their mitochondria (145) so it is possible that the imbalance can also occur in the cytosol.

7 – Conclusion

PEPCK-C plays an important role in the regulation of lipid metabolism as mice lacking this enzyme in the liver show an increase in extrahepatic production of lipids as well as an inability to correctly downregulate their lipogenic flux when fasting. In fact, the calculated flux coefficient controls (FCC) of PEPCK-C over the pathways of lipid production seem to be higher than FCC of PEPCK-C over gluconeogenesis, where PEPCK-C is considered to be the rate controlling enzyme. These mice also show clear impairments in the fate of the acetyl-CoA carbons produced during β-oxidation. Though the exact mechanism through which PEPCK-C regulates lipid metabolism in not clear, mice with a knockdown and knockout of this enzyme in the liver show altered concentrations of key TCA cycle intermediates in both their hepatic mitochondrial and cytosol fractions. This could impair these mice's ability to export citrate from the mitochondria to the cytosol, which is an essential prerequisite for the synthesis of fatty acids via DNL.

Final remarks

In this dissertation a novel hybrid $^{1}H/^{2}H$ NMR methodology was developed for the determination of lipid biosynthetic fluxes. This method allows the simultaneous, non-destructive analysis of several fluxes: 1) *De novo* lipogenesis 2) fatty acid desaturation, 3) fatty acid elongation, 4) glycerol production, 5) cholesterol synthesis. To confirm that the method accurately informs biologically relevant changes in these fluxes, several validation experiments were made. DNL, glycerol and cholesterol flux were validated using mice overexpressing a truncated, constitutively active form of SREBP-1c, which have been previously reported to have significantly increased production of fatty acids, triglycerides and cholesterol. Validation of fatty acid desaturation flux was performed using an inhibitor of SCD-1, one of the main enzymes responsible for the desaturation of fatty acids in mammals. Finally, validation of fatty acid elongation flux was performed in mice that were administered coconut oil containing a significant amount of short-medium chain fatty acids, the preferential substrate of ELOVL enzymes. In all cases, the NMR method detected the expected changes in metabolic fluxes. The developed NMR method also provided a partial lipidomic analysis, allowing the identification of multiple lipid classes, such as ω-3 fatty acids, saturated fatty acids, mono- and poly-unsaturated fatty acids, average fatty acid length as well as two individual fatty acids: docosahexaenoic acid and linoleic acid.

One poorly understood aspect of diabetes is the paradox of selective insulin resistance, i.e., the state in which insulin's actions on the glucoregulatory arm of insulin signaling are resistant (suppression of glycogen synthesis, increase in gluconeogenesis) while the effect of insulin on lipid metabolism (increase in lipogenesis) remain responsive or even elevated. In order to elucidate this apparent paradox, the NMR method was applied to diabetic mice. Both the % contribution of lipogenesis to total fatty acid synthesis and the total amount of newly made fatty acids were significantly reduced in HFD-induced diabetic animals, suggesting that, at least under the condition of high fat diet induced diabetes, there is no significant selective insulin resistant phenotype.

Finally, in order to understand the effects of PEPCK-C in the regulation of lipid metabolism, the NMR method was applied to mice that express different levels of PEPCK-C. It was found that this enzyme has a higher control over the production of fatty acids than over the production of glucose, both in the fed (where lack of PEPCK-C limits fatty acid synthesis) and in the fasted state (where lack of PEPCK-C increases fatty acid

synthesis). These animals also show significantly impaired ability to dispose of hepatic fatty acids, either via β-oxidation or by VLDL export. These mice also had extremely altered concentrations of total cytosolic and mitochondrial organic acids, as well as severe changes in the ratio of concentrations between these two compartments, suggesting the possibility of impaired transport from the mitochondria to the cytosol and vice-versa.

REFERENCES

1. Flegal, K. M., M. D. Carroll, B. K. Kit, and C. L. Ogden. 2012. Prevalence of obesity and trends in the distribution of body mass index among US adults, 1999-2010. *JAMA : the journal of the American Medical Association* **307**: 491-497.
2. Berghofer, A., T. Pischon, T. Reinhold, C. M. Apovian, A. M. Sharma, and S. N. Willich. 2008. Obesity prevalence from a European perspective: a systematic review. *BMC public health* **8**: 200.
3. Wang, Y., M. A. Beydoun, L. Liang, B. Caballero, and S. K. Kumanyika. 2008. Will all Americans become overweight or obese? estimating the progression and cost of the US obesity epidemic. *Obesity* **16**: 2323-2330.
4. Ogden, C. L., S. Z. Yanovski, M. D. Carroll, and K. M. Flegal. 2007. The epidemiology of obesity. *Gastroenterology* **132**: 2087-2102.
5. Oguma, Y., H. D. Sesso, R. S. Paffenbarger, Jr., and I. M. Lee. 2005. Weight change and risk of developing type 2 diabetes. *Obesity research* **13**: 945-951.
6. Finkelstein, E. A., J. G. Trogdon, J. W. Cohen, and W. Dietz. 2009. Annual medical spending attributable to obesity: payer-and service-specific estimates. *Health affairs* **28**: w822-831.
7. Bugg, T. D. 2001. The development of mechanistic enzymology in the 20th century. *Natural product reports* **18**: 465-493.
8. Brownsey, R. W., A. N. Boone, J. E. Elliott, J. E. Kulpa, and W. M. Lee. 2006. Regulation of acetyl-CoA carboxylase. *Biochemical Society transactions* **34**: 223-227.
9. Abu-Elheiga, L., W. R. Brinkley, L. Zhong, S. S. Chirala, G. Woldegiorgis, and S. J. Wakil. 2000. The subcellular localization of acetyl-CoA carboxylase 2. *Proceedings of the National Academy of Sciences of the United States of America* **97**: 1444-1449.
10. Saggerson, D. 2008. Malonyl-CoA, a key signaling molecule in mammalian cells. *Annual review of nutrition* **28**: 253-272.
11. Tong, L. 2005. Acetyl-coenzyme A carboxylase: crucial metabolic enzyme and attractive target for drug discovery. *Cellular and molecular life sciences : CMLS* **62**: 1784-1803.
12. Maier, T., S. Jenni, and N. Ban. 2006. Architecture of mammalian fatty acid synthase at 4.5 A resolution. *Science* **311**: 1258-1262.
13. Smith, S., A. Witkowski, and A. K. Joshi. 2003. Structural and functional organization of the animal fatty acid synthase. *Progress in lipid research* **42**: 289-317.
14. Hagve, T. A. 1988. Effects of unsaturated fatty acids on cell membrane functions. *Scandinavian journal of clinical and laboratory investigation* **48**: 381-388.
15. Calder, P. C. 2006. n-3 polyunsaturated fatty acids, inflammation, and inflammatory diseases. *The American journal of clinical nutrition* **83**: 1505S-1519S.
16. Georgiadi, A., and S. Kersten. 2012. Mechanisms of gene regulation by fatty acids. *Advances in nutrition* **3**: 127-134.
17. Miyazaki, M., and J. M. Ntambi. 2008. Chapter 7 - Fatty acid desaturation and chain elongation in mammals. *In* Biochemistry of Lipids, Lipoproteins and Membranes (Fifth Edition). D. E. Vance and J. E. Vance, editors. Elsevier, San Diego. 191-V.
18. Guillou, H., D. Zadravec, P. G. Martin, and A. Jacobsson. 2010. The key roles of elongases and desaturases in mammalian fatty acid metabolism: Insights from transgenic mice. *Progress in lipid research* **49**: 186-199.

19. Heinemann, F. S., and J. Ozols. 2003. Stearoyl-CoA desaturase, a short-lived protein of endoplasmic reticulum with multiple control mechanisms. *Prostaglandins, leukotrienes, and essential fatty acids* **68**: 123-133.
20. Tabor, D. E., J. B. Kim, B. M. Spiegelman, and P. A. Edwards. 1998. Transcriptional activation of the stearoyl-CoA desaturase 2 gene by sterol regulatory element-binding protein/adipocyte determination and differentiation factor 1. *The Journal of biological chemistry* **273**: 22052-22058.
21. Zheng, Y., S. M. Prouty, A. Harmon, J. P. Sundberg, K. S. Stenn, and S. Parimoo. 2001. Scd3--a novel gene of the stearoyl-CoA desaturase family with restricted expression in skin. *Genomics* **71**: 182-191.
22. Miyazaki, M., M. J. Jacobson, W. C. Man, P. Cohen, E. Asilmaz, J. M. Friedman, and J. M. Ntambi. 2003. Identification and characterization of murine SCD4, a novel heart-specific stearoyl-CoA desaturase isoform regulated by leptin and dietary factors. *The Journal of biological chemistry* **278**: 33904-33911.
23. Miyazaki, M., S. M. Bruggink, and J. M. Ntambi. 2006. Identification of mouse palmitoyl-coenzyme A Delta9-desaturase. *Journal of lipid research* **47**: 700-704.
24. de Antueno, R. J., L. C. Knickle, H. Smith, M. L. Elliot, S. J. Allen, S. Nwaka, and M. D. Winther. 2001. Activity of human Delta5 and Delta6 desaturases on multiple n-3 and n-6 polyunsaturated fatty acids. *FEBS letters* **509**: 77-80.
25. Ikeda, M., Y. Kanao, M. Yamanaka, H. Sakuraba, Y. Mizutani, Y. Igarashi, and A. Kihara. 2008. Characterization of four mammalian 3-hydroxyacyl-CoA dehydratases involved in very long-chain fatty acid synthesis. *FEBS letters* **582**: 2435-2440.
26. Arner, P. 2002. Insulin resistance in type 2 diabetes: role of fatty acids. *Diabetes/metabolism research and reviews* **18 Suppl 2**: S5-9.
27. Chen, J. L., E. Peacock, W. Samady, S. M. Turner, R. A. Neese, M. K. Hellerstein, and E. J. Murphy. 2005. Physiologic and pharmacologic factors influencing glyceroneogenic contribution to triacylglyceride glycerol measured by mass isotopomer distribution analysis. *The Journal of biological chemistry* **280**: 25396-25402.
28. Wilcox, C. B., G. O. Feddes, J. E. Willett-Brozick, L. C. Hsu, J. A. DeLoia, and B. E. Baysal. 2007. Coordinate up-regulation of TMEM97 and cholesterol biosynthesis genes in normal ovarian surface epithelial cells treated with progesterone: implications for pathogenesis of ovarian cancer. *BMC cancer* **7**: 223.
29. Lambert, J. E., M. A. Ramos-Roman, J. D. Browning, and E. J. Parks. 2014. Increased de novo lipogenesis is a distinct characteristic of individuals with nonalcoholic fatty liver disease. *Gastroenterology* **146**: 726-735.
30. Bickerton, A. S., R. Roberts, B. A. Fielding, L. Hodson, E. E. Blaak, A. J. Wagenmakers, M. Gilbert, F. Karpe, and K. N. Frayn. 2007. Preferential uptake of dietary Fatty acids in adipose tissue and muscle in the postprandial period. *Diabetes* **56**: 168-176.
31. Gagne, S., S. Crane, Z. Huang, C. S. Li, K. P. Bateman, and J. F. Levesque. 2007. Rapid measurement of deuterium-labeled long-chain fatty acids in plasma by HPLC-ESI-MS. *Journal of lipid research* **48**: 252-259.
32. Ecker, J., G. Liebisch, M. Grandl, and G. Schmitz. 2010. Lower SCD expression in dendritic cells compared to macrophages leads to membrane lipids with less mono-unsaturated fatty acids. *Immunobiology* **215**: 748-755.
33. Mosley, E. E., B. Shafii Dagger, P. J. Moate, and M. A. McGuire. 2006. cis-9, trans-11 conjugated linoleic acid is synthesized directly from vaccenic acid in lactating dairy cattle. *The Journal of nutrition* **136**: 570-575.
34. Collins, J. M., M. J. Neville, K. E. Pinnick, L. Hodson, B. Ruyter, T. H. van Dijk, D. J. Reijngoud, M. D. Fielding, and K. N. Frayn. 2011. De novo lipogenesis in the differentiating human adipocyte can provide all fatty acids necessary for maturation. *Journal of lipid research* **52**: 1683-1692.

35. Bederman, I. R., A. E. Reszko, T. Kasumov, F. David, D. H. Wasserman, J. K. Kelleher, and H. Brunengraber. 2004. Zonation of labeling of lipogenic acetyl-CoA across the liver: implications for studies of lipogenesis by mass isotopomer analysis. *The Journal of biological chemistry* **279**: 43207-43216.
36. Turner, S. M., E. J. Murphy, R. A. Neese, F. Antelo, T. Thomas, A. Agarwal, C. Go, and M. K. Hellerstein. 2003. Measurement of TG synthesis and turnover in vivo by 2H2O incorporation into the glycerol moiety and application of MIDA. *American journal of physiology. Endocrinology and metabolism* **285**: E790-803.
37. Lee, W. N., S. Bassilian, H. O. Ajie, D. A. Schoeller, J. Edmond, E. A. Bergner, and L. O. Byerley. 1994. In vivo measurement of fatty acids and cholesterol synthesis using D2O and mass isotopomer analysis. *American. Journal. of. Physiology.* **266**: E699-E708.
38. Brunengraber, D. Z., B. J. McCabe, T. Kasumov, J. C. Alexander, V. Chandramouli, and S. F. Previs. 2003. Influence of diet on the modeling of adipose tissue triglycerides during growth. *American journal of physiology. Endocrinology and metabolism* **285**: E917-925.
39. Murphy, E. J. 2006. Stable isotope methods for the in vivo measurement of lipogenesis and triglyceride metabolism. *Journal of animal science* **84 Suppl**: E94-104.
40. Katz, J., and R. Rognstad. 1966. The metabolism of tritiated glucose by rat adipose tissue. *The Journal of biological chemistry* **241**: 3600-3610.
41. Jungas, R. L. 1968. Fatty acid synthesis in adipose tissue incubated in tritiated water. *Biochemistry* **7**: 3708-3717.
42. Rognstad, R., G. Clark, and J. Katz. 1974. Glucose synthesis in tritiated water. *European journal of biochemistry / FEBS* **47**: 383-388.
43. Kuwajima, M., S. Golden, J. Katz, R. H. Unger, D. W. Foster, and J. D. McGarry. 1986. Active hepatic glycogen synthesis from gluconeogenic precursors despite high tissue levels of fructose 2,6-bisphosphate. *The Journal of biological chemistry* **261**: 2632-2637.
44. Hellerstein, M. K., and R. A. Neese. 1992. Mass isotopomer distribution analysis: a technique for measuring biosynthesis and turnover of polymers. *The American journal of physiology* **263**: E988-1001.
45. Lee, W. N., S. Bassilian, Z. Guo, D. Schoeller, J. Edmond, E. A. Bergner, and L. O. Byerley. 1994. Measurement of fractional lipid synthesis using deuterated water (2H2O) and mass isotopomer analysis. *American. Journal. of. Physiology.* **266**: E372-E383.
46. Diraison, F., C. Pachiaudi, and M. Beylot. 1996. In vivo measurement of plasma cholesterol and fatty acid synthesis with deuterated water: determination of the average number of deuterium atoms incorporated. *Metabolism:. Clinical. &. Experimental.* **45**: 817-821.
47. Ajie, H. O., M. J. Connor, W. N. Lee, S. Bassilian, E. A. Bergner, and L. O. Byerley. 1995. In vivo study of the biosynthesis of long-chain fatty acids using deuterated water. *The American journal of physiology* **269**: E247-252.
48. Seubert, W., and E. R. Podack. 1973. Mechanisms and physiological roles of fatty acid chain elongation in microsomes and mitochondria. *Molecular and cellular biochemistry* **1**: 29-40.
49. Bederman, I. R., S. Foy, V. Chandramouli, J. C. Alexander, and S. F. Previs. 2009. Triglyceride synthesis in epididymal adipose tissue: contribution of glucose and non-glucose carbon sources. *The Journal of biological chemistry* **284**: 6101-6108.
50. Diraison, F., C. Pachiaudi, and M. Beylot. 1997. Measuring lipogenesis and cholesterol synthesis in humans with deuterated water: Use of simple gas chromatographic mass spectrometric techniques. *Journal of Mass Spectrometry* **32**: 81-86.
51. Foster, D. W., and J. Katz. 1966. The distribution of tritium in fatty acids synthesized from tritiated glucose and tritiated water by rat adipose tissue. *Biochimica et biophysica acta* **125**: 422-427.
52. Lakshmanan, M. R., and R. L. Veech. 1977. Measurement of rate of rat liver sterol synthesis in vivo using tritiated water. *The Journal of biological chemistry* **252**: 4667-4673.

53. Delgado, T. C., D. Pinheiro, M. Caldeira, M. M. Castro, C. F. Geraldes, P. Lopez-Larrubia, S. Cerdan, and J. G. Jones. 2009. Sources of hepatic triglyceride accumulation during high-fat feeding in the healthy rat. *NMR in biomedicine* **22**: 310-317.
54. Hamilton, J. G., and K. Comai. 1988. Rapid separation of neutral lipids, free fatty acids and polar lipids using prepacked silica Sep-Pak columns. *Lipids* **23**: 1146-1149.
55. Jones, J. G., M. Merritt, and C. Malloy. 2001. Quantifying tracer levels of (2)H(2)O enrichment from microliter amounts of plasma and urine by (2)H NMR. *Magnetic resonance in medicine : official journal of the Society of Magnetic Resonance in Medicine / Society of Magnetic Resonance in Medicine* **45**: 156-158.
56. Carvalho, F., J. Duarte, A. R. Simoes, P. F. Cruz, and J. G. Jones. 2013. Noninvasive measurement of murine hepatic acetyl-CoA (1)(3)C-enrichment following overnight feeding with (1)(3)C-enriched fructose and glucose. *BioMed research international* **2013**: 638085.
57. Folch, J., M. Lees, and G. H. Sloane Stanley. 1957. A simple method for the isolation and purification of total lipides from animal tissues. *The Journal of biological chemistry* **226**: 497-509.
58. Willker, W., and D. Leibfritz. 1998. Assignment of mono- and polyunsaturated fatty acids in lipids of tissues and body fluids. *Magn Reson Chem* **36**: S79-S84.
59. Siddiqui, N., J. Sim, C. J. Silwood, H. Toms, R. A. Iles, and M. Grootveld. 2003. Multicomponent analysis of encapsulated marine oil supplements using high-resolution 1H and 13C NMR techniques. *Journal of lipid research* **44**: 2406-2427.
60. Burr, G. O., M. M. Burr, and E. S. Miller. 1932. On the fatty acids essential in nutrition. *The Journal of biological chemistry* **97**: 1-9.
61. Shimano, H., J. D. Horton, R. E. Hammer, I. Shimomura, M. S. Brown, and J. L. Goldstein. 1996. Overproduction of cholesterol and fatty acids causes massive liver enlargement in transgenic mice expressing truncated SREBP-1a. *The Journal of clinical investigation* **98**: 1575-1584.
62. Xin, Z., H. Zhao, M. D. Serby, B. Liu, M. Liu, B. G. Szczepankiewicz, L. T. Nelson, H. T. Smith, T. S. Suhar, R. S. Janis, N. Cao, H. S. Camp, C. A. Collins, H. L. Sham, T. K. Surowy, and G. Liu. 2008. Discovery of piperidine-aryl urea-based stearoyl-CoA desaturase 1 inhibitors. *Bioorganic & medicinal chemistry letters* **18**: 4298-4302.
63. von Roemeling, C. A., L. A. Marlow, J. J. Wei, S. J. Cooper, T. R. Caulfield, K. Wu, W. W. Tan, H. W. Tun, and J. A. Copland. 2013. Stearoyl-CoA desaturase 1 is a novel molecular therapeutic target for clear cell renal cell carcinoma. *Clinical cancer research : an official journal of the American Association for Cancer Research* **19**: 2368-2380.
64. Moon, Y. A., R. E. Hammer, and J. D. Horton. 2009. Deletion of ELOVL5 leads to fatty liver through activation of SREBP-1c in mice. *Journal of lipid research* **50**: 412-423.
65. Miyazaki, M., M. T. Flowers, H. Sampath, K. Chu, C. Otzelberger, X. Liu, and J. M. Ntambi. 2007. Hepatic stearoyl-CoA desaturase-1 deficiency protects mice from carbohydrate-induced adiposity and hepatic steatosis. *Cell metabolism* **6**: 484-496.
66. Ntambi, J. M., M. Miyazaki, J. P. Stoehr, H. Lan, C. M. Kendziorski, B. S. Yandell, Y. Song, P. Cohen, J. M. Friedman, and A. D. Attie. 2002. Loss of stearoyl-CoA desaturase-1 function protects mice against adiposity. *Proceedings of the National Academy of Sciences of the United States of America* **99**: 11482-11486.
67. Tripathy, S., M. Torres-Gonzalez, and D. B. Jump. 2010. Elevated hepatic fatty acid elongase-5 activity corrects dietary fat-induced hyperglycemia in obese C57BL/6J mice. *Journal of lipid research* **51**: 2642-2654.
68. Tripathy, S., and D. B. Jump. 2013. Elovl5 regulates the mTORC2-Akt-FOXO1 pathway by controlling hepatic cis-vaccenic acid synthesis in diet-induced obese mice. *Journal of lipid research* **54**: 71-84.
69. Abu-Elheiga, L., H. Wu, Z. Gu, R. Bressler, and S. J. Wakil. 2012. Acetyl-CoA carboxylase 2-/- mutant mice are protected against fatty liver under high-fat, high-carbohydrate dietary and de novo lipogenic conditions. *The Journal of biological chemistry* **287**: 12578-12588.

70. McGarry, J. D. 1992. What if Minkowski had been ageusic? An alternative angle on diabetes. *Science* **258**: 766-770.
71. Guo, S. 2014. Insulin signaling, resistance, and the metabolic syndrome: insights from mouse models into disease mechanisms. *The Journal of endocrinology* **220**: T1-T23.
72. Dong, X. C., K. D. Copps, S. D. Guo, Y. D. Li, R. Kollipara, R. A. DePinho, and M. F. White. 2008. Inactivation of hepatic Foxo1 by insulin signaling is required for adaptive nutrient homeostasis and endocrine growth regulation. *Cell metabolism* **8**: 65-76.
73. Michael, M. D., R. N. Kulkarni, C. Postic, S. F. Previs, G. I. Shulman, M. A. Magnuson, and C. R. Kahn. 2000. Loss of insulin signaling in hepatocytes leads to severe insulin resistance and progressive hepatic dysfunction. *Molecular cell* **6**: 87-97.
74. Biddinger, S. B., A. Hernandez-Ono, C. Rask-Madsen, J. T. Haas, J. O. Aleman, R. Suzuki, E. F. Scapa, C. Agarwal, M. C. Carey, G. Stephanopoulos, D. E. Cohen, G. L. King, H. N. Ginsberg, and C. R. Kahn. 2008. Hepatic insulin resistance is sufficient to produce dyslipidemia and susceptibility to atherosclerosis. *Cell metabolism* **7**: 125-134.
75. Long, Y. C., Z. Y. Cheng, K. D. Copps, and M. F. White. 2011. Insulin Receptor Substrates Irs1 and Irs2 Coordinate Skeletal Muscle Growth and Metabolism via the Akt and AMPK Pathways. *Molecular and cellular biology* **31**: 430-441.
76. Araki, E., M. A. Lipes, M. E. Patti, J. C. Bruning, B. Haag, R. S. Johnson, and C. R. Kahn. 1994. Alternative Pathway of Insulin Signaling in Mice with Targeted Disruption of the Irs-1 Gene. *Nature* **372**: 186-190.
77. Gutierrez, J. S., D. J. Withers, H. Towery, D. J. Burks, J. M. Ren, S. Previs, G. I. Shulman, S. Bonner-Weir, and M. F. White. 1998. Disruption of IRS-2 causes type 2 diabetes in mice. *Diabetes* **47**: A57-A57.
78. Taniguchi, C. M., K. Ueki, and C. R. Kahn. 2005. Complementary roles of IRS-1 and IRS-2 in the hepatic regulation of metabolism. *Journal of Clinical Investigation* **115**: 718-727.
79. Copps, K. D., and M. F. White. 2012. Regulation of insulin sensitivity by serine/threonine phosphorylation of insulin receptor substrate proteins IRS1 and IRS2. *Diabetologia* **55**: 2565-2582.
80. Laplante, M., and D. M. Sabatini. 2009. mTOR signaling at a glance. *J Cell Sci* **122**: 3589-3594.
81. Laplante, M., and D. M. Sabatini. 2009. An Emerging Role of mTOR in Lipid Biosynthesis. *Curr Biol* **19**: R1046-R1052.
82. Peterson, T. R., S. S. Sengupta, T. E. Harris, A. E. Carmack, S. A. Kang, E. Balderas, D. A. Guertin, K. L. Madden, A. E. Carpenter, B. N. Finck, and D. M. Sabatini. 2011. mTOR Complex 1 Regulates Lipin 1 Localization to Control the SREBP Pathway. *Cell* **146**: 408-420.
83. Huffman, T. A., I. Mothe-Satney, and J. C. Lawrence. 2002. Insulin-stimulated phosphorylation of lipin mediated by the mammalian target of rapamycin. *Proceedings of the National Academy of Sciences of the United States of America* **99**: 1047-1052.
84. Duvel, K., J. L. Yecies, S. Menon, P. Raman, A. I. Lipovsky, A. L. Souza, E. Triantafellow, Q. C. Ma, R. Gorski, S. Cleaver, M. G. V. Heiden, J. P. MacKeigan, P. M. Finan, C. B. Clish, L. O. Murphy, and B. D. Manning. 2010. Activation of a Metabolic Gene Regulatory Network Downstream of mTOR Complex 1. *Molecular cell* **39**: 171-183.
85. Porstmann, T., C. R. Santos, B. Griffiths, M. Cully, M. Wu, S. Leevers, J. R. Griffiths, Y. L. Chung, and A. Schulze. 2008. SREBP activity is regulated by mTORC1 and contributes to Akt-dependent cell growth. *Cell metabolism* **8**: 224-236.
86. Hagiwara, A., M. Cornu, N. Cybulski, P. Polak, C. Betz, F. Trapani, L. Terracciano, M. H. Heim, M. A. Ruegg, and M. N. Hall. 2012. Hepatic mTORC2 Activates Glycolysis and Lipogenesis through Akt, Glucokinase, and SREBP1c. *Cell metabolism* **15**: 725-738.
87. Yuan, M., E. Pino, L. Wu, M. Kacergis, and A. A. Soukas. 2012. Identification of Akt-independent regulation of hepatic lipogenesis by mammalian target of rapamycin (mTOR) complex 2. *The Journal of biological chemistry* **287**: 29579-29588.

88. Ricoult, S. J., and B. D. Manning. 2013. The multifaceted role of mTORC1 in the control of lipid metabolism. *EMBO reports* **14**: 242-251.
89. Betz, C., and M. N. Hall. 2013. Where is mTOR and what is it doing there? *Journal of Cell Biology* **203**: 563-574.
90. Horton, J. D., J. L. Goldstein, and M. S. Brown. 2002. SREBPs: activators of the complete program of cholesterol and fatty acid synthesis in the liver. *The Journal of clinical investigation* **109**: 1125-1131.
91. Shimomura, L., Y. Bashmakov, S. Ikemoto, J. D. Horton, M. S. Brown, and J. L. Goldstein. 1999. Insulin selectively increases SREBP-1c mRNA in the livers of rats with streptozotocin-induced diabetes. *Proceedings of the National Academy of Sciences of the United States of America* **96**: 13656-13661.
92. Hegarty, B. D., A. Bobard, I. Hainault, P. Ferre, P. Bossard, and F. Foufelle. 2005. Distinct roles of insulin and liver X receptor in the induction and cleavage of sterol regulatory element-binding protein-1c. *Proceedings of the National Academy of Sciences of the United States of America* **102**: 791-796.
93. Horton, J. D., I. Shimomura, M. S. Brown, R. E. Hammer, J. L. Goldstein, and H. Shimano. 1998. Activation of cholesterol synthesis in preference to fatty acid synthesis in liver and adipose tissue of transgenic mice overproducing sterol regulatory element-binding protein-2. *The Journal of clinical investigation* **101**: 2331-2339.
94. Shimano, H., J. D. Horton, I. Shimomura, R. E. Hammer, M. S. Brown, and J. L. Goldstein. 1997. Isoform 1c of sterol regulatory element binding protein is less active than isoform 1a in livers of transgenic mice and in cultured cells. *Journal of Clinical Investigation* **99**: 846-854.
95. Eberle, D., B. Hegarty, P. Bossard, P. Ferre, and F. Foufelle. 2004. SREBP transcription factors: master regulators of lipid homeostasis. *Biochimie* **86**: 839-848.
96. Geiszt, M. 2006. NADPH oxidases: new kids on the block. *Cardiovascular research* **71**: 289-299.
97. Mahadev, K., H. Motoshima, X. Wu, J. M. Ruddy, R. S. Arnold, G. Cheng, J. D. Lambeth, and B. J. Goldstein. 2004. The NAD(P)H oxidase homolog Nox4 modulates insulin-stimulated generation of H2O2 and plays an integral role in insulin signal transduction. *Molecular and cellular biology* **24**: 1844-1854.
98. Goldstein, B. J., K. Mahadev, and X. Wu. 2005. Redox paradox: insulin action is facilitated by insulin-stimulated reactive oxygen species with multiple potential signaling targets. *Diabetes* **54**: 311-321.
99. Loh, K., H. Deng, A. Fukushima, X. Cai, B. Boivin, S. Galic, C. Bruce, B. J. Shields, B. Skiba, L. M. Ooms, N. Stepto, B. Wu, C. A. Mitchell, N. K. Tonks, M. J. Watt, M. A. Febbraio, P. J. Crack, S. Andrikopoulos, and T. Tiganis. 2009. Reactive oxygen species enhance insulin sensitivity. *Cell metabolism* **10**: 260-272.
100. Bedard, K., and K. H. Krause. 2007. The NOX family of ROS-generating NADPH oxidases: physiology and pathophysiology. *Physiological reviews* **87**: 245-313.
101. Otero, Y. F., J. M. Stafford, and O. P. McGuinness. 2014. Pathway-Selective Insulin Resistance and Metabolic Disease: The Importance of Nutrient Flux. *The Journal of biological chemistry*.
102. Furtado, L. M., R. Somwar, G. Sweeney, W. Niu, and A. Klip. 2002. Activation of the glucose transporter GLUT4 by insulin. *Biochemistry and cell biology = Biochimie et biologie cellulaire* **80**: 569-578.
103. Hernandez-Ono, A., Y. L. Zhang, J. Chiang, B. Moon, C. R. Kahn, and H. Ginsberg. 2005. Lipoprotein metabolism in the liver insulin receptor knockout (LIRKO) mouse: Critical role of insulin signaling in the regulation of very low density lipoprotein (VLDL) secretion. *Diabetes* **54**: A2-A2.
104. Brown, M. S., and J. L. Goldstein. 2008. Selective versus total insulin resistance: a pathogenic paradox. *Cell metabolism* **7**: 95-96.

105. Shimomura, I., M. Matsuda, R. E. Hammer, Y. Bashmakov, M. S. Brown, and J. L. Goldstein. 2000. Decreased IRS-2 and increased SREBP-1c lead to mixed insulin resistance and sensitivity in livers of lipodystrophic and ob/ob mice. *Molecular cell* **6**: 77-86.
106. Li, S., M. S. Brown, and J. L. Goldstein. 2010. Bifurcation of insulin signaling pathway in rat liver: mTORC1 required for stimulation of lipogenesis, but not inhibition of gluconeogenesis. *Proceedings of the National Academy of Sciences of the United States of America* **107**: 3441-3446.
107. Nakae, J., W. H. Biggs, 3rd, T. Kitamura, W. K. Cavenee, C. V. Wright, K. C. Arden, and D. Accili. 2002. Regulation of insulin action and pancreatic beta-cell function by mutated alleles of the gene encoding forkhead transcription factor Foxo1. *Nature genetics* **32**: 245-253.
108. Ferre, P., M. Foretz, D. Azzout-Marniche, D. Becard, and F. Foufelle. 2001. Sterol-regulatory-element-binding protein 1c mediates insulin action on hepatic gene expression. *Biochemical Society transactions* **29**: 547-552.
109. Leavens, K. F., R. M. Easton, G. I. Shulman, S. F. Previs, and M. J. Birnbaum. 2009. Akt2 is required for hepatic lipid accumulation in models of insulin resistance. *Cell metabolism* **10**: 405-418.
110. Ferre, P., and F. Foufelle. 2010. Hepatic steatosis: a role for de novo lipogenesis and the transcription factor SREBP-1c. *Diabetes, obesity & metabolism* **12 Suppl 2**: 83-92.
111. Lee, A. H., E. F. Scapa, D. E. Cohen, and L. H. Glimcher. 2008. Regulation of hepatic lipogenesis by the transcription factor XBP1. *Science* **320**: 1492-1496.
112. Kammoun, H. L., H. Chabanon, I. Hainault, S. Luquet, C. Magnan, T. Koike, P. Ferre, and F. Foufelle. 2009. GRP78 expression inhibits insulin and ER stress-induced SREBP-1c activation and reduces hepatic steatosis in mice. *The Journal of clinical investigation* **119**: 1201-1215.
113. Wu, X., and K. J. Williams. 2012. NOX4 pathway as a source of selective insulin resistance and responsiveness. *Arteriosclerosis, thrombosis, and vascular biology* **32**: 1236-1245.
114. Turner, S. M., S. Roy, H. S. Sul, R. A. Neese, E. J. Murphy, W. Samandi, D. J. Roohk, and M. K. Hellerstein. 2007. Dissociation between adipose tissue fluxes and lipogenic gene expression in ob/ob mice. *American Journal of Physiology-Endocrinology and Metabolism* **292**: E1101-E1109.
115. Bandsma, R. H., C. H. Wiegman, A. W. Herling, H. J. Burger, A. ter Harmsel, A. J. Meijer, J. A. Romijn, D. J. Reijngoud, and F. Kuipers. 2001. Acute inhibition of glucose-6-phosphate translocator activity leads to increased de novo lipogenesis and development of hepatic steatosis without affecting VLDL production in rats. *Diabetes* **50**: 2591-2597.
116. Mutel, E., A. Abdul-Wahed, N. Ramamonjisoa, A. Stefanutti, I. Houberdon, S. Cavassila, F. Pilleul, O. Beuf, A. Gautier-Stein, A. Penhoat, G. Mithieux, and F. Rajas. 2011. Targeted deletion of liver glucose-6 phosphatase mimics glycogen storage disease type 1a including development of multiple adenomas. *Journal of hepatology* **54**: 529-537.
117. Irimia, J. M., C. M. Meyer, C. L. Peper, L. Zhai, C. B. Bock, S. F. Previs, O. P. McGuinness, A. DePaoli-Roach, and P. J. Roach. 2010. Impaired glucose tolerance and predisposition to the fasted state in liver glycogen synthase knock-out mice. *The Journal of biological chemistry* **285**: 12851-12861.
118. Oosterveer, M. H., T. H. van Dijk, U. J. Tietge, T. Boer, R. Havinga, F. Stellaard, A. K. Groen, F. Kuipers, and D. J. Reijngoud. 2009. High fat feeding induces hepatic fatty acid elongation in mice. *PloS one* **4**: e6066.
119. Castro-Perez, J. M., T. P. Roddy, V. Shah, D. G. McLaren, S. P. Wang, K. Jensen, R. J. Vreeken, T. Hankemeier, D. G. Johns, S. F. Previs, and B. K. Hubbard. 2011. Identifying static and kinetic lipid phenotypes by high resolution UPLC-MS: unraveling diet-induced changes in lipid homeostasis by coupling metabolomics and fluxomics. *Journal of proteome research* **10**: 4281-4290.
120. Hull, R. L., K. Kodama, K. M. Utzschneider, D. B. Carr, R. L. Prigeon, and S. E. Kahn. 2005. Dietary-fat-induced obesity in mice results in beta cell hyperplasia but not increased insulin release: evidence for specificity of impaired beta cell adaptation. *Diabetologia* **48**: 1350-1358.

121. Karasawa, H., S. Nagata-Goto, K. Takaishi, and Y. Kumagae. 2009. A novel model of type 2 diabetes mellitus based on obesity induced by high-fat diet in BDF1 mice. *Metabolism: clinical and experimental* **58**: 296-303.
122. Satapati, S., N. E. Sunny, B. Kucejova, X. Fu, T. T. He, A. Mendez-Lucas, J. M. Shelton, J. C. Perales, J. D. Browning, and S. C. Burgess. 2012. Elevated TCA cycle function in the pathology of diet-induced hepatic insulin resistance and fatty liver. *Journal of lipid research* **53**: 1080-1092.
123. Sunny, N. E., S. Satapati, X. R. Fu, T. T. He, R. Mehdibeigi, C. Spring-Robinson, J. Duarte, M. J. Potthoff, J. D. Browning, and S. C. Burgess. 2010. Progressive adaptation of hepatic ketogenesis in mice fed a high-fat diet. *American Journal of Physiology-Endocrinology and Metabolism* **298**: E1226-E1235.
124. Kozawa, S., A. Honda, N. Kajiwara, Y. Takemoto, T. Nagase, H. Nikami, Y. Okano, S. Nakashima, and N. Shimozawa. 2011. Induction of peroxisomal lipid metabolism in mice fed a high-fat diet. *Molecular medicine reports* **4**: 1157-1162.
125. DiTullio, N. W., C. E. Berkoff, B. Blank, V. Kostos, E. J. Stack, and H. L. Saunders. 1974. 3-mercaptopicolinic acid, an inhibitor of gluconeogenesis. *The Biochemical journal* **138**: 387-394.
126. Groen, A. K., C. W. van Roermund, R. C. Vervoorn, and J. M. Tager. 1986. Control of gluconeogenesis in rat liver cells. Flux control coefficients of the enzymes in the gluconeogenic pathway in the absence and presence of glucagon. *The Biochemical journal* **237**: 379-389.
127. Burgess, S. C., T. He, Z. Yan, J. Lindner, A. D. Sherry, C. R. Malloy, J. D. Browning, and M. A. Magnuson. 2007. Cytosolic phosphoenolpyruvate carboxykinase does not solely control the rate of hepatic gluconeogenesis in the intact mouse liver. *Cell metabolism* **5**: 313-320.
128. Chakravarty, K., H. Cassuto, L. Reshef, and R. W. Hanson. 2005. Factors that control the tissue-specific transcription of the gene for phosphoenolpyruvate carboxykinase-C. *Critical reviews in biochemistry and molecular biology* **40**: 129-154.
129. Yang, J., S. C. Kalhan, and R. W. Hanson. 2009. What is the metabolic role of phosphoenolpyruvate carboxykinase? *The Journal of biological chemistry* **284**: 27025-27029.
130. She, P., M. Shiota, K. D. Shelton, R. Chalkley, C. Postic, and M. A. Magnuson. 2000. Phosphoenolpyruvate carboxykinase is necessary for the integration of hepatic energy metabolism. *Molecular and cellular biology* **20**: 6508-6517.
131. Guan, H. P., Y. Li, M. V. Jensen, C. B. Newgard, C. M. Steppan, and M. A. Lazar. 2002. A futile metabolic cycle activated in adipocytes by antidiabetic agents. *Nature medicine* **8**: 1122-1128.
132. Bederman, I. R., S. Foy, V. Chandramouli, J. C. Alexander, and S. F. Previs. 2009. Triglyceride Synthesis in Epididymal Adipose Tissue CONTRIBUTION OF GLUCOSE AND NON-GLUCOSE CARBON SOURCES. *Journal of Biological Chemistry* **284**: 6101-6108.
133. Nye, C. K., R. W. Hanson, and S. C. Kalhan. 2008. Glyceroneogenesis is the dominant pathway for triglyceride glycerol synthesis in vivo in the rat. *The Journal of biological chemistry* **283**: 27565-27574.
134. Martins-Santos, M. E., V. E. Chaves, D. Frasson, R. P. Boschini, M. A. Garofalo, C. Kettelhut Ido, and R. H. Migliorini. 2007. Glyceroneogenesis and the supply of glycerol-3-phosphate for glyceride-glycerol synthesis in liver slices of fasted and diabetic rats. *American journal of physiology. Endocrinology and metabolism* **293**: E1352-1357.
135. Kalhan, S. C., E. Bugianesi, A. J. McCullough, R. W. Hanson, and D. E. Kelley. 2008. Estimates of hepatic glyceroneogenesis in type 2 diabetes mellitus in humans. *Metabolism: clinical and experimental* **57**: 305-312.
136. Franckhauser, S., S. Munoz, A. Pujol, A. Casellas, E. Riu, P. Otaegui, B. Su, and F. Bosch. 2002. Increased fatty acid re-esterification by PEPCK overexpression in adipose tissue leads to obesity without insulin resistance. *Diabetes* **51**: 624-630.
137. Olswang, Y., H. Cohen, O. Papo, H. Cassuto, C. M. Croniger, P. Hakimi, S. M. Tilghman, R. W. Hanson, and L. Reshef. 2002. A mutation in the peroxisome proliferator-activated receptor gamma-binding site in the gene for the cytosolic form of phosphoenolpyruvate carboxykinase

reduces adipose tissue size and fat content in mice. *Proceedings of the National Academy of Sciences of the United States of America* **99**: 625-630.
138. Ferramosca, A., and V. Zara. 2014. Dietary fat and hepatic lipogenesis: mitochondrial citrate carrier as a sensor of metabolic changes. *Advances in nutrition* **5**: 217-225.
139. Owen, O. E., S. C. Kalhan, and R. W. Hanson. 2002. The key role of anaplerosis and cataplerosis for citric acid cycle function. *The Journal of biological chemistry* **277**: 30409-30412.
140. Hakimi, P., M. T. Johnson, J. Yang, D. F. Lepage, R. A. Conlon, S. C. Kalhan, L. Reshef, S. M. Tilghman, and R. W. Hanson. 2005. Phosphoenolpyruvate carboxykinase and the critical role of cataplerosis in the control of hepatic metabolism. *Nutrition & metabolism* **2**: 33.
141. She, P., S. C. Burgess, M. Shiota, P. Flakoll, E. P. Donahue, C. R. Malloy, A. D. Sherry, and M. A. Magnuson. 2003. Mechanisms by which liver-specific PEPCK knockout mice preserve euglycemia during starvation. *Diabetes* **52**: 1649-1654.
142. Millar, J. S., D. A. Cromley, M. G. McCoy, D. J. Rader, and J. T. Billheimer. 2005. Determining hepatic triglyceride production in mice: comparison of poloxamer 407 with Triton WR-1339. *Journal of lipid research* **46**: 2023-2028.
143. Dohm, G. L., R. L. Huston, E. W. Askew, and P. C. Weiser. 1972. Effects of exercise on activity of heart and muscle mitochondria. *The American journal of physiology* **223**: 783-787.
144. Des Rosiers, C., C. A. Fernandez, F. David, and H. Brunengraber. 1994. Reversibility of the mitochondrial isocitrate dehydrogenase reaction in the perfused rat liver. Evidence from isotopomer analysis of citric acid cycle intermediates. *The Journal of biological chemistry* **269**: 27179-27182.
145. Burgess, S. C., N. Hausler, M. Merritt, F. M. Jeffrey, C. Storey, A. Milde, S. Koshy, J. Lindner, M. A. Magnuson, C. R. Malloy, and A. D. Sherry. 2004. Impaired tricarboxylic acid cycle activity in mouse livers lacking cytosolic phosphoenolpyruvate carboxykinase. *The Journal of biological chemistry* **279**: 48941-48949.